Development of Hydrogen Storage Materials Based on Amine-Boranes

Presented to the

Faculty of Computing, Engineering and Sciences

University of South Wales

By

Sam Baker

Supervisor: Dr Nildo Costa

(October 2021 – September 2022)

This work was carried out in fulfilment of the requirements for MRes Degree.

Dissertation Committee:

Dr Ben Ward, Cardiff University

Dr Christian Laycock, University of South Wales

Acknowledgments

I would like to express my sincere gratitude to my supervisor, Dr Nildo Costa, for his guidance, patience, and encouragement throughout the entire process. His insight and feedback have been instrumental in shaping the direction and scope of this study.

I would also like to thank Dr Gareth Owen for his support during my time working on this research project. I have the utmost respect and admiration for you both.

I would like to thank Dr Issam Abdalghani for his help and assistance in the laboratory.

Finally, I would like to express my gratitude to the KESS2 program and TATA Steel; for providing the sponsorship that enabled me to undertake this project in the first place; and the University of South Wales for providing the resources and facilities to carry out this research.

Abstract

The production of coke oven gas (COG) from Port Talbot steelmaking generates several side-products, (e.g. CH_4, CO, CO_2, NH_3, H_2, H_2S, organic aromatic compounds, cresols, etc), that can enable possibilities for the recovery of energy (e.g. via utilisation of generated H_2 and potential utilisation of ammonia gas as energy vectors) and valuable compounds. Particularly, the mandatory removal of ammonia, as either $NH_4^+{}_{(aq)}$ or $NH_{3\ (g)}$, from COG provides a foundation to be utilised as a precursor for hydrogen storage in the form of amine-boranes; where ammonia as a Lewis base forms Lewis adducts with boranes. In the Lewis adducts involving ammonia and boranes, the control of substituents on the boron can serve to influence the hydrogen storage characteristics of the Lewis pair. In this study, boron-methyl and boron-phenyl amine boranes were selected as targets for their potential exploration as hydrogen storage materials. Meanwhile, literature analysis indicates the possibility of boron-diethyl and boron-*bis*(trifluoromethyl) phenylamine-borane as synthetic targets with improved product selectivity and potential for reversibility. Such characteristics could show an improved practicality for application at TATA Steel; although these are very reactive species and limited success in the preparation of these compounds was achieved. In addition to investigating the thermolytic character of synthesised boron-substituted amine boranes, the activation of H_2 was also investigated via catalytic methods involving ruthenium complexes. Catalytic reactions showed H_2 release was possible at room temperature, and in loadings reduced to 0.1 mol% at 70°C. Further, ^{11}B and ^{1}H NMR spectroscopy showed the catalytic release of all available H_2 making them advantageous as hydrogen storage materials at TATA Steel. The potential direct involvement of the ligand in these catalytic methods, allowed us to speculate on a plausible mechanism of action via a metal ligand cooperation regime. This was possible by utilising phosphine ligands containing an OH functional group i.e. phosphinous acids [Ru-P(O**H**)] in $RuCl_2$(*p*-cymene)PR_2(OH)-type complexes. Thus, drawing on similar literature precedents, a bifunctional ligand co-operative mechanism was anticipated. This comprised of the transfer of hydridic BH to the metal center and NH proton activation to the basic oxygen functionality. Accordingly, the inclusion of phosphorous acid (PA) as a ligand was assessed and comparison studies were carried out with catalysts containing analogous functionality (Ru-**H**N-Propyl) or without (Ru-PPh_3) as a benchmark. The activation of H_2 from low catalytic loadings served to better understand the catalytic activity as well as explore cost implications for TATA Steel. Probing experiments such as stoichiometric reactions or independent hydride preparations

which relate to detailing the mechanism of dehydrogenation were also explored based on initial NMR spectroscopy (^{31}P, ^{1}H, ^{11}B) observations.

Table of Contents

List of Figures

Chapter 1: Introduction

Chapter 2: Results & Discussions

List of Schemes

List of Tables

List of Equations

1. Introduction

1.1 Project Main Idea/Concept

As described above, the removal of ammonia is an integral component of steel-making. This can facilitate a sizeable feedstock of the material. While this could serve towards agricultural demands, the high hydrogen content within ammonia (NH_3; 17.8 wt% H_2) has made its prospective use as a hydrogen carrier conceivable. Through the process of its removal in the steel production, waste ammonia may be delivered as $NH_4^+X^-$ solutions from the washing stages, or as NH_3(g) after subsequent stripping. Theoretically, both can support the formation of amine-borane adducts as prospective hydrogen storage materials via known synthetic routes. For instance, reactions of NH_3 (g) with solutions of boron-substituted (BH_2R-THF) solutions are well-known,[1] whilst ammonium salts NH_4X can react with alkali borohydrides, MBH_4, to support adduct formation with the concomitant formation of hydrogen gas.[2] Naturally, the application of these reactions towards an industrial setting would require considerations towards purity, contaminants and stability of reactants and products. Moreover, the nature of substituents on the boron centre can influence these and can lead to the opportunity for the synthesis of new amine-boranes as hydrogen storage materials with direct industrial links. To date there are a limited number of articles on B-substituted amine boranes and fewer on systems developed to pilot scale.[3,4] The main idea of this thesis consists of the synthesis of amine boranes and the investigation of their dehydrogenation reactivity for the generation of hydrogen gas. Amine boranes can be dehydrogenated thermolytically and catalytically. In this work, catalysts based on ruthenium cymene and phosphine ligands were utilised.

1.2 Background on Industrial Partner Tata Steel

TATA Steel is one of Europe's largest steelmakers, with a production of 34 million tonnes of crude steel per annum.[5] In the UK, the Port Talbot integrated plant produces 3.4 million tonnes of liquid steel, the majority of which services a number of downstream domestic markets. In connection with British Steel Scunthorpe, the two sites are responsible for 95% of all emissions arising from steelmaking in the UK.[6] This contributes to the UK steel and iron industry generating 14% of UK greenhouse gas emissions. In the case of Tata Port Talbot, 6,07 Mt of CO_2 emission were emitted and verified by the European Emission and Trade System (EU ETS) in 2019[7] with a 2.14 (t/tcs) carbon intensity (tonnes of CO_2 per tonne of crude steel) for the years of 2020-2021. This means that on average, for each tonne of steel produced, approximately 2 tonnes of CO_2 are emitted. Nevertheless, a step-change reduction in CO_2

emission by the steel industry is paramount to safeguard a low-carbon footprint and meet UK net-zero commitments by 2050.[8] For the same reason, other exhaust gases, namely from coke oven gas (COG) are receiving increased attention for the recovery of energy and valuable compounds.[9]

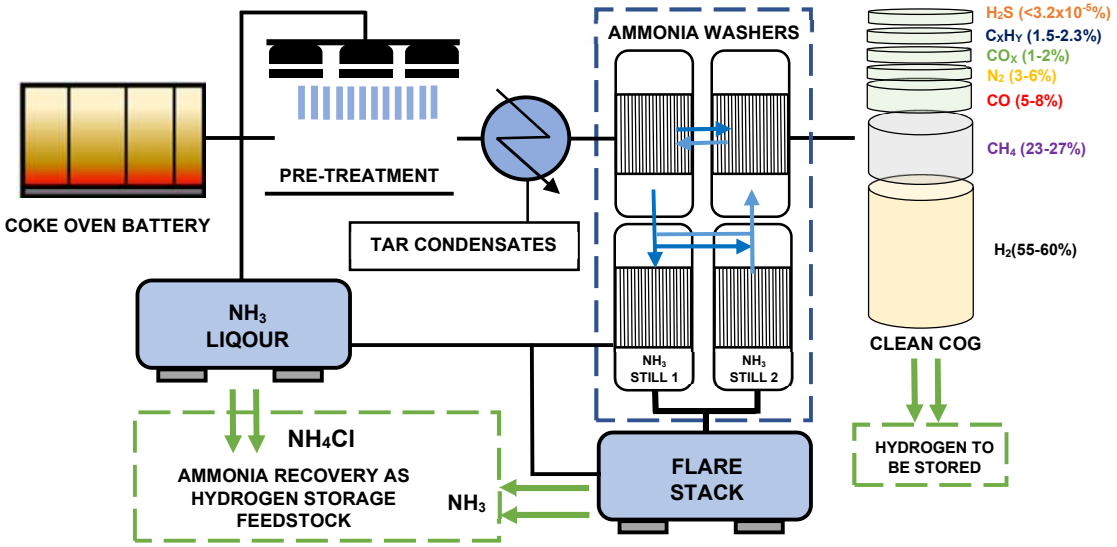

Figure 1: A simplified schematic representation of COG handling with respect to NH_3 removal

Coke serves as an essential input as a reducing agent for ironmaking, and is generated by treatment of coal in airtight ovens at temperatures between 1200-1300 ºC. Minor compounds such as ammonia, tar (semisolid mixture of condensable aromatic hydrocarbons) or hydrogen sulfide are present within COG at this stage, and must be eliminated to prevent fouling and corrosion across the plant pipelines. Raw gases (COG) funnelled out of coke oven batteries are retrieved via a collection systems (exhausters). Since exhausters cause the compression of the gas, secondary cooling is necessary to attain suitable processing conditions for the NH_3/H_2S removal stage at around 27 ºC. Simultaneously, secondary cooling causes tar droplets to separate from the condensate streams which are carried out in a decanter. Ammonia removal is a well-established process consisting of driving the unclean gas counter current to an ammonia washing solvent (washers). After successive cycles through the washers, low-ammonia content gas is then transferred onward through other cleaning cycles while the concentrated ammonia liquor exits the washers (Figure 1). The in-situ generated $NH_4^+X^-$ solutions are then treated further via steam and sodium hydroxide stripping before disposal via incineration at the coke oven flare stack. Typically, every metric ton of steel manufactured in blast furnaces generates approximately 1.5 kg of ammonia vapour as a by-product from the cleansing of COG.[10] At current volume, the Port Talbot site produces 44,000 m^3 of COG every

hour from its coke ovens, roughly responsible for 264 kg of concomitant NH_3 per hour. Presently, treatment of COG can be pursued to obtain valuable products by separation or conversion techniques, while in high production rates surplus COG can be potentially used for heating purposes or burnt in flares and discharged into the atmosphere. Ammonia has also been proposed as a source of energy by Hewlett *et al.* to produce power using gas turbine technology.[10]

An approximate 55% hydrogen content in the COG (dependent on the coal utilised) after the appropriate conditioning also positions it as promising source toward a hydrogen-based economy that could drive economic and environmental benefits within the steel industry. To this extent, a number of decarbonisation strategies focused on a net-zero CO_2 steel supply are increasingly based on the utilisation of green hydrogen, ammonia production and CO_2 sequestration.[7] Hydrogen produced within the process can be recycled throughout the site as a fuel[11] - although given the transition required for a circular steel economy, lifecycle assessments of large-scale H_2 production will require considerations towards storage and distribution. Thus, establishing practices targeting ammonia and hydrogen are at the forefront of chemical and industrial strategies.

1.3 Hydrogen as a Fuel

Securing access to new sources of inexpensive and sustainable energy is critical to facilitate continued economic security and provide flexibility to future energy portfolios.[12] Whilst the current dependency on fossil fuels covers a dominant portion of immediate and short-term demands, future energy sources must reconcile against challenges (fuel exhaustion, environmental damage, health implications) associated with their current practice and inevitable withdrawal.[13,14] In recognition of these concerns, the President of the USA, George W. Bush commissioned in 2003 the development of new hydrogen technologies in order to safeguard USA environmental quality, energy resiliency and economic vitality.[15] Today, over 228 hydrogen projects have been announced across Europe by governments and stakeholders; 17 of which now contribute to giga-scale hydrogen production.[16]

As a fuel, hydrogen has the potential to be a clean, source-independent energy carrier. Notably, it has a favourable energy content compared to petroleum (120 MJ kg^{-1} *versus.* 44 MJ kg^{-1} for petroleum) and can provide a mechanism for flexible energy transfer that can counterbalance electricity.[17,18] Additionally, fuel cell devices operating on hydrogen can lead to significant increases in efficiency over internal combustion engines (32% efficiency for diesel-electric;

90% potential efficiency for fuel cell with heat capture) while eliminating end-use formation of sulphur or carbon particulates.[19] Quiet operation, cold-start capability, low maintenance and high reliability are other significant advantages of fuel cell systems that render them encouraging for roll-out to stationary, transportation and portable applications. To date, hydrogen and fuel cell technologies are central in plans to transitioning towards net-zero; it is becoming an integral feature of government and shareholder strategies.[16,20] The UK government have pledged the introduction of 5 GW of low-carbon hydrogen production by 2030 which could help deliver emissions savings of 41 $MtCO_2e$ between 2023 and 2032.[21] Still, a successful transition towards a hydrogen economy will ultimately require several technological, economic and institutional breakthroughs (i.e. storage) over a series of decades. Furthermore, the scale up of hydrogen-based technologies from marginal to commercial events will require regulatory frameworks that support the execution of delivery infrastructure, and ensure robust supply and demand.

1.3.1 Department of Energy & Hydrogen Storage

Transport modes, notably light-duty vehicles are a continued driver of CO_2 emissions, and must be dramatically off-set to meet both domestic and global clean air targets.[22] As of 2021, the International Energy Agency (IEA) reported transport remained highly reliant on fossil fuels and accounted for 37% of global CO_2 emissions.[23] In the UK, transport is the largest emitting sector of greenhouse gas emissions, producing 24% of the UK's total emissions in 2020 (406 $MtCO_2e$).[24] For stationary energy applications, resultant CO_2 may be sequestered. However, for portable energy, the solution must involve a shift to non-carbon intensive carriers. Hydrogen fuel cell vehicles (FCEV's) are one of the main options for future low-carbon transport alongside electric vehicles (EV's). While EV's are significantly ahead in maturity, the simultaneous buildout of a hydrogen fleet can extend flexibility to resolve the diverse nature of the sector in geographic coverage, convenience, and user-acceptability. Furthermore, the extended ranges and faster recharging times of FCEV's are expected to be positive attributes that resonate well with future vehicle purchase decisions, even if ultimate cost parity is not met.[16] In scenarios where road transport can be defined in drive cycles of extended ranges or higher payloads (return to base fleets) requiring fast, infrequent refuelling, FCEVs already show a high technological readiness.[25] However, for passenger vehicles, the low volumetric density of liquid H_2 (8 MJ/L versus 32 MJ/L for gasoline) creates the requirement to store hydrogen without adversely affecting vehicle size. The Department of Energy (DOE) have established a series of metrics that hydrogen must meet or exceed to become viable as a

gasoline equivalent.[26] These include the necessity for a 300-mile range, hydrogen purity of 99.99%, temperature operability between −20 ºC to 40 ºC as well as cost parity estimates (Table 1). Current FCEV's consist of carbon nano-fiber tanks that can store up to 700 bar of compressed H_2. Beyond the safety concerns linked to the use of high pressure H_2 in public areas, the storage density of the system is decreased by the conformity demands of pressure stable tanks (volume) to maintain passenger or cargo space. Equally, an analysis by Hua concluded this technology was unlikely to successfully meet DOE targets associated to volumetric capacity or cost.[27] Liquefying hydrogen, which can offer improvements in H_2 density, creates critical issues of pressure build-up from the strong temperature gradient between liquid hydrogen (−239.96 ºC) and environment. Thus, the permanent evaporation of H_2 is inevitable to relieve tank pressure, which together with the upfront energy intensive liquefication (10-13 kWh/kg) process inhibits practicality of the technology.[28] Hydrogen UK anticipates 45 TWh of hydrogen could be demanded for UK transport by 2035.[29]

Table 1: Selected DOE Targets for Hydrogen Fuel Vehicles (From Ref 26)

STORAGE PARAMETER	UNITS	2020	2025	ULTIMATE
System Gravimetric Capacity				
Usable, specific-energy from H_2 (net useful energy/max system mass)	kWh/kg (kg H_2/kg system)	1.5 (0.045)	1.8 (0.055)	2.2 (0.065)
System Volumetric Capacity				
Usable energy density from H_2 (net useful energy/max system volume)	kWh/L (kg H_2/L system)	1.0 (0.030)	1.3 (0.040)	1.7 (0.050)
Min/max delivery temperature	°C	-40/85	-40/85	-40/85
Minimum full flow rate (e.g., 1.6 g/s target for 80 kW rated fuel cell power)	(g/s)/kW	0.02	0.02	0.02
Storage system cost	$/kWh net ($/kg H_2)	10 (333)	9 (300)	8 (266)
Operational cycle life (1/4 tank to full)	Cycles	1,500	1,500	1,500
Fuel Quality (H_2 from storage)	%H_2	99.99	99.99	99.99

The DOE commissioned the Chemical Hydrogen Storage Center of Excellence (CHSCoE), a solicitation of US departments and national laboratories to discover, explore and recommend the feasibility of storing onboard H_2 within storage materials (chemically). The center was one of three formulative segments of the DOE, and joined the Metal Hydride Center and Sorption Center as integral contributors to the National Hydrogen Storage Project. The mission was to select and/or rank candidate materials with promising characteristics (release process, kinetics,

regeneration etc.) to fulfil DOE specifications towards sub-scale prototype demonstration. Other metrics for technical targets such as total system weight relating to the material storage weight of H_2 divided by the fuel system weight including tanks, heaters, tubing, solvents etc have also been proposed. Additionally, qualitative analysis of onboard storage requirements recognised liquid storage materials are preferable in view of minimal engineering turnover and improved loading logistics. For Chemical Hydrogen Storage, the inclusion of several boundary gravimetric and volumetric conditions established amine boranes/borohydrides as the direct candidates for investigation (Figure 2).[30]

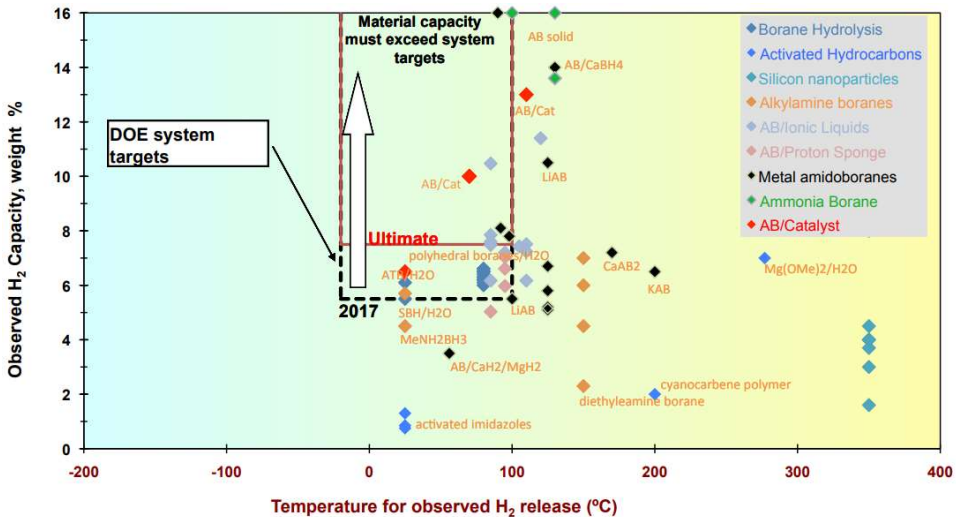

Figure 2: A plot of the temperature & quantity of hydrogen metrics of the DOE populated by the general type of families of storage materials after completion of the CHSCoE activities (2010). Taken from Ref [30]

Borohydrides (BH_4^-) have shown promising capabilities as a hydrogen storage material, where hydrogen is stored within the B-H chemical bond. Still, the decomposition temperatures reported to effect hydrogen loss are exceedingly high; $LiBH_4$ undergoes hydrogen desorption over four endothermic events with 9 wt% loss between 400-680 °C.[31,32] Instead, hydrolysis of the material is needed to liberate hydrogen gas which causes decomposition of the borohydride. Thus, a subsequent mandatory chemical regeneration of the borohydride is needed which makes it less practical to implement as a hydrogen storage material. Boron and nitrogen are both lightweight elements capable of bearing multiple hydrogens of hydridic and protic character, respectively; they also present scope for the favourable activation of H_2 at low temperatures. Additionally, the parent adduct, ammonia borane (NH_3BH_3) theoretically shows promise of a 19.6 wt% H_2 capacity and stability across a range of requirements in keeping with DOE targets.[34] As such, amine boranes have been considered as a potential hydrogen storage

material. The next section discusses the general characteristics and chemistry of amine boranes including their potential application as hydrogen storage materials.

1.4 Amine Boranes (AB) as Hydrogen Storage Materials

Amine boranes are Lewis adducts, consisting of a dative bond between the lone pair of ammonia and vacant orbital on the borane group (Figure 3). Crystalline NH_3BH_3 (AB) was first reported by Shore and Parry in 1955 from the metathesis reaction of lithium borohydride and ammonium chloride in diethyl ether.[34] Since its discovery, the solid state structure of NH_3BH_3 has been determined by X-ray and neutron diffraction. Solid NH_3BH_3 exists in a staggered conformation and exhibits short BH···HN intermolecular distances of 2.02 Å inside the Van der Waals distance of 2.4 Å, constituting a dihydrogen bond.[35] As a result of the dihydrogen bond, a stabilisation energy of 90.4 kJ mol^{-1} contributes to the solid structure of NH_3BH_3 at standard conditions. The electronegativity difference between B (2.04) and N (3.04) results in protic N-H and B-H hydrogens that leads to the favourable elimination of H_2 by reaction $H^{\delta+}$ and $H^{\delta-}$.

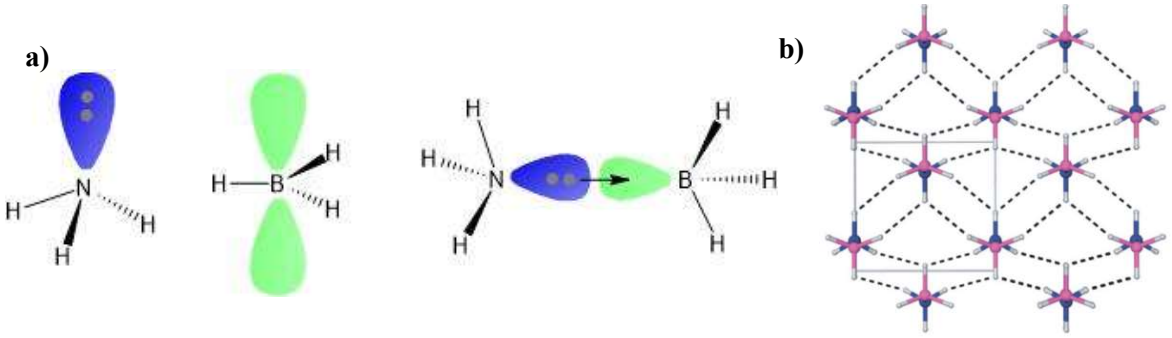

Figure 3: (a) The bonding involved in the Lewis adduct of ammonia borane **(b)** Low-temperature (orthorhombic) crystal structure of H_3NBH_3. Nitrogen, Boron, and Hydrogen atoms are depicted in blue, purple, and grey respectively. The dihydrogen bonds are delineated by dashed lines. The unit cell is shown by grey lines. From Ref [35].

1.4.1 Dehydrogenation of Amine Boranes

Ammonia borane (AB; NH_3BH_3) has been core to the discussion of potential solid/liquid state hydrogen storage materials because of its potential high volumetric capacity of H_2 (19.6 wt% H_2). The presence of equimolar protic and hydridic hydrogens suggests stepwise H_2 loss in successive 6.5 wt% releases; this occurs via the generation of polyaminoborane $(H_2NBH_2)_X$ and polyiminoborane $(HNBH)_X$ intermediates in sequence until the formation of boron-nitrides (BN). Such a pathway was originally postulated by Hu *et. al.,* and can serve as a straight-forward mechanism for the thermal dehydrogenation of AB.[36] Within the literature the formation of dimers, trimers, oligomers, and BN-polymers upon dehydrogenation of amine

boranes through B-H and N-H combination are normally referred to as dehydrocoupling reactions.

$$nNH_3BH_3 \rightarrow (NH_2BH_2)_n + nH_2 \text{ (100 °C) (} \textbf{Equation 1.1}\text{)}$$

$$(NH_2BH_2)_n \rightarrow (NHBH)_n + nH_2 \text{ (150 °C) (}\textbf{Equation 1.2}\text{)}$$

$$(NHBH)_n \rightarrow nBN + nH_2 \text{ (>500 °C) (}\textbf{Equation 1.3}\text{)}$$

Instead, thermogravimetric analysis of H_2 release measured up to 200 °C concludes the mass losses of ~35 wt% from AB towards a complex mixture of straight, branched and cyclic structures (Figure 4).[37] As part of a recent mechanistic insight review, Demirci highlighted there was consistency between groups that reported on detectable volatile emissions.[38] Baitalow *et al* reported small quantities of diborane, borazine and aminoborane NH_2BH_2 during the first decomposition, while Wolf et al detected NH_2BH_2 prior to borazine.[39,40] Roy *et al* suggested that intramolecular hydrogen loss to NH_2BH_2 was primary and led to an autocatalytic effect through reactions with AB.[41]

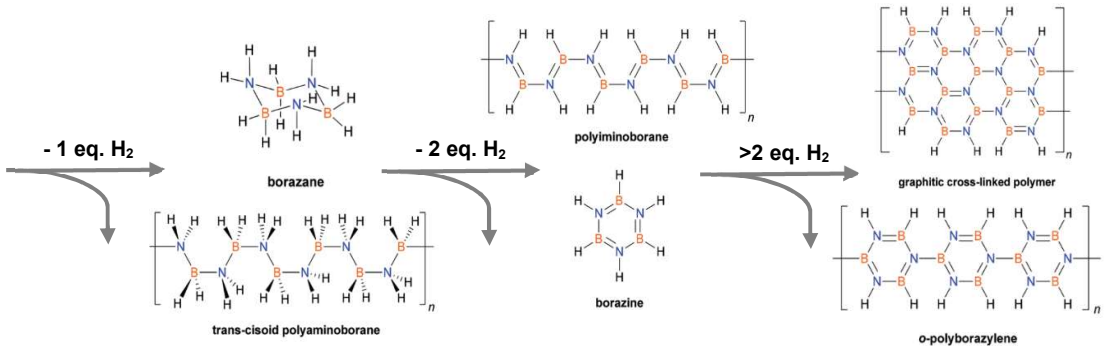

Figure 4: The products of ammonia borane thermal dehydrogenation.
Image adapted from Ref [47]

Stowe and co-workers studied the mechanism of thermal decomposition of AB by solid state ^{11}B NMR spectroscopy and provided first evidence towards the presence of a new mobile phase of AB, denoted as AB* formed by the disruption of the hydrogen bonding network.[42] This new phase was critical to the architecture of an ionic-dimer DABD ($[(NH_3)_2BH_2^+][BH_4^-]$) comprised of 2 AB* units. At isothermal heating of AB between 70 °C to 90 °C, reaction courses appear sigmoidal indicative of nucleation and growth periods in AB solids – notably the formation of DABD as a reactive precursor for chain growth. Minor additions of NH_4Cl or DABD have since been shown to reduce the induction period of neat AB. Further, metal chloride additives such as $CuCl_2$ have been reported to initiate AB catalysis through $[NH_4]^+[BCl_4]^-$ intermediates that lead to significant improvements in release temperatures and

borazine reduction.[43,44] Counter-intuitively, homopolar B-H couplings are also expected to contribute moderately with dehydrocoupling.[45]

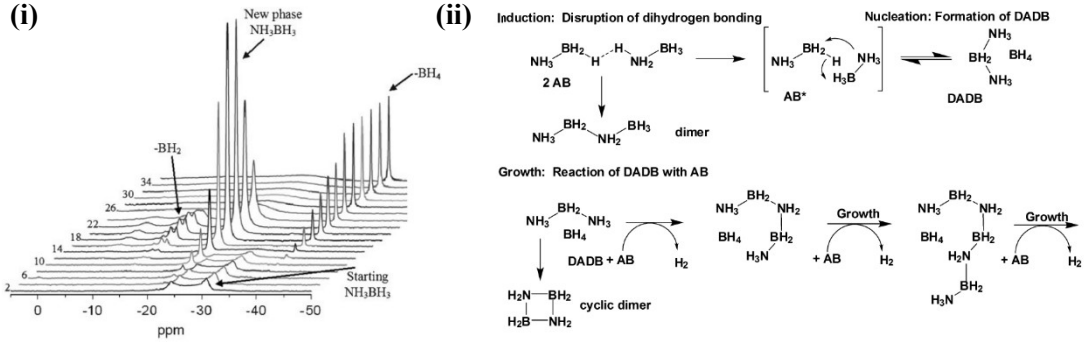

Figure 5: **(i)** Time resolved $^{11}B\{^{1}H\}$ MAS-NMR spectra for the thermal dehydrogenation of AB at 88 °C depicting the growth of new phase AB (–23 ppm) **(ii)** Proposed thermal dehydrogenation mechanism of AB showing discrete induction, nucleation, and growth steps. From Ref [42]

The evolution of borazine and ammonia from solid AB causes concern in relation to DOE targets of hydrogen quality. Moreover, ammonia is known to react irreversibly with the acidic polymer electrolyte to form ammonium ions, with concomitant loss in proton transport and fuel cell performance.[30] In scoping experiments, PEM fuel cells conditioned with pure hydrogen and exposed to ammonia borane thermolysis experienced 30% loss in current after minutes and full loss after 3 hours. Furthermore, the formed structure of AB monitored by IR spectroscopy is observed to change over the course of dehydrogenation, characterised by foaming and significant volume expansion. Choi and co-workers showed that addition of 15wt% methyl cellulose (MC) was found to be a promising antifoaming agent, while also enhancing the thermal propagation of AB.[46] Most detrimental, the formation of a π-bond within the amine borane in place of the dative interaction is highly exothermic and incurs self-propagation (runaway) and thermal management issues. Wolf et al determined a mean enthalpy of –21.7 kJ mol^{-1} for the first decomposition stage.[40] This results in an impossibility of direct rehydrogenation under H_2 pressure and necessitates that spent-residues undergo off-board chemical recycling as part of novel energy-intensive processes. This is exacerbated by considering the complexity of the spent residue, in which cyclotriborazane $(H_2NBH_2)_3$, aminodiborane $NH_2B_2H_5$, borazine *c*-$B_3N_3H_6$, polyaminoborane $(NH_2BH_2)_n$, polyiminoborane $(NHBH)_n$ and polyborazylene $(\{B_3N_3H_4\}_n)$ create a diverse mixture which cannot be treated uniformly. Although many elegant approaches have been put forward towards solving off-board regeneration, none offer an efficient, scalable and economic method.[47-49] Thus, in reference to the aforementioned challenges, use of pristine AB for on-board fuel cells cannot be pursued. Following down selection criteria of the HSECoE, a center wide repertoire of remediative strategies have been developed that include; nanoconfinement, chemical

modification, the inclusion of additives/dopants, catalytic dehydrogenation and solvent activation. A few of these areas are expanded upon in the next section. Of note, hydrolysis strategies of AB although attractive for the rapid kinetics of H_2 release are discarded based on the formation of spent borates (B-O) that are too energy intensive to regenerate.[30]

1.4.2 Dehydrogenation of Nitrogen-Alkyl Substituted Amine Boranes

Following reports by the Manners group and others, substitution of hydrogen at the nitrogen atom with electron donating groups as been readily investigated. After an original report by Beachley, Bowden and co-workers updated the study of methylamine borane (MeAB) with respect to DOE commitments.[50,51] MeAB exhibits similar character to AB, with an activation energy of 115 kJ mol^{-1} and enthalpy of –25 kJ mol^{-1} for the first equivalent of hydrogen to be evolved. Following TG and DSC traces, hydrogen loss is accompanied with significant contamination of N-trimethylcycloborazane and MeAB sublimation in losses totalling 70wt%. To this extent, ^{11}B mechanistic studies indicate a mechanism consistent with that reported for AB; comprised of an initial induction step towards a DADB species ($[H_2B(NH_2CH_3)_2]^+[BH_4]^-$) and cyclic polyborazine products. Equally, expanded searches incorporating larger alkyl motifs such as Me_2NH-BH_3 and $^tBuNH_2$-BH_3 ultimately yield similar results and suggest impracticality.[52,53] More recently, Confer and co-workers suggested that G3(MP2)-based predictions achieved for C, Si, N and P centered amine boranes show them to be promising synthetic targets and warrant further investigation.[54] Yang et al reported that a composite material of MeAB and poly (methyl acrylate) could result in lower onset hydrogen desorption and improved kinetics.[55] The as-prepared PMA/MeAB100 blend showed significant improvement in reducing the emission of selective volatilities, reporting a weight loss reduction from 92 wt% to 45 wt% for MeAB and PMA/MeAB100 over 107 ºC - 220 ºC. Accordingly, no MeAB sublimation was reported during dehydrogenation, and onset release was achieved at 90.5 ºC, roughly 20 ºC lower than pristine MeAB.

Contrary to MeAB, independent systems incorporating an AB unit as part of a chain show significant advantages in hydrogen delivery. Li and co-workers reported that 1,2/1,3-di-aminopropane borane produces hydrogen in two separate steps with no impurities.[56] Promisingly, up to 7.4 and 6.3 wt% pure H_2 can be liberated between 20 ºC – 250 ºC with a heating rate of 5 ºC min^{-1} respectively. Additionally, characteristic N-H and B-H stretching bands in the FT-IR spectra indicate the formation of C-B-N polymers with hydrogen release facilitated from $B\text{-}H^{\delta-}$ and $N\text{-}H^{\delta+}$ combination. Similarly, Neiner et al reported that

dehydrogenation of ethylene diamine bisborane ($BH_3NH_2CH_2CH_2NH_2BH_3$; EDAB) (9.4 wt%) occurs over two mildly exothermic stages (–10 kJ mol^{-1} & – 4 kJ mol^{-1}) below 200ºC releasing *ca*. 10 wt%, where the introduction of an ethyl-bridge mitigates contaminant release, with no detectable presence of gaseous $B_3N_3H_6$ and NH_3.[57] Steeper temperature dependencies are also a feature of EDAB in comparison to AB allowing beneficial release control in practical devices. At temperatures below 100 ºC, hydrogen release occurs more slowly than AB (60x slower at 60 ºC); whereas above 130 ºC hydrogen can be delivered at higher rates. Additionally, no mass loss events are detected for EDAB after extended heating at elevated temperatures (72 h at 80 ºC) representing stability targets for vehicular storage, albeit at higher thresholds. Both, Neiner and Leardini[58] concluded EDAB to undergo dehydrogenation through an intermolecular pathway, citing poor solubility within the competing intramolecular pathway (Figure 6).

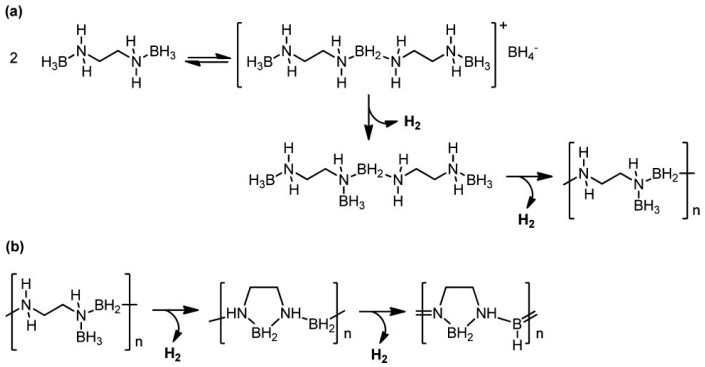

Figure 6: Proposed mechanism for the first **(a)** and second **(b)** hydrogen desorption steps of EDAB thermolysis below 500K. Taken from Ref [58]

Similar to AB, EDAB initially dimerises to produce a BH_4^- unit which differentially reacts with a nearby NH_2, polymerising and forming longer chains. The second desorption is resultant of hydridic and protic combinations on the polymer to yield cyclic BH_2 groups and B=N linkages. Identical results are suggested by Zhang *et al* on inspection of diethylenetriamine-borane ($C_4H_{13}N_3$-$3BH_3$, DETAB), triethylenetetramine-borane ($C_6H_{18}N_4$-$4BH_3$, TETAB) and tetraethylenepentamine-borane ($C_8H_{23}N_5$-$5BH_3$, TEPAB).[59] These structures can release 7.6, 6.8 and 5.9 wt% respectively between 50 – 250 ºC with a ramp of 5 ºC min^{-1}. Moreover, analogous to EDAB, increased alkyl modification results in even greater reductions in activation energies (101.76, 66.85, 61.19 kJ mol^{-1}) and the sole release of pure hydrogen. Regeneration of these compounds can be afforded with use of energy intensive HCOOH and $LiAlH_4$ in moderate success of 77% for EDTAB. Analogous ethylene diamine monoborane materials are also receiving close attention.

1.4.3 Dehydrogenation of Boron-Alkyl Substituted Amine Boranes

In response to the assertion that electron withdrawing groups on boron may encourage thermoneutrality, these systems have not received equal attention. Hawthorne first reported that B-substituted amine boranes prepared as Me_3NBRH_2 (R = ^{i}Pr, ^{n}Pr, ^{n}Bu, ^{i}Bu, n-pentyl and n-hexyl) in the presence of ammonia and catalytic NH_4Cl could afford B-substituted borazines $[HNBR]_3$ in moderate yields (65-91%) between 100 – 150 °C.[60] Alternatively, $^{i}Pr_2NH$-$BH(C_6F_5)_2$ prepared as a model substrate with EDGs on N and EWGs on B only produced $^{i}Pr_2N{=}B(C_6F_5)_2$ in a 23% yield at 100 °C after 70 h.[61] Attempts to prepare the aminoborane under milder conditions via use of transition metal catalysts proved unsuccessful - believed to be dependent on the high steric bulk at boron and nitrogen impairing co-ordination. Moreover, the interest of hydrogenation of the aminoborane ($^{i}Pr_2N{=}B(C_6F_5)_2$) could not be demonstrated under 100 bar H_2 (100 °C) or catalytically. Resendiz-Lara and co-workers explored the dehydrocoupling of NH_3-$BH_2(p\text{-}CF_3C_6H_4)$ towards poly(B-aryl)aminoboranes as inorganic analogues of polystyrene.[62] Indeed, the inclusion of an electron withdrawing *p*-CF_3 proved sufficient to inhibit redistribution reactions and NH_3-$BH_2(p\text{-}CF_3C_6H_4)$ is found to be stable at 20 °C in THF for 170 h. Heating to 70 °C in THF (170 h) achieved the following distribution; $[HN\text{-}B(p\text{-}CF_3C_6H_4)]_3$ [δ_B 31.5 (s)] (ca. 80 %), $[NH_2{-}BH(p\text{-}CF_3C_6H_4)]_n$ [δ_B −6.1 (br)] (ca. 15 %) and an unidentified product [δ_B 9.3 (s, br)] (ca. 5 %). Yields of 40% $[NH_2{-}BH(p\text{-}CF_3C_6H_4)]_n$ were achieved through reaction with 5 mol% $[IrH_2(POCOP)]$ (POCOP = $[\eta^3\text{-}1,3\text{-}(OP^{t}Bu_2)_2C_6H_3]$) in THF for 1 h.

1.4.4 Dehydrogenation of Cyclic Amine Boranes

Liu and co-workers prepared a series of CBN heterocyclic systems; imagining that incorporation of NH_2BH_2 units into carbocyclic systems would provide a rigid framework that could produce a single well-defined product and limit volatile by-products.[63] Additionally, the coupling of endothermic C-H release with the exothermic release of amine boranes could accomplish free energy neutrality and gas-liquid hydrogenation.

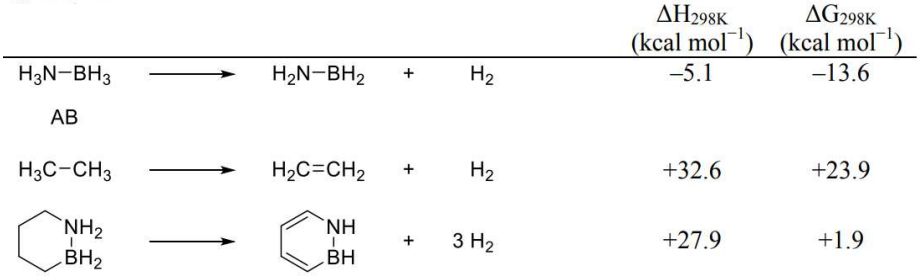

Figure 7: Calculated thermodynamics for isolated BN and CC dehydrogenation reactions and their combined occurrence in a single molecular entity. From Ref [63]

Despite developing a number of systems in view of producing reversible, liquid, and high wt% structures, two main systems have been reported in literature: namely 3-methyl-1,2-BN-cyclopentane (4.7 wt%) and 1,2-BN-cyclohexane (4.7 wt%).[64,65] In the former case, $FeCl_2$ (5 mol%) catalysed dehydrogenation at 80 ºC yields the quantitative trimer, likely proceeding through a bimolecular mechanism. An analogous reaction is reported for 1,2-BN-cyclohexane using either $CoCl_2$ or $FeCl_2$ at 150 ºC. Luo also demonstrated that these systems are reversible and can be converted back to a charged state with MeOH and BH_3·THF in high yields (71%), which could be improved on scale up. Considering this, 3-methyl-1,2-BN-cyclopentane was considered in a scaled-up process, with a rate of production of 100 kg/h^{-1}. After initially being powered by facility H_2, Liu and co-workers tested the ability of 3-methyl-1,2-BN-cyclopentane to power a fuel stack (12 cell, 9.5 cm^2 active area PEM stack to provide 30 W of power at 0.3 sLpm H_2 consumption). They reported no noticeable difference in stack performance throughout material delivery. Despite this, these systems are only achievable through multistep synthesis and the ambition to couple C-H dehydrogenation remains impractical at moderate temperatures.

1.4.5 Dehydrogenation of Amine Borane Blends

Grant and co-workers reported that mixtures of AB and methyl amine-borane could achieve melting points lower than their corresponding constituents.[1] In this vein, blends of amine boranes could provide a practical route to liquid storages where the solvent also contributes to H_2 capacity. Groshens & Hollins reported remarkable improvement in the purity and suppression of NH_3 in guanidinium borohydride (GBH) when blended with EDAB.[66] Mixtures of 46:54 and 40:60 GBH-EDAB reported 9.6 and 10.1 wt% hydrogen emission with negligible ammonia generation (0.026 mol%). Liquid solutions were reported for *sec*-butylamineborane (SBAB) and ammonia borane blends.[67] Unfortunately, the reaction precipitated out linear poly(aminoborane), which could be inhibited with (EMIM)[$EtSO_4$] as an ionic liquid, but at the expense of capacity (3.6 wt%). With this in mind, it appears possible to re-utilise liquid amine boranes with insufficient amounts of H_2 independently as "solvents" for AB to generate single-phase fuels. To this extent, Carre-Burritt et al utilised blends of hexylamineborane (3.5 wt%) and 3-methoxypropylamine (3.9 wt%) with AB to formulise slurries.[68] They reported the formation of high molecular weight co-oligomerizaiton products (M_W: 400-700), which do not freeze down to –60 ºC. Whittemore et al utilised 3-methyl-1,2-dihydro-1,2-azaborolidine as a liquid blending agent with AB.[69] Blends of closely related azaborolidine species and EDAB with 3-methyl-1,2-dihydro-1,2-azaborolidine were trialled but ultimately dismissed through

lack of stability or poor solubility. Moreover, a 2:1 blend with AB showed remarkable improvement over AB alone. The absence of an induction period indicated that AB and 3-methyl-1,2-dihydro-1,2-azaborolidine were in fact reacting together, and forming mixed non-volatile trimeric products. These beliefs were confirmed by GC-MS, with additionally a 676-fold reduction in borazine evolution. Not only this, but the mixture could also be regenerated through a similar pathway developed for cyclic CBN compounds. Nakagawa et al also commented on the possibility to use slurries of AB.[70] They determined 30wt% AB threshold as the optimised concentration for liquid formation and desirable engineering properties, far below the requirement of 68.2 wt% AB for H_2 supply. These optimised mixtures show relatively low viscosities of 150 - 200 cP at RT, whereas mixtures exceeding 30wt% lose their fluidity becoming sticky and solid.[71] An interesting solid fuel blend was reported by Zhang et al utilising EDAB and ethylene diamine (ED) to generate 5-membered CBN rings at room temperature.[72] In general, one equivalent of ED reacts with EDAB in a Pt-assisted formation of two N=B-NH pentacyclic systems yielding 8.2 wt%. In reality, species where ED acts as both a co-ordinating solvent and reactant exist, and the resultant capacity is between 4.5 – 5.8wt%. Intriguingly, EDAB within this system could be regenerated at room temperature using $NaBH_4$ and H_2O allowing a possible cyclic system.

1.4.6 Computational Analysis of Amine Boranes as Storage Materials

Theoretical work performed by Staubitz and Manners in 2008 established guiding principles for reversible amine-borane storage materials.[73] Loss of H_2 from amine boranes is too exergonic for reversibility. For initial calculations addressed to $R_2^1NH\text{-}BHR_2^2$ based systems, substitution on nitrogen with more electron donating groups was suggested to lead to a generalised 4 kcal/mol increase in ΔH relative to AB. Similarly, halogen substituents on boron observed a trend in the series R^2=F, Cl, Br to give an increasingly positive dehydrogenation enthalpy. In a desire to elucidate the factors governing hydrogen storage, Staubitz et al conceived a thermodynamic cycle measuring the contributions of bond-types on the overall enthalpy of reaction. Interestingly combined contributions of H_A (bond dissociation) and H_D (newly formed π-bonds) which describe the change in bond after the elimination of hydrogen produce a strong correlation ($R^2 = 0.91$) with the overall dehydrogenation reaction. As such, the reaction enthalpy directly depends on the relative strengths of the dative bonds in the starting material and the product. Thus, in order to obtain more-positive overall reaction enthalpies, a strong dative σ bond in the starting material should be combined with a weaker π bond in the product. In general, combinations of electron donating groups on nitrogen (resulting

in a more lewis-basic amine) and electron withdrawing groups on boron (resulting in a more lewis-acid borane) can lead to favourable systems. Evaluation of a series of cyclic amines indicated that six-membered rings are more endothermic than four- and five-membered.

1.5 Potential Ligand Cooperation in the Catalysed Dehydrogenation of Amine Boranes

The employment of transition metal catalysts for the activation of H_2 from amine boranes is commonplace in literature.[33,35,74] Typically, homogeneous catalysts contain ligands able to stabilise the metal centre throughout the fundamental steps of a catalytic cycle. Within the last two decades or so, a new strategy where the ligand is directly involved in the transformation of substrates within the catalysis cycle has been developed. In these scenarios, the ligand assists the metal centre by interacting with the substrate and facilitating bond activation, promoting bond breakage or formation, as well as other transformations (Figure 8). In this way, the ligand participates in the transformation of substrates into products or intermediate species and this strategy has been named ligand cooperativity or cooperation. The use of metal-ligand cooperation by transition metal bifunctional catalyst has emerged at the forefront for activation of small molecules.[75] The incorporation of "actor ligands" in opposition to "spectator ligands" that can directly participate in the crucial bond breaking/forming of amine borane dehydrogenation has provided a powerful tool to optimise electronic properties of metal complexes. Transition-metal complexes containing ligands based on Bronsted basic sites have been shown to promote H_2 release from amine boranes through the transfer of the hydridic hydrogen in the BH moiety to the acidic metal center and the transfer of proton from the NH moiety to the basic ligand functionality.

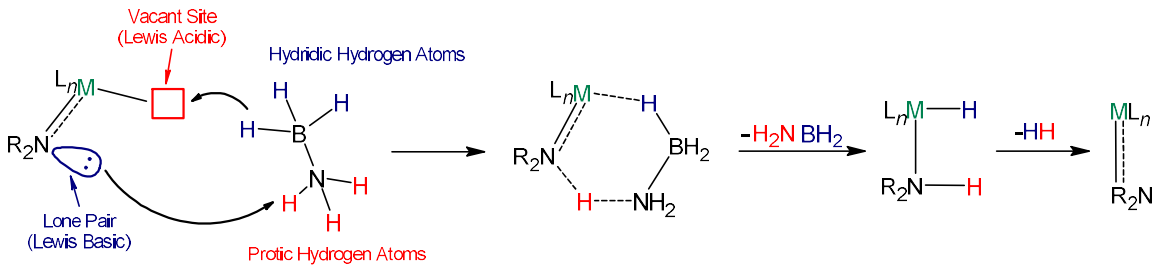

Figure 8: Generalised mechanism for the activation of AB via ligand co-operative catalysts based on Bronsted basic sites

The iridium pincer catalyst IrH_2POCOP (POCOP= [η^3-1,3-$(OP^tBu_2)_2C_6H_3$]) reported by Denney & Goldberg is regarded as a benchmark for the dehydrocoupling of amine boranes.[76] At room temperature, NH_3BH_3 can be dehydrogenated towards $[H_2NBH_2]_5$ in 14 minutes using

the iridium catalyst (0.5 mol%). The catalyst is also highly active in the dehydrocoupling of substituted amine boranes, and is highly cited in the literature.

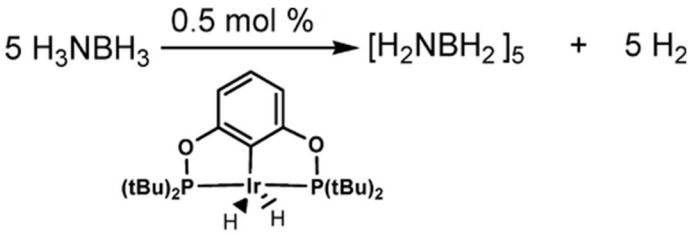

Figure 9: The dehydrogenation of ammonia borane by Golderg's IrH_2POCOP catalyst

Recently, the development of ligand cooperative catalysts has established catalysts capable of matching or surpassing the activity demonstrated by Goldberg. Catalysts **1-6** in Figure 10 are primary examples of ligand cooperative catalysts reported for the dehydrocoupling of amine-boranes. In catalysts **1-4**, the active species' for these catalysts contain amine boranes interacting with both the metal centre and the basic centre leading to a reversible metal-amine/metal-amido interconversion.[77-83]

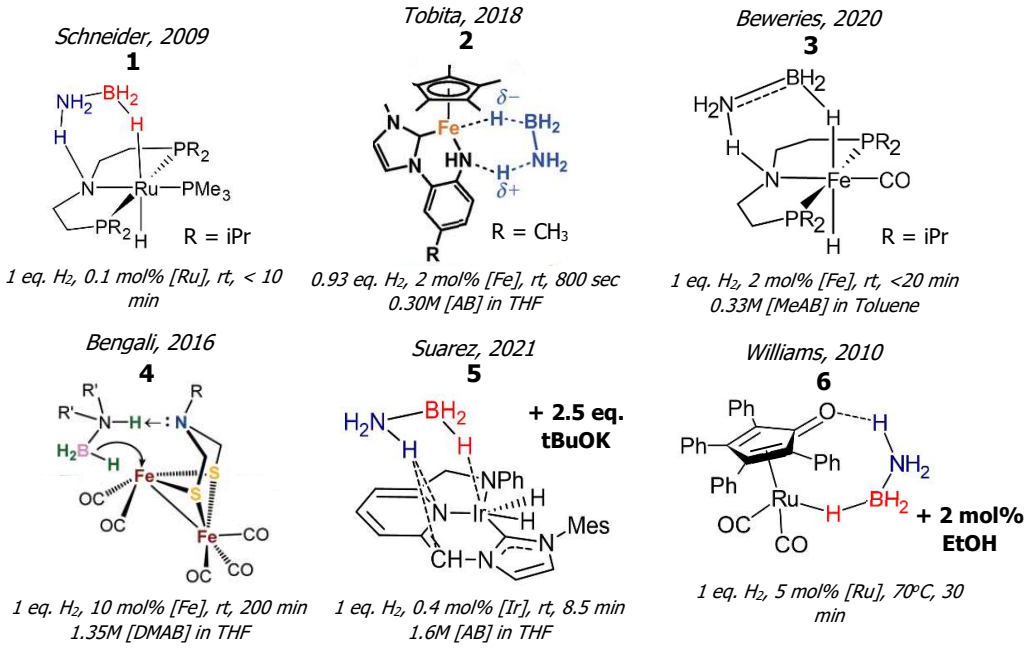

Figure 10: Literature examples of ligand co-operative catalysts for amine-borane dehydrogenation

Anke and co-workers provided further mechanistic details from DFT calculations for **3** [FeH(CO)(PNP)] (PNP = N $(CH_2CH_2P^iPr_2)_2$). The lowest energy pathways starts with proton transfer of NH_3 to the metal hydride to form Ru-H_2. The resulting aminoborate anion is stabilized by hydrogen bonding of the pincer ligand, such that the N-H of the ligand interacts with NH_2 through N-H···NH_2-BH_3. Subsequent H_2 loss is irreversible (ΔG^0= –20.6 kcal/mol)

and is followed by an interaction of the unsaturated Ru centre with the hydride of the BH_3 moiety to form a bridging dihydride. Final loss of the aminoborane from the bridging hydride is thermoneutral and readily feasible ($\Delta^{\ddagger}G$ = 5.4 kcal/mol).

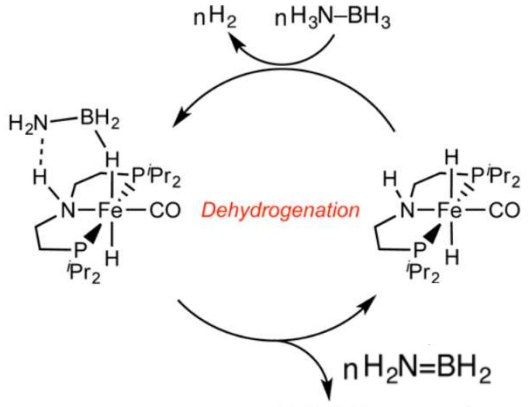

Figure 11: The dehydrogenation of ammonia borane by [FeH(CO)(PNP)] through a bridging hydride

There is comparatively less literature dedicated for synergistic metal-ligand cooperation using oxygen/OH as a Bronsted basic site. The Wang group recently utilized a cooperative phosphinopyridonate ligand for Co-catalyzed sequential transformation of terminal arylalkynes to (E,Z)-1,3-dienes using ammonia-borane.[84] Prior to this work, Liu applied a half-sandwich Ni(II) complex bearing a phosphinophenolato ligand for the activation of pyridines with HBpin.[85] The involvement of the phosphinophenolato ligand was highlighted by Ni-alkoxide assisted cleavage of the B-H bond to afford a Ni-H hydride and oxygen-stabilized boron moiety (Scheme 1).

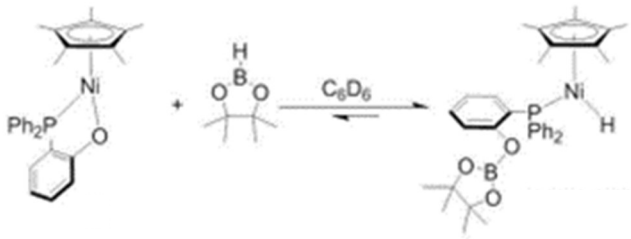

Scheme 1: The activation of HBpin with a Ni(II) complex bearing a phosphinophenolato ligand

Wang developed another similar system where an additional methylene was incorporated between the phosphine group and the pyridine unit (which has replaced the phenyl unit). In this Co-based system, the active catalyst **7** reacts with amine borane in a similar way, *i.e.* via cobalt-pyridonate cooperation to yield a cobalt-hydride intermediate (Figure 12; Left). Coordination and insertion of the alkyne in the (E)-1,3-enyne into Co–H allows a final exergonic deprotonation of the amine group and eliminates the aminoborane along with the reduced

product and regenerated catalyst. DFT studies suggested that the uncoordinated oxygen plays both a deprotonation (of the alkyne) and H-bonding role.

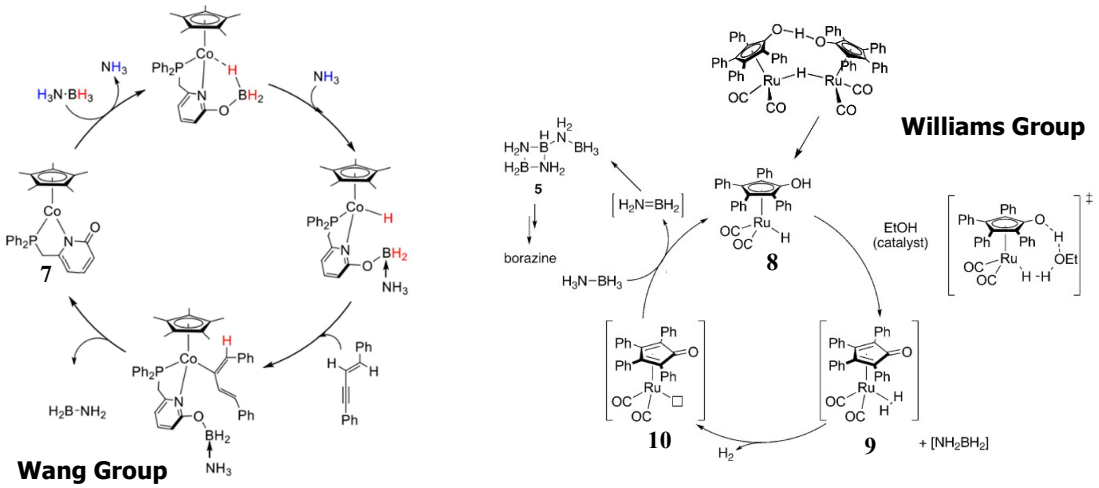

Figure 12: Mechanistic cycles for AB dehydrogenation using ligand assisted oxygen motifs

Alternately, the Williams group reported the dehydrogenation of amine boranes by Shvo's catalyst (Figure 12; Right).[83] The Shvo dimer reacts by splitting heterolytically into an oxidizing fragment and a reducing fragment. The reducing fragment (**8**) consists of a metal hydride and acidic proton which contributes to its metal−ligand cooperative reactivity. From here, a concerted, bifunctional transition state for B–H and N–H transfer to the metal centre and oxygen is predicted. However, unlike Wang, deactivation of the mechanistic regime was identified as the reaction between borazine to hydroborate intermediate **10**. To this extent, reactions of amine boranes with protic dopants [86-88] or capped nano-material supports[89,90] in the absence of a metal centre have been shown to result in O-B-O that are irreversible without chemical regeneration. In subsequent papers, the group successfully developed a "semi-site protection" strategy to inhibit hydroboration and NH_3 ligation as competing deactivation pathways and maintain catalytic performance.[91]

Taking into account these previous studies with catalysts based on oxygen co-operative ligands, we prepared complexes based on ruthenium-cymene complexes which contain phosphinous acid, methylene phosphinous acid or amide-phosphinous acid as co-ligands (Figure 13). Our aim was to explore the potential involvement of these co-ligands via cooperativity in the dehydrogenation of amine boranes. The complexes utilised have the general formulae $RuCl_2$(*p*-cymene)PR_2R'. We also anticipated a similar mechanism of action as those proposed above.

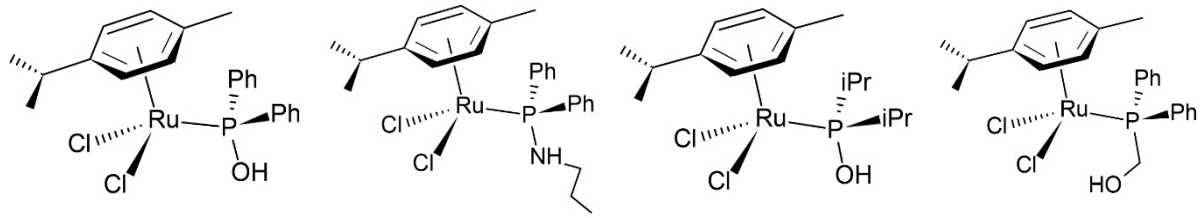

Figure 13: $RuCl_2$(*p*-cymene)PR_2R' complexes to be assessed for AB dehydrogenation

These complexes have been previously explored as catalysts in nitrile reduction reactions with high success.[92,93] They are air stable, and can be prepared by introduction of a phosphine oxide/amide to the $[RuCl_2(p\text{-cymene})]_2$ dimer. Additionally, examples of application of catalysts containing these ligands in the dehydrogenation of amine boranes are very limited; these have been mainly applied in amine borane hydrolysis studies with the mechanisms of action being largely unexplored.[94-96] Generally, the presence of auxiliary ligands in the co-ordination sphere of the metal that are able to activate water by hydrogen bonding has been recognised as a key factor to reduce the activation barrier of the hydration process towards amine boranes. Ciganda and co-workers reported $[IrHCl\{PPh_2(o\text{-}C_6H_4CO))_2H\}]$ as a homogenous catalyst with a hydridoirida-β-diketone motif featuring intramolecular hydrogen bonds from component acyl and hydroxycarbene moieties.[97] Hydrolysis of solutions of amine boranes (0.46M) in THF-H_2O (1:1) mixtures was accomplished in as little as 19 minutes (2.73 equiv. H_2, 0.5 mol% [Ir]). Likewise, Azpeitia developed Rh-complexes containing strong PPh_2OH hydrogen bonds which were highly active at 30 °C, in air and 0.2 mol% Rh loading.[94] The best complex featuring N-H hydrogen bonds was capable of 97% hydrogen content release within 9 minutes. A relevant mechanism for $[Cp^*Ir(6,6'\text{-}(OH)_2\text{-bpy})(OH_2)]SO_4$ was highlighted by Wang *et al,* constructed of synergistic effects between pendent hydroxyl group and metal center.[98] Early mechanistic steps revealed the activation of $B\text{-}H^{\delta-}$ and $N\text{-}H^{\delta+}$ by Ir and O^- respectively, with successive co-ordinations installing an additional OH on $BH(OH)_R\text{-}NH_3$ via hydrolysis with H_2O (Figure 14; Left).

It is interesting to consider the latter mechanism alongside the hydrolysis of amine borane by a metal-free chiral phosphonic acid (CPA) catalyst described by Zhou *et al*.[99] Here, reaction of CPA and amine borane quickly results in H_2 release and formation of OBH_2NH_3 as a notable intermediate. After hydrogen transfer reactions via a concerted 6-membered ring transition state, the catalyst is recovered from hydrolysis of boron-nitride [B-N] products (Figure 14; Right). This is similar to the mechanism described by Wang, while the prior relates to the regime proposed by the Williams group. It suggests that the metal is a key prerequisite for ligand cooperation, as Ir and Ru examples favour [M]···H-B pathways whilst Co prefers to

form OBH_2 intermediate species. In either case, catalysts bearing these motifs are generally active in air and are highly reusable making them attractive for an industrial process.

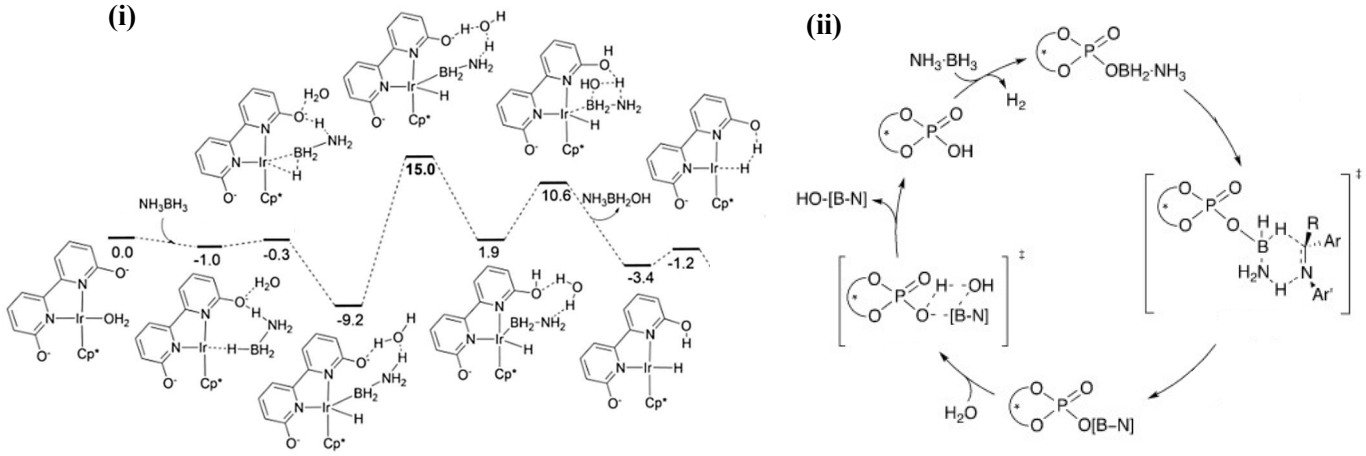

Figure 14: Examples of AB dehydrogenation with catalytic OH functionality
(i): Wang ligand co-operative regime. Relative energies are given in kcal/mol
(ii) Zhou regime based on metal free catalysis

2 Results & Discussion

2.1 Preparation of Amine Boranes and Their Reactivity upon Heating in Solution

The synthesis of mono-organyl borohydrides was carried out via the reduction of commercially available $RB(OH)_2$ with 1.5 equivalents of $LiAlH_4$ (Scheme 2) in THF.[100,101]

$$LiAlH_4 + B(OH)_2R \xrightarrow{THF,\ RT,\ 2h} LiBH_3R + AlH(OH)_2$$
$$LiAlH_4 + BR_2(OMe) \xrightarrow{THF,\ RT,\ 2h} LiBH_2R_2 + AlH(OMe)_2$$

Scheme 2 : Synthetic route to B-substituted borohydrides

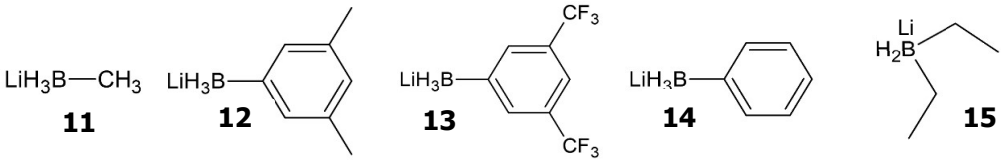

Figure 15: Series of B-substituted borohydrides covered in this study

As expected, $LiBH_3Me$ and $LiBH_3Ph$ were isolated as colourless solids. The ^{11}B NMR spectra for $LiBH_3Me$ and $LiBH_3Ph$ exhibited quartet resonances at $\delta = -31.00$ (q, $^1J_{BH} = 76$ Hz) and -25.85 (q, $^1J_{BH} = 80$ Hz), respectively.[102] The ^1H NMR spectra although unremarkable, did serve to quantify the residual THF content present in both structures. The synthesis of boron-substituted amine boranes was carried out via metathesis between $LiBH_3Me$ or $LiBH_3Ph$ and NH_4Cl in THF as solvent. Furthermore, ^{11}B NMR spectra acquired for amine borane products; B(Me)-amine borane and B(Ph)-amine borane exhibited a triplet resonance with coupling constant value of 95 Hz at –13 ppm and –16 ppm, respectively. The appearance of a broad

triplet signal for the N-H group in the ^{1}H NMR spectrum also served to confirm the formation of the Lewis adducts. In trial preparations of B-PhAB, the growth of adjacent resonances at –10.80 (t, $^{1}J_{BH}$ = 95 Hz) and –13.85 (t, $^{1}J_{BH}$ = 95 Hz) were observed in cases where acetonitrile was used as the solvent instead of THF (Figure 16). The $^{1}H\{^{11}B\}$ confirmed the presence of inequivalent B-H environments, suggesting adduct formation between CN and BH_3Ph units via a possible CN:→BH_2Ph interaction. Lewis adducts of acetonitrile and boranes have been previously reported. [103]

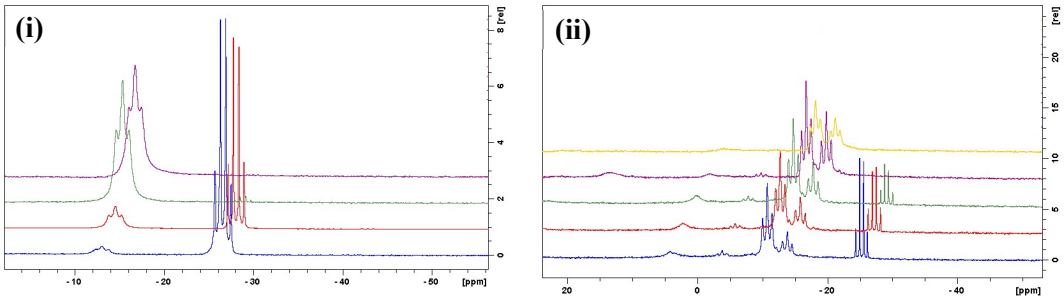

Figure 16: Trial preparation of (Phenyl)B-amine borane via ^{11}B NMR spectroscopy
(i) THF solvent **(ii)** CD_3CN solvent

Switching the reaction solvent to THF produced the desired compound exclusively. In practical terms, however, the use of THF as a solvent introduced challenges for the isolation of the (Ph)B-amine borane. A very fine powder was obtained which led to prolonged filtration time of the reaction mixture. As a consequence, a minor co-product formed (<5%) during the filtration of the reaction mixture. This appeared in the ^{11}B NMR spectrum at 29.09 ppm concurrent with the presence of aromatic protons in the ^{1}H NMR spectrum. The final product was isolated as a sticky material, and was presumably contaminated with $B(OH)_2Ph$. Still, the removal of solvent under vacuum from the reaction flask resulted in a free-flowing powder with clean ^{11}B NMR spectrum and only solvent contamination. Attempts to use diethyl ether as the solvent, led to the formation of the dehydrogenated amine borane (*i.e.* amino borane) as evidenced by the broad signal observed at $\delta_{B,lit}$ –6.2 (br) in the ^{11}B NMR spectrum of the isolated product. This is consistent with previous reports by Manners et al.[104] which showed the spontaneous dehydrocoupling formation of aromatic amino boranes at ambient temperature. The authors assigned the broad signal to the formation of oligomeric amino borane $[NH_2\text{-}BHPh]_n$. Additionally, hydrogen was observed as a singlet at 4.55 ppm in the ^{1}H NMR spectrum.

On the other hand, (Me)B-amine borane was synthesised in reasonable purity via NH_4Cl in THF with no detectable hydrogen loss. Thus, the thermolysis of (Me)B-amine borane was

investigated in both acetonitrile (CD_3CN) and benzene (C_6D_6) as solvents. It is important to highlight that redistributions reactions towards NH_3BH_3 and NH_3BHMe_2 can occur at elevated temperatures.[105] The partial ^{11}B NMR spectra for the thermolysis of (Me)B-amine borane in CD_3CN is shown in Figure 17. Relative integration of the signal for the starting material and the products showed that a 28% conversion was observed after 20h at 40 °C. As observed during the synthesis of NH_3BH_2Ph, the formation of an adjacent triplet at –13.38 ppm alongside (Me)B-amine borane (–15.94 ppm, $^1J_{BH}$ = 93 Hz) was also observed upon heating a solution of the starting amine borane at 40 °C in acetonitrile as a solvent.

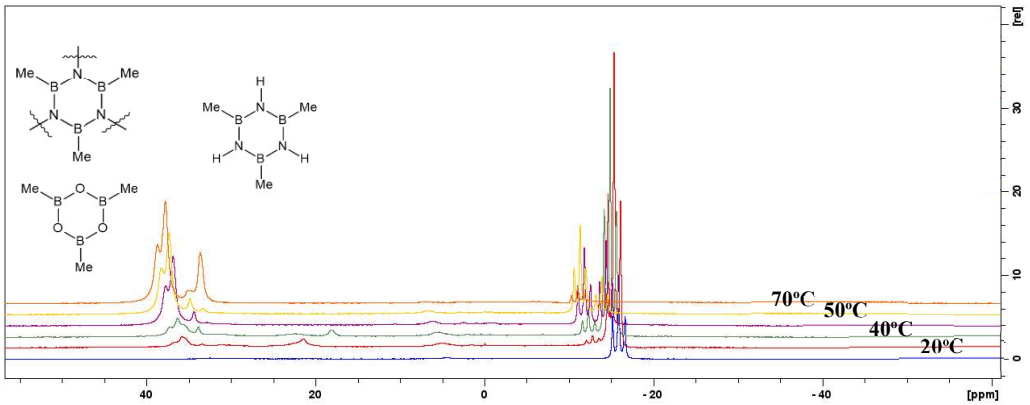

Figure 17: Reaction course for the thermolysis of (Me)B-AB in CD_3CN (20 °C - 70 °C; <70 h) monitored by ^{11}B NMR spectroscopy

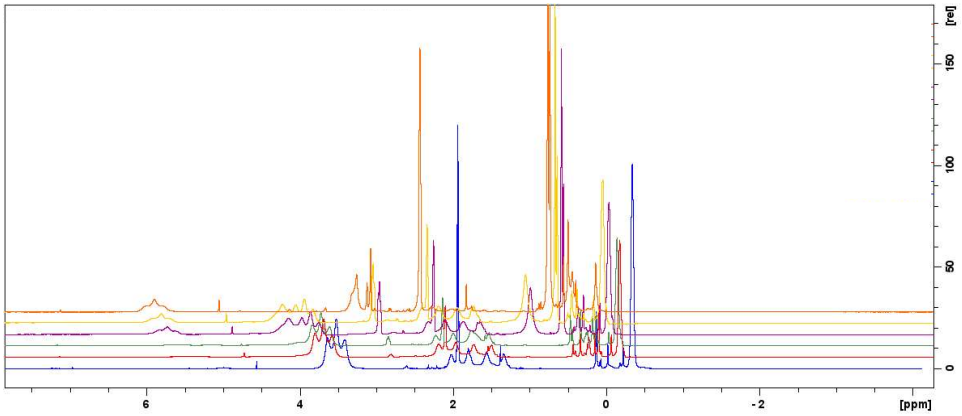

Figure 18: ^1H NMR spectrum comparison of (Me)B-AB through the thermolysis reaction in CD_3CN

This provides direct evidence for B-N bond cleavage and that BH_2Me fragments are stabilised by CD_3CN. Two minor signals were detected at δ = –23.16 ppm and 32.82 ppm which may correspond to μ-(amino)diborane and diaminoborane, respectively. These can be formed by reaction of $MeBH_2$-NH_3 with B-N bond cleavage products NH_3 and BH_2Me. Such reactions were originally identified by Helten *et al.* who postulated that such intermediates are responsible for the formation of cyclotriborazanes from amine-boranes.[104] The full ^{11}B NMR spectrum showed further broad resonances at δ = 4.46 ppm, 20.98 ppm, 30.59 ppm and 35.26

ppm. The latter of which was tentatively assigned as [NH-BMe]$_3$ based on a similar shift to literature on the dehydrogenation of (Me)B-amine borane.[106] Extended heating of the mixture causes MeBH$_2$-NH$_3$ to converge towards [NH-BMe]$_3$ through a CD$_3$CN assisted pathway. After 80 h, the ^{11}B NMR spectrum shows two overlapping singlets as the main signals at δ = 36.26 and 35.37 ppm. A 66% conversion of the starting material into these two new main products could be calculated by relative integration. Two unassigned additional signals at 32.67 ppm and 31.20 ppm were also observed corresponding to two minor co-products in a 34% concentration. The decoupled experiment (^{11}B{^{1}H}) confirmed the absence of remaining B-H species since no change in the spectrum was observed within this experiment. The presence of trimeric cyclised species [NH-BMe]$_3$ could also be observed in the ^{1}H NMR spectrum which showed that the N-H bond is shifted to a higher chemical shift (δ = 5.40 ppm) over the reaction course (Figure 18), consistent with the previous literature report.[105] Additionally, B(Me) signals can be viewed as sharp singlets in the ^{1}H{^{11}B} at 0.23 ppm and 0.26 ppm. The growth of the ^{11}B NMR signal at δ = 36.26 ppm suggests the presence of either cross linked borazine units generated through the further loss of H$_2$ from equivalent N-H bonds or a potential contamination of methylated boroxine as a result of unintentional exposure to air. The thermolysis of the B(Me)-amine borane was also carried out in benzene as solvent. In this case, dehydrogenation also led to the formation of several compounds as judged by the development of multiple signals in the ^{11}B NMR spectrum (Figure 19).

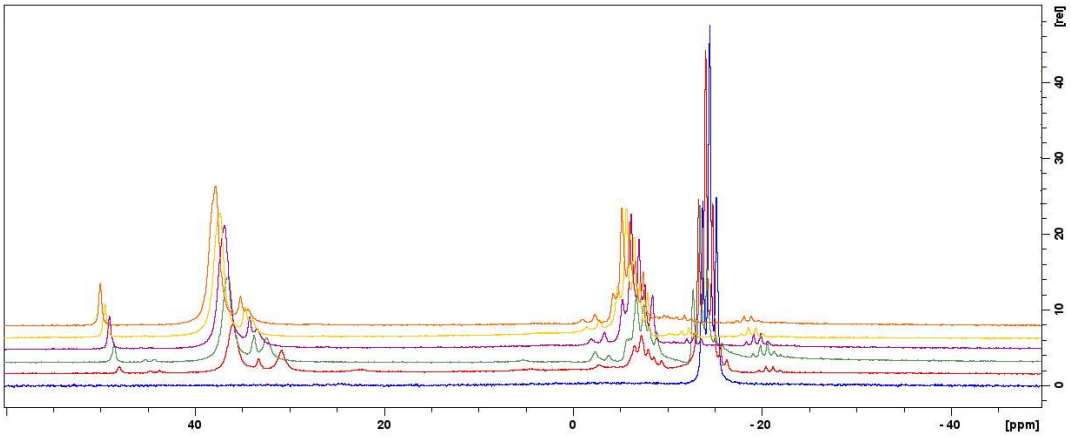

Figure 19: Reaction course for the thermolysis of B-MeAB in C$_6$D$_6$ by ^{11}B NMR spectroscopy

As early as 1h, heating at 35 °C, the ^{11}B NMR spectrum reveals a doublet at δ = –7.42 ppm, with a coupling constant value of 106 Hz. This is likely to be oligomeric species of the type [NH$_2$-BHMe]$_X$. After 20 h, the region between δ = –7.00 ppm and –9.94 ppm becomes increasingly complex due to the formation of several products involving exchange/redistribution of the substituents. Resonances assignable to NH$_3$BH$_3$ at –21.30 ppm as a doublet with a coupling constant of 94 Hz, to (NH)$_2$BMe at 32.68 ppm as a singlet, to [NH-

BMe]$_3$ at 35.43 ppm as a singlet, to NH_2=BHMe at 43.70 ppm as a doublet with coupling constant of 125 Hz and to NH_2=BMe_2 at 47.43 ppm as a singlet are all observed. The mechanism by which methyl and hydrogen substituents are exchanged between B-methylated amine-boranes has been previously postulated.[105] Dimerization of deficient borane molecules is theorised to arise from the initial dissociation of the B-N bond (Scheme 3).

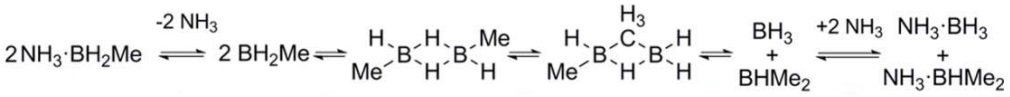

Scheme 3: Mechanism Proposed by Manners for Redistribution Reactions of NH_3BH_2Me

This is followed by the subsequent cleavage and bonding steps of the bridging moiety to establish mixed boranes that reassociate to free amine. In relation to redistribution reactions, DFT calculations show that the installation of a CH_3 bridging bond is found to endergonic by +112.9 kJ mol^{-1}, whilst initial B-N bond dissociation is only +70.7 kJ mol^{-1}. After re-dimerization (+66.9 kJ mol^{-1}), reassociation of ammonia is found to be favourable towards NH_3BH_3 (–85.9 kJ mol^{-1}) and NH_3BHMe_2 (–74.4 kJ mol^{-1}) with a free energy (ΔG^{298}) values of +22.9 and +34.4 kJ mol^{-1}, respectively. Interestingly, the effect of the solvent was found to be largely invariant for this process. Instead, the polarity of THF alone is in theory responsible for the lack of redistribution products as it provides stability to N-H and B-H bonds at 20 ºC. Nonetheless, both $MeBH_2$-NH_3 and $PhBH_2NH_3$ are known to redistribute at 70 ºC in THF, although the process is minimized for $PhBH_2NH_3$ as bridged phenyl motifs are expected to be highly endergonic. In our case, over a longer reaction period (80 h) at 70 ºC, the quantitative consumption of NH_3-BH_2Me yields [NH-BMe]$_3$ (47%), NH_2=BMe_2 (5%), NH_3BH_3 (3%), [NH_2-BHMe]$_X$ (40%) and [NH_2-BH_2]$_X$ (5%) based on relative integrations of the ^{11}B NMR spectrum. Boron decoupled experiments, ^{1}H{^{11}B} NMR spectroscopy, show the formation of oligomeric products as B-H bonds are detected after B(Me)-amine borane consumption.

In order to investigate the effect of different substituents on the boron atom on the distribution of products of dehydrogenation under catalytic conditions, we pursued the preparation of an amine borane containing fluorinated phenyl substituents as electron-withdrawing groups. The amine borane NH_3-BH_2(*m*-$(CF_3)_2C_6H_3$) was targeted based on computational suggestions of introducing electron-withdrawing groups on boron motifs.[73] Additionally, the Manners group investigation on NH_3-BH_2(*p*-$CF_3C_6H_4$) showed promising results for selective, non-redistributive thermolysis of the substrate towards poly(B(aryl) aminoboranes as inorganic analogues of polystyrene.[62] Instead, the polymeric [NH_2-BHR]$_n$ and trimeric [NH-BR]$_3$ amino-boranes are observed as products when NH_3-BH_2(*p*-$CF_3C_6H_4$) was heated to 70 ºC in THF.

Further, the catalysis of NH_3-BH_2(*p*-$CF_3C_6H_4$) with IrH_2(POCOP) produced the polymeric product in 40% yield. The substrate, $^{i}Pr_2NH$-$BH(C_6F_5)_2$ is another example where perfluorinated boron substituents were trailed under thermolysis and catalysis. In this case, no dehydrogenation of the substrate was observed.

In our initial investigations, the preparation of $LiBH_3$(*m*-$(CF_3)_2C_6H_3$) was achieved by analogous reduction of $B(OH)_2$($(CF_3)_2C_6H_3$) with $LiAlH_4$. The ^{11}B NMR spectrum exhibited a quartet signal at –27.80 ppm with a coupling constant of 80 Hz in consistency with four-coordinate boron species. An unknown species present in 30% relative to the product exhibited a broad resonance at δ_B = –5.89 ppm. This was believed to be the partially reduced product ($BH_2(OH)$($(CF_3)_2C_6H_3$)) which remained unchanged after the addition of a further 0.5 equiv. of $LiAlH_4$. After extraction with toluene (2 x 50 mL) and isolation, this product proved to be shock sensitive. The attempt to scrape the product off the sides of the reaction flask with a spatula led to rapid decomposition and evolution of a brown gas. Therefore, for safety reasons, the synthesis of NH_3-BH_2(m-$(CF_3)_2C_6H_3$) was discontinued for this project. Nonetheless, it is anticipated that the direct conversion of this borohydride into the corresponding amine borane without its isolation as a solid may lead to a synthetic method.

An amine borane containing electron-donating groups such as $LiBH_2(C_2H_5)_2$ was also synthesised. This would have allowed reactivity and selectivity comparisons with the amine borane containing electro-withdrawing groups above. In this case, the borinic acid $B(OH)(C_2H_5)_2$ was reduced with 1.5 equiv. of $LiAlH_4$ in THF at room temperature. The reaction was monitored by ^{11}B and ^{1}H NMR spectroscopy. After 1h, ^{11}B NMR spectrum showed a triplet at δ = –16.82 ppm with a coupling constant of 69.4 Hz. The triplet multiplicity confirms the presence of two hydrides on the boron. The product formed almost exclusively in 91% conversion together with two minor contaminants. One of the contaminants was the monoalkylated borohydride (BH_3Et), based on the quartet multiplicity ($^{1}J_{BH}$ = 75 Hz) and its chemical shift δ = –27.15 ppm. This was present in 7% based on relative integrations. The other contaminant corresponded to $LiBH_4$ as a multiplet in the ^{11}B NMR spectrum and chemical shift δ = –41.39 ppm. In this case, no further purification was attempted and the product was subsequently reacted with NH_4Cl in THF overnight at room temperature. Contrary to the methyl and phenyl substituted amine borane preparations, this gave a white precipitate. ^{11}B NMR spectroscopy revealed the presence of a weak doublet (–6.45 ppm, $^{1}J_{BH}$ = 89.7 Hz) consistent with the expected product NH_3-$BH(Et)_2$ and a large singlet (48.35 ppm) (Figure 20) corresponding to a side-product.

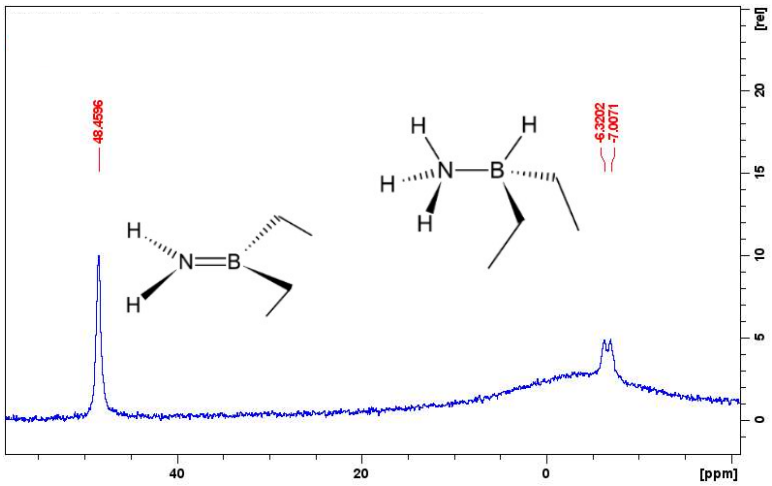

Figure 20: ^{11}B NMR spectrum of (Diethyl)B-amine borane

Isolation of the white precipitate produced a solid that was largely insoluble in a range of solvents; THF, $CDCl_3$, CD_3CN, DMSO, C_6D_6. To this extent, it is plausible that the singlet at 48.35 ppm represents the aminoborane NH_2=B(Et)$_2$ (cf. e.g NH_2=BMe_2; δ = 46.3 (s), NH_2=BPh_2; δ = 41.0) and dehydrogenation has occurred during this preparation of amine borane at room temperature. In relation to this, Grant and co-workers predicted the amine borane NH_3-BHMe_2 as an unstable compound. Their calculation indicates H_2 loss and formation of the aminoborane $(CH_3)_2$B=NH_2 as a highly exothermic process with free energy values of –11.7 and –13.3 kcal/mol at 298K at CCSD(T) and G3(MP2) theory levels, respectively.[1] The inclusion of electron-donating ethyl groups may have led to a significantly favored B=N bond formation which prevents the isolation of the amine borane NH_3-BH(Et)$_2$ at RT. Since the isolation of the NH_3-BH_2(*m*-$(CF_3)_2C_6H_3$) and Et_2BHNH_3 proved challenging, the dehydrogenation studies within this thesis focused on the use of $MeBH_2NH_3$ and BH_3NHMe_2 (DMAB) as starting materials. Two main approaches were utilised, namely, the dehydrogenation of the starting materials by heating their solutions (thermolysis) as described above and the dehydrogenation of the starting materials catalysed by ruthenium chloride cymene complexes containing phosphine as co-ligands. The nature of the phosphine co-ligands was vitally important to understand the potential mechanisms where these co-ligands are directly involved in the dehydrogenation catalysis by cooperating with the transition metal centre. The sections below describe the results for the catalysed dehydrogenation of the amine boranes starting materials.

2.2 Catalytic Dehydrogenation of Me(B) Amine Borane

2.2.1 Catalytic Dehydrogenation of (Me)B-Amine Borane with $RuCl_2$(*p*-cymene)PPh_2OH

In an attempt to favour dehydrocoupling over redistributions reaction of the (Me)B-amine borane substrate, the catalytic ability of $RuCl_2$(p-cymene)PPh_2(OH), $RuCl_2$(p-cymene) $PPh_2(CH_2OH)$ and $RuCl_2$(p-cymene)PPh_3 was investigated. The catalysts were assessed by their ability to consume (Me)B-amine borane, which was measured by the ^{11}B NMR spectroscopy. The reactions were also measured by ^{31}P and ^{1}H NMR spectroscopy.

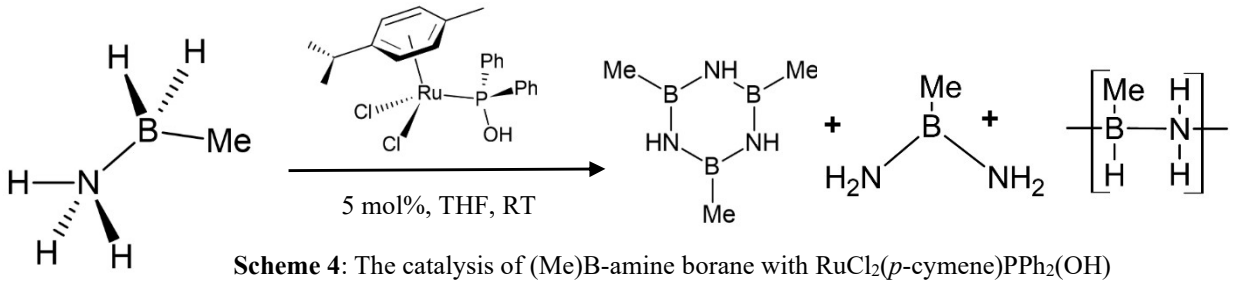

Scheme 4: The catalysis of (Me)B-amine borane with $RuCl_2$(*p*-cymene)PPh_2(OH)

The Young's tubes were charged with the solid starting materials and complexes and the appropriate amount of solvent were added under inert atmosphere. The reaction course was monitored by ^{11}B, ^{1}H, $^{31}P\{^{1}H\}$ NMR spectroscopy. A control experiment where no catalyst was used, was also carried out and monitored under similar conditions. Immediately after addition of the solvent, gas evolution was observed. The triplet signal for the (Me)B-amine borane at δ_B –14.31 ppm, ($^{1}J_{BH}$ = 96 Hz) in the ^{11}B NMR spectrum had mostly disappeared (6% relative to all the other signals present). A new broad doublet at δ_B –16.62 ppm, ($^{1}J_{BH}$ = 147 Hz) was observed. This became a singlet signal by removing the proton-boron coupling in a $^{11}B\{^{1}H\}$ experiment, which confirms the presence of B-H bond in this new compound. The formation of several other species can be deduced by the presence of several signals in the ^{11}B NMR spectrum. This shows a similar behaviour to previous dehydrogenation experiments, where the main signals observed had the following chemicals shifts: a multiplet at δ = –7.17 ppm , a singlet at 33.18 ppm, a doublet at 43.96 ppm ($^{1}J_{BH}$ = 120 Hz) and another singlet at 47.95 ppm. The corresponding ^{1}H NMR spectra showed the presence of *mono*-hydride and *bis*-hydride ruthenium complexes. These separate species appeared as doublets at –8.49 ppm (J_{HP} = 56 Hz) and at –10.98 ppm (J_{HP} = 45 Hz) due to the coupling to the phosphorus of the co-ligand. Additionally, a minor alternate set of *mono*-hydride and *bis*-hydride could be observed as underlying –8.04 ppm (d, J_{HP} = 52 Hz) and –10.92 ppm (d, J_{HP} = 45 Hz) resonances. Two unresolved broad signals were also observed at δ = –4.80 ppm and –14.07 ppm in the ^{1}H NMR spectrum. These latter signals resolved into a singlet and doublet (J_{BH} = 19.67 Hz) in the $^{1}H\{^{11}B\}$ suggesting a potential connectivity of the borane to the Ru-centre and the presence of a BH bond, respectively. On this point, the coordination of a borane unit as part of a

metallacycle architecture has been previously demonstrated within ligand cooperativity catalysis.[77,79] Both, Anke and Gluer demonstrated the formation of a BH_2NMe_2 amide adduct during the dehydrogenation of amine boranes catalysed by iron and ruthenium pincer complexes (M-PNP). The authors highlight that such adducts can form via an independent pathway (Figure 21). In the latter case, [Ru(H)(PMe_3)(PNP^{BH_2,NMe_2})] showed a broad hydride signal at –8.02 ppm for the bridging hydride attached to the boron [Ru(μ-H)B)], and a quartet signal at –13.55 ppm (J = 24.8 Hz) for a Ru-H. Given these observations, it is possible a similar reactivity is occurring in our catalytic system involving $RuCl_2$(cymene)PPh_2(OH). The relative integration of the singlet signal at –4.80 ppm and the doublet at –14.07 ppm in the $^1H\{^{11}B\}$ NMR spectrum appear to show a 1:0.65 ratio.

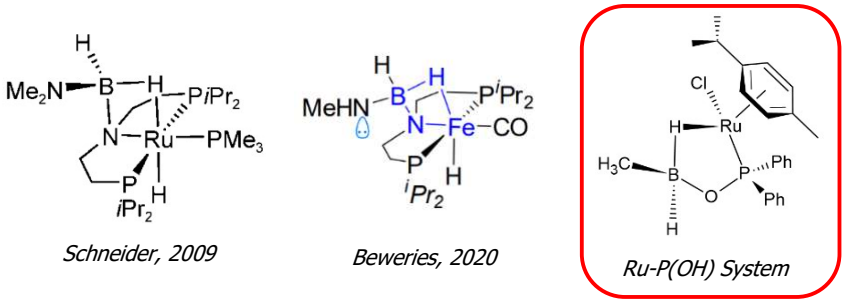

Figure 21 : Examples of borane metallacycles in ligand co-operative catalysis

As these signals appear secondary to the growth of apparent *mono* and *bis*-hydride species, a separate mechanistic regime might be occurring. The proposed mechanism by Titova *et al.* for an iridium-based system [(^{tBu}POCOP)IrHCl] can provide potential insight.[107] In this particular case, DFT calculations supported the interaction between the catalyst and Me_2NH-BH_3 to precede via N-H---Cl hydrogen bonding. This interaction could be observed by ^1H NMR spectroscopy at 200 K. Consequently, the N-H---Cl interaction results in strong activation of the Ir-Cl bond and is relieved by simultaneous N-H and B-H cleavage to generate catalytically active (^{tBu}POCOP)IrH_4 and $[Me_2N\text{-}BHCl]_2$. In this case, the borane unit functions as a halide abstractor. It is anticipated that a similar pre-activation is occurring in our system involving the $RuCl_2$(p-cymene)PPh_2(OH) whereby the active *mono*-hydride results from B-H activation to the metal centre and addition of Cl^- to the borane (Figure 22). However, in our own case the doublet signal observed at δ_B = –16.62 ppm in the ^{11}B NMR spectrum, (with a coupling constant of $^1J_{BH}$ = 147 Hz) likely indicates the formation of $BClHMe\text{-}NH_3$ as a new amine-borane adduct, in contrast to the anticipated hydrogen activation across the amine-borane as in the literature report described above. Indeed, Lu reported an identical procedure for the activation of a *bis*(borane) Lewis acid catalyst with an amine borane substrate.[108] Admittedly, the relative formation of this species ($BClHMe\text{-}NH_3$) is significantly higher (20% by ^{11}B

integration) than could be expected from a 5 mol% catalyst loading (10 mol% Cl), indicating a potential involvement of the chlorinated solvent ($CDCl_3$) as a halide source.

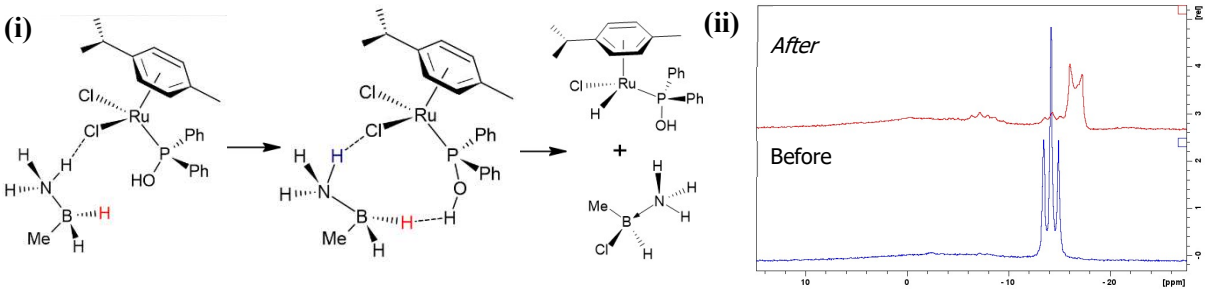

Figure 22: **(i)** Activation of $RuCl_2$(*p*-cymene)$PPh_2(OH)$ via Me(B)-AB **(ii)** ^{11}B NMR spectrum for Me(B)-AB before & after addition of $RuCl_2$(*p*-cymene)$PPh_2(OH)$

This may be supported by change within the ^{11}B NMR spectrum in the control experiment, where additional resonances at δ_B –6.23 ppm and δ_B –7.11 ppm accompany the starting material. Continuing the analogy, (^{tBu}POCOP)IrH_2 was shown to generate a complex containing a BH_4 ligand [(^{tBu}PCP)$IrH(\mu^2\text{-}H_2BH_2)$] through σ-borane interaction and dissociation of the B-N bond. Within this process, the authors stipulate that presence of a nucleophile (either BH unit or water) may promote this pathway. Given the observation that BH appears as the source of the hydride to the metal, the P-OH motif is not expected to act co-operatively. However, it may occur that the presence of P-O^- in a state of the complex may be conducive of this pathway; In our case, it is anticipated that once the (Me)B-amine borane gets involved in hydrogen bonding via NH…Cl which facilitates the removal of one of the chloride ligands, it may undergo intramolecular nucleophilic attack by P-O^-. This intramolecular pathway is actively discussed as a main mechanistic proposal for nitrile hydration reactions catalysed by Ru(II)arene complexes.[93]

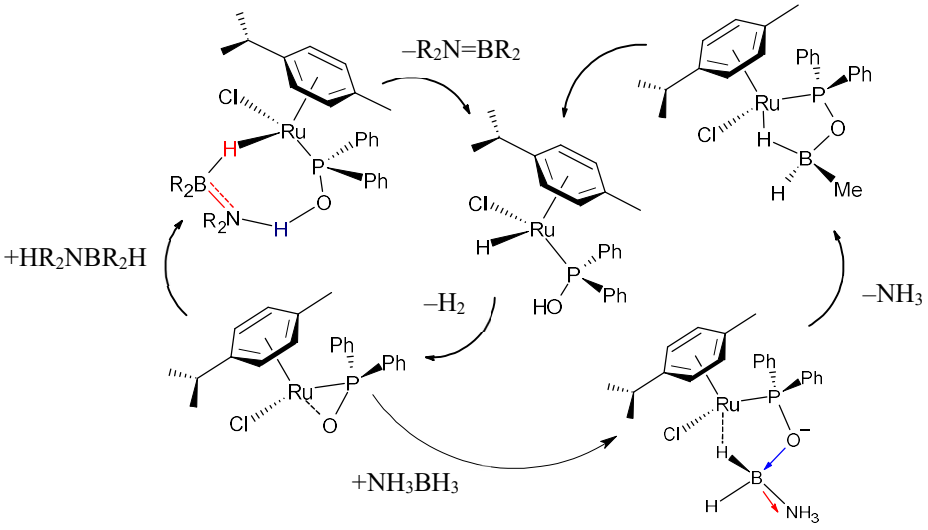

Figure 23: **Left:** Suggested catalytic cycle of (Me)B-amine borane by RuHCl(*p*-cymene)$PPh_2(OH)$

Furthermore, the existence of a dominant ligand cooperative pathway is supported in this view by the formation of a *mono*-hydride as theorised. Equally, the formation of the *bis*-hydride ([$Ru(H)_2$]) can be conceived by a secondary abstraction of chloride from the *mono*-hydride species with excess (Me)B-amine borane. After 1h, the complete consumption of (Me)B-amine borane is observed by disappearance of the triplet signal at –15.37 ppm in the ^{11}B NMR spectrum along with appearance of a new species as evidenced by the growth of a broad singlet at 35.38 ppm. This signal was shown to continually grow over the reaction course, until it is produced with the singlet at 33.18 ppm after 4h.

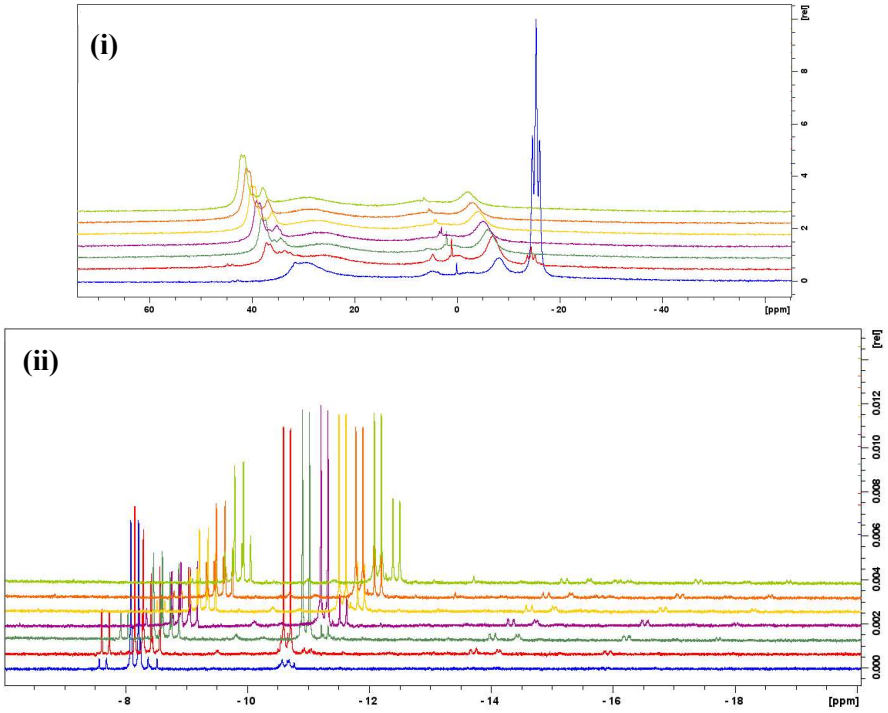

Figure 24: Reaction course (1-6 h) in THF for $RuCl_2$(*p*-cymene)PPh_2(OH) catalysis of (Me)B-amine borane **(i)** ^{11}B NMR Spectrum **(ii)** Hydride ^{1}H NMR Spectrum

The suggestion that $CDCl_3$ participates in the previous reaction is supported by differences for a parallel reaction conducted in THF. Notably, in this case, the ^{11}B NMR spectrum shows the absence of the doublet at –16.62 ppm, whilst (Me)B-amine borane remains in large excess (50%) after addition of the solvent (Figure 24). A broad signal is visible at 31.67 ppm which begins to develop after 1 h towards co-products at 36.03 ppm and 31.89 ppm conditional with the consumption of (Me)B-amine borane. Additionally, a broad signal at –7.93 ppm (assigned to $[NH_2\text{-}BHMe]_X$) is consistent since it is observed in both experiments in $CDCl_3$ and THF. This gradually forms over the course of the reaction (18 h). After 2 h, (Me)B-amine borane is fully consumed as judged by ^{11}B NMR spectroscopy. The ^{1}H NMR spectrum shows a complex hydride region after addition of the solvent. It exhibits several doublet signals corresponding

to different hydride species with the following chemical shifts and coupling constants: –7.64 ppm (J_{HP} = 50 Hz), –8.18 ppm (J_{HP} = 50 Hz), –8.45 (J_{HP} = 58 Hz) and –10.61 ppm (J_{HP} = 46 Hz). After 1 h, the consumption of (Me)B-amine borane is correlated with a significant growth in the *bis*-hydride (at –10.61 ppm) signal suggesting that this is the catalytically active species. Its formation, however, is sluggish in THF relative to the reaction in $CDCl_3$. Additionally, a sequence of weak unknown doublets is observed at the following chemical shifts and coupling constants in the ^1H NMR spectrum; –13.38 ppm (J_{HP} = 38 Hz), –13.83 ppm (J_{HP} = 20 Hz), –15.63 ppm (J_{HP} = 35 Hz), and –17.11 ppm (J_{HP} = 22 Hz). The coupling of the hydride to the phosphorus in the co-ligand was confirmed by carrying out $^{31}P\{^1H\}$ experiments which remove such couplings. In these cases, all observed doublets transform into singlets. A peak at 20.74 ppm in the ^{31}P NMR spectrum also indicates a species where loss of PPh_2OH may occur. The presence of multiple *mono*-hydride species suggests the pathway not to be selective for ligand co-operativity. Equally, the co-ordinating effect of THF may enable the formation of alternative complexes not previously observed.

2.2.2 Catalytic Dehydrogenation of (Me)B-Amine Borane with $RuCl_2$(*p*-cymene)PPh_3

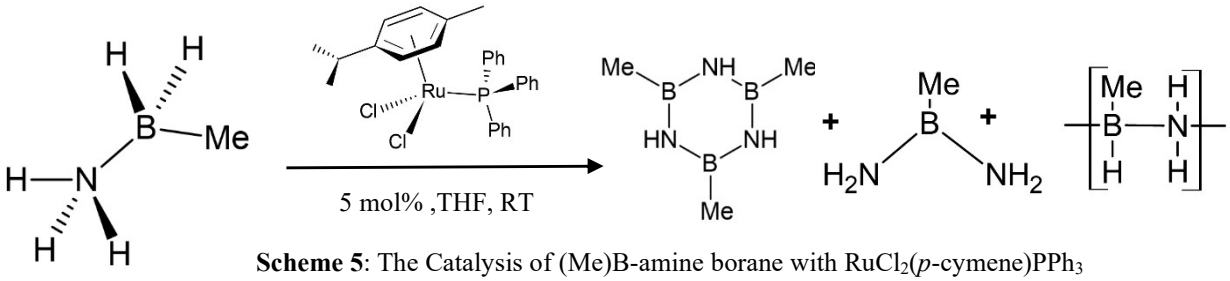

Scheme 5: The Catalysis of (Me)B-amine borane with $RuCl_2$(*p*-cymene)PPh_3

The catalytic dehydrogenation of (Me)B-amine borane with $RuCl_2$(*p*-cymene)PPh_3 was investigated as a benchmark on which to compare and assess the effect of the phosphinous acid co-ligand. The catalysis of (Me)B-amine borane via $RuCl_2$(*p*-cymene)PPh_3 (5 mol%) in THF at room temperature was also monitored by ^{11}B, ^1H, $^{31}P\{^1H\}$ NMR spectroscopy. In comparison to experiments with the catalyst $RuCl_2$(*p*-cymene)PPh_2(OH), in this case, the ^{11}B shows a similar product distribution is achieved. However, notably, the consumption of (Me)B-amine borane was approximately three times slower. Full consumption of the starting amine borane occurred after 6 h. The generation of a small doublet at 43.18 ppm ($^1J_{HB}$ = 126 Hz) and a small singlet at 47.06 ppm are observed similarly to reaction carried out using $RuCl_2$(*p*-cymene)PPh_2(OH) as catalyst. Ultimately, the spectrum exhibits a broad singlet at 35.80 ppm (s) ([NH-BMe]$_3$) as the main product signal (Figure 25). A broad signal is also visible at 25.98

ppm in the ^{11}B NMR spectrum. When compared with the previous results obtained with $RuCl_2$(*p*-cymene)$PPh_2(OH)$, the corresponding ^{1}H NMR spectrum when $RuCl_2$(*p*-cymene)PPh_3 was used was much simpler. After the start of the reaction, a single set of doublet resonances are observed corresponding to the *mono*-hydride and *bis*-hydride at –7.34 ppm (J_{HP} = 54 Hz) and at –10.57 ppm (J_{HP} = 44 Hz), respectively. Equally, for the same conditions, the ^{1}H NMR spectrum shows 30% generation of the *bis*-hydride relative to the *mono*-hydride (70%). These exist in a 6:4 (3:2) *mono*:*bis* relationship for the duration of the reaction and remain present after the substrate is fully consumed. The *mono*-hydride and *bis*-hydride appear to correlate to signals at 51.67 ppm and 66.64 ppm respectively in the ^{31}P NMR spectrum.

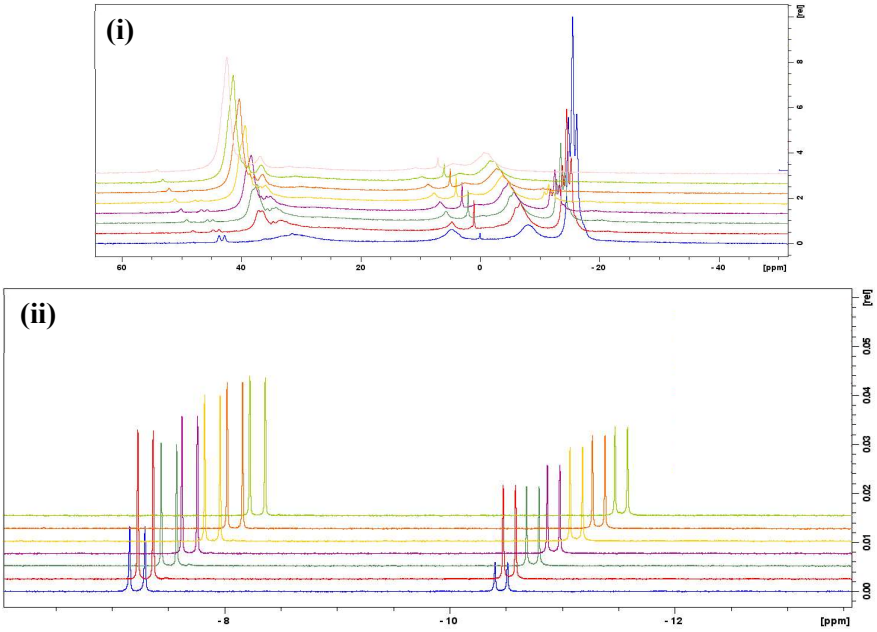

Figure 25 : Reaction course in THF for $RuCl_2$(*p*-cymene)PPh_3 with (Me)B-amine borane
(i) ^{11}B NMR Spectrum **(ii)** Hydride Region ^{1}H NMR Spectrum

2.2.3 Catalytic Dehydrogenation of (Me)B-Amine Borane with $RuCl_2$(*p*-cymene)$PPh_2(CH_2OH)$

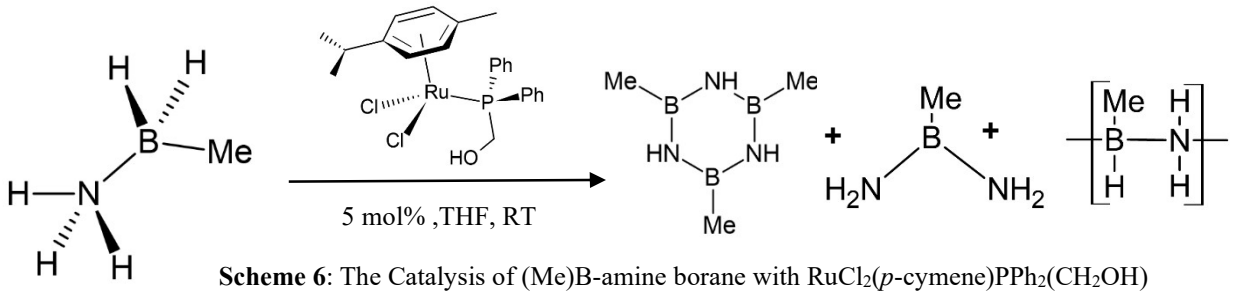

Scheme 6: The Catalysis of (Me)B-amine borane with $RuCl_2$(*p*-cymene)$PPh_2(CH_2OH)$

Dehydrogenation of Me(B)-amine borane with 5 mol% of the catalyst $RuCl_2$(*p*-cymene)$PPh_2(CH_2OH)$ was carried out in THF at room temperature. Monitoring of the reaction by NMR spectroscopy showed similarity to the previous results obtained with catalysts

$RuCl_2$(*p*-cymene)PPh_2(OH) and $RuCl_2$(*p*-cymene)PPh_3 under similar conditions. While the ^{11}B NMR spectrum resembles a similar landscape to the case of $RuCl_2$(*p*-cymene)PPh_2(OH), the inclusion of a methylene group as CH_2OH produced different hydride scenarios. Firstly, there is commonality in the creation of broad resonances at –4.11 ppm and –12.91 ppm in the ^1H NMR spectrum, similar to the reaction profile of Me(B)-amine borane in $CDCl_3$. These were absent for $RuCl_2$(*p*-cymene)PPh_2(OH) in THF, and hypothesised to be dependent on the formation of a metallacycle structure favoured and dependent on the involvement of the chlorinated solvent. However, their inclusion in this reaction suggests a similar pathway where a metallacycle may be present involving $RuCl_2$(*p*-cymene)$PPh_2(CH_2OH)$ when THF is used as solvent. To this extent, the inclusion of CH_2 as a spatial linker for OH may encourage the formation of a 6-membered metallacycle (Figure 26).

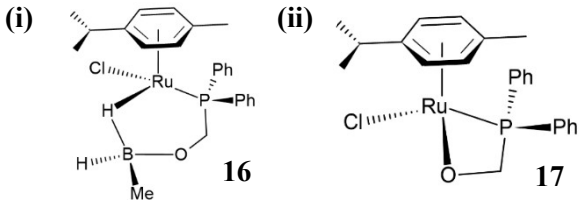

Figure 26: **(i)** Metallacycle formation with $RuCl_2$(*p*-cymene)$PPh_2(CH_2OH)$ **(ii)** κ^2 P-O bonding motif in $RuCl_2$(*p*-cymene)$PPh_2(CH_2OH)$

Similarly, to the $RuCl_2$(*p*-cymene)PPh_2(OH) case, the region for *mono* and *bis*-hydride also show a high degree of complexity. A myriad of closely related *mono*-hydride signals were observed between –7.85 ppm and –8.07 ppm in the ^1H NMR spectrum. This correlated with the ^{31}P NMR spectrum which equally indicated the presence of several signals between 51 and 53 ppm. Moreover, signals at –10.94 ppm (J_{HP} = 44 Hz) and at –10.97 ppm (J_{HP} = 44 Hz) are observed as sets of doublets relating to bis-hydride species. These seem to be consistent with downfield field signals observed at 63.91 ppm and 63.50 ppm in the ^{31}P NMR spectrum. The ^{31}P NMR chemical shifts for species observed when $RuCl_2$(*p*-cymene)$PPh_2(CH_2OH)$ was used as catalyst are consistent with those observed when $RuCl_2$(*p*-cymene)PPh_3 was used instead. This suggests that the CH_2OH inclusion does not strongly impact the metal-hydride species and that the same hydrides are formed during the catalysis. Nevertheless, resonances at 28.50 ppm are unique to the catalyst containing the methylene unit [$RuCH_2OH$]. This potentially indicates a co-operativity effect of this ligand to the metal centre. Diaz-Alvarez and co-workers investigated similar complexes for C-H versus O-H activation in phosphino-alcohol ligands.[109] They reported that bidentate κ^2 binding modes are possible for [$RuCl_2${2-$Ph_2PC_6H_4CH(R)OH$}(η^6-arene)] systems such as $RuCl\{\kappa^2$-(P,O)-2-$Ph_2PC_6H_4CH_2OH\}(\eta^6$-*p*-cymene)][Cl] and [$RuCl\{\kappa^2$-(P,C)-2-$Ph_2PC_6H_4CH_2OH\}(\eta^6$-*p*-cymene)]. These are observed as

singlet signals at 28.1 ppm and 52.8 ppm, respectively in the ^{31}P NMR spectra. They can interconvert under basic conditions. Again, it is possible these bonding modes are also available to $RuCl_2$(*p*-cymene)$PPh_2(CH_2OH)$, with $RuCl\{\kappa^2$-(P,O)-2-$Ph_2PCH_2OH\}(\eta^6$-*p*-cymene)][Cl] being directly comparable, albeit with a smaller ring size (Figure 26; **17**). After 1 h, (Me)B-amine borane is completely consumed. This catalyst promoted faster dehydrogenation when compared to $RuCl_2$(*p*-cymene)PPh_2(OH) and $RuCl_2$(*p*-cymene)PPh_3. The decomposition of the hydrides may provide some mechanistic insight of how H_2 is eliminated. After 2 h, a doublet at –15.30 ppm (J_{HP} = 16.19 Hz) begins to grow in intensity in the ^{1}H NMR spectrum over the next several hours, while the *mono*- and *bis*-hydride species disappear. Indeed, the ^{31}P NMR spectrum shows that all hydrides are most intense at 1 h, and are depleted sequentially over 12 h. Contrarily, the ^{31}P indicates low field resonances at 33.35 ppm, 29.03 ppm and 28.17 ppm all increase in size over the same period. This could be derived from the further elimination of H_2 towards the κ^2 bonding motif Ru-P,O. This cannot be corroborated by an increase on H_2 in the ^{1}H NMR spectrum, as the signal cannot be assigned. Still, the pathway in which hydrogen is rapidly eliminated from the complex initially may have been demonstrated by the demise of the hydrides on a longer timeframe.

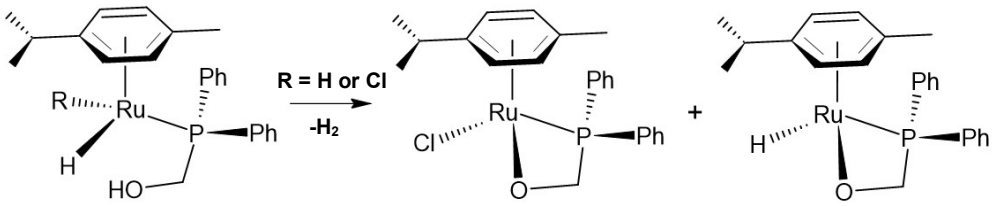

Figure 27: Proposed mechanism for hydrogen loss from $RuCl_2$(*p*-cymene)$PPh_2(CH_2OH)$

2.3 Catalytic Dehydrogenation of Dimethyl Amine Borane (Me_2NHBH_3)

To establish the catalytic ability of the phosphinous acid-based catalysts, experiments with a 5 mol% catalyst loading were carried out. The catalysts $RuCl_2$(*p*-cymene)PPh_2(OH), $RuCl_2$(*p*-cymene)P^iPr_2(OH), $RuCl_2$(*p*-cymene)PPh_3, $RuCl_2$(*p*-cymene)$PPh_2(CH_2OH)$ and $RuCl_2$(*p*-cymene)PPh_2(HN-Propyl) were utilised in the dehydrogenation of Me_2NH-BH_3 at RT. Commercially available Me_2NH-BH_3 was chosen as a substrate since it is often employed as a model for catalysis due to being less labile than amine borane (H_3N-BH_3). Its dehydrogenation forms 1 equiv. of H_2 which potentially facilitates mechanistic investigations. The reaction course was monitored by ^{11}B, ^{1}H, ^{31}P NMR spectroscopy. Early catalytic tests showed the class of catalysts to be active without additional activation, such as base or irradiation.

For the catalytic dehydrogenation of Me_2NH-BH_3, the same ^{11}B product distribution was observed regardless of the catalyst used (Figure 28; Scheme 7). These products were identified based on literature assignments for the same transformation.[33,35,107] As in previous articles, the cyclic dimer $[Me_2N\text{-}BH_2]_2$ is formed in <90% concentrations, along with minor side-products such as monomeric aminoborane $[Me_2N\text{-}BH_2]$ and $(NMe_2)_2BH$. However, the linear dimer $HMe_2NBH_2NMe_2BH_3$ is not observed in this system (*Section 2.5*) leading to the belief that $[Me_2N\text{-}BH_2]_2$ forms via an off-metal dimerization and not a chain length mechanism. An additional signal is often observed at δ = ~21.00 in the ^{11}B NMR spectrum resulting from water content in the reaction, and subsequent formation of (poly)boric acid. The following sections provide experimental observations based on ^{1}H, ^{31}P and ^{11}B NMR measurements for the catalysis of dimethyl amine borane with respect to each catalyst.

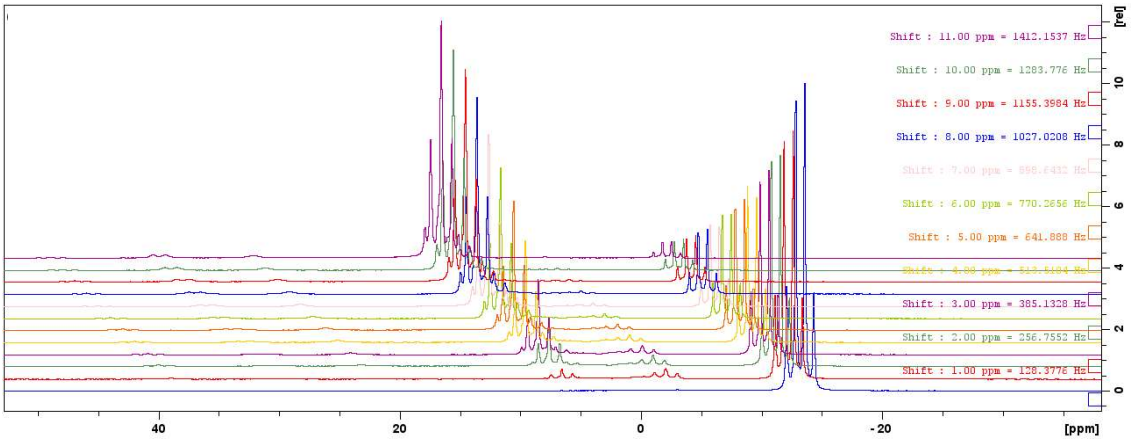

Figure 28 : The catalytic conversion of Me_2NH-BH_3 monitored by ^{11}B NMR spectroscopy

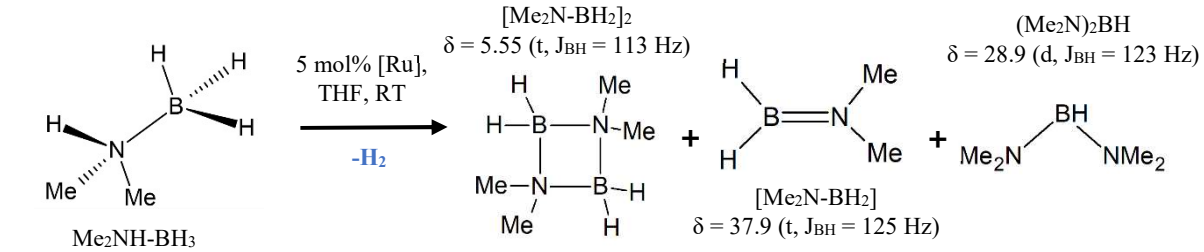

Me_2NH-BH_3
δ = -13.19 (q, J_{BH} = 95 Hz)

Catalysts Under Investigation:

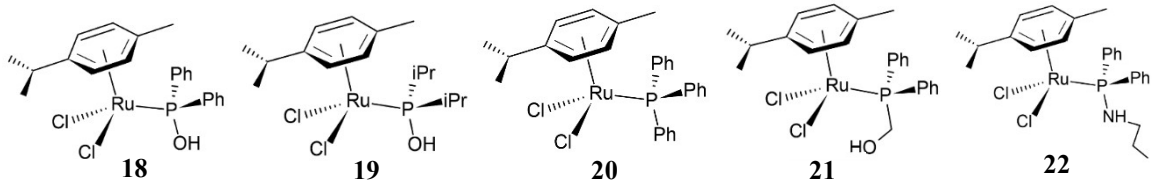

18 **19** **20** **21** **22**

Scheme 7: Reaction products of Me_2NH-BH_3 catalysis with ruthenium cymene catalysts

2.3.1 Catalytic Dehydrogenation of Dimethyl Amine Borane with $RuCl_2$(*p*-cymene)PPh_2(OH)

It is evident from the ^{31}P and ^{1}H NMR spectra of the reaction mixtures during catalytic dehydrogenation experiments, that the catalyst precursor $RuCl_2$(*p*-cymene)PPh_2(OH) shows an exclusive 18% conversion to the *mono*-hydride (125.33 ppm), consistent with the –8.15 (J_{HP} = 54 Hz) signal in the ^{1}H NMR spectrum at the start of the catalysis. Based on the ^{11}B NMR spectra, the generation of the *mono*-hydride appears to have been initiated by the conversion of Me_2NH-BH_3 to $(Me_2N)_2BH$ (0.45%) and Me_2NH-BH_2Cl[110] (2.50%). After 12 h, dimethyl aminoborane $[Me_2N$-$BH_2]_2$ emerges in 4% concentration as a secondary triplet in ^{11}B NMR spectrum, along with monomeric Me_2N-BH_2 as a minor product. Conversion to Me_2NH-BH_2Cl increases from 2.5% to 8% in the product distribution along with the appearance of the *bis*-hydride at –10.68 ppm (J_{HP} = 45 Hz) in the ^{1}H NMR spectrum. This is consistent with the activation of the second chloride on the ruthenium centre by Me_2NH-BH_3. The reaction was also monitored over the first 12 hours. Initially, four sets of doublets corresponding to two *mono*- and two *bis*-hydride species are observed as judged by their chemical shifts in the ^{1}H NMR spectra.

After 1h, the ^{31}P NMR spectrum shows the main species at 125.26 ppm in 97% excess. This quickly converts into a species at 129.15 ppm. This becomes the dominant species 2 h later. Analysing the ^{1}H NMR spectra, this change from 125.33 ppm to 129.15 seems to reflect the formation of a new *mono*-hydride species. Whilst the first species formed at 125.33 ppm seems to be related to the formation of the *mono*-hydride at –8.16 ppm (as judged by the ^{1}H NMR spectrum), the second species observed at 129.15 ppm seems to be related to the formation of a different *mono*-hydride complex at –7.99 ppm according to the ^{1}H NMR spectrum. A similar conversion is observed related to the *bis*-hydride in the ^{1}H NMR spectrum. While a signal at –11.00 ppm is originally observed, after 4h, the *bis*-hydride at –10.68 ppm is dominant thereafter. Analysing the corresponding ^{11}B NMR spectra, these transformations also reflect the initial formation of Me_2NH-BH_2Cl (pre-activation associated with the formation of the –8.16 ppm *mono*-hydride) and the formation of $(Me_2N)_2BH$ and $[Me_2N$-$BH_2]_2$ (associated with the formation of the –7.99 ppm *mono*-hydride complex). This creates difference between the events of the formation of the *mono*-hydride and its role in the reaction once formed. After 5 h, only a single set for the *mono*-hydride and *bis*-hydride were observed in the ^{1}H NMR spectrum. After 12 h, several downfield signals were observed in the ^{31}P NMR spectrum at δ (ppm) = 143.18, 140.58, 135.63 and 131.10 as the signal at 129.15 ppm is consumed. After 24 h, the $^{1}H\{^{31}P\}$ indicates splitting of the dihydride to separate signals which fully diverge over the reaction course to –10.39 ppm (J_{HP} = 47 Hz) and –10.43 ppm (J_{HP} = 45 Hz). The ^{11}B NMR

spectrum shows that growth of $[Me_2N\text{-}BH_2]_2$ throughout is promoted by consumption of Me_2NHBH_3. Resonances assigned to $(Me_2N)_2BH$ and monomeric Me_2NBH_2 appear constant in integration throughout (<3%), while $Me_2NH\text{-}BH_2Cl$ triplet is only slowly consumed. The intensity of the ^{31}P signals appear to decrease throughout the reaction, furnishing only minor resonances at 143.20 ppm and 140.70 ppm when two dihydride signals are observed. $Me_2NH\text{-}BH_3$ is fully consumed after 156 h, generating $[Me_2NBH_2]_2$ in a 90% yield by relative integration.

2.3.2 Catalytic Dehydrogenation of Dimethyl Amine Borane with $RuCl_2$(*p*-cymene)P^iPr_2(OH)

The effect of the phosphine substituents on the reaction profiles for the dehydrogenation of amine boranes was also investigated. For this purpose, $RuCl_2$(*p*-cymene)PR_2(OH) where R= ^{i}Pr or Ph) were used as catalysts. This section describes the use of the $RuCl_2$(*p*-cymene)P^iPr_2(OH) as a catalyst. It is anticipated that it should access the same reactivity pathway as $RuCl_2$(*p*-cymene)PPh_2(OH) allowing the effect of the substituent to be analysed. Similar to the phenyl analogue, the activation of the *mono*-hydride as a doublet at –8.47 ppm (J_{HP} = 50 Hz) appears to dependent on the formation of $Me_2NH\text{-}BH_2Cl$. The ^{31}P NMR spectrum confirms this selective pathway as the *mono*-hydride resonance at 158.7 ppm in the ^{31}P NMR spectrum is formed in equimolar ratios after introduction. This becomes the only species present after 1h by ^{31}P NMR spectrum. However, unlike $RuCl_2$(*p*-cymene)PPh_2(OH) which rapidly converted to an alternate hydride along with the appearance of the dehydrogenated products, $RuCl_2$(*p*-cymene)P^iPr_2(OH) appears non-progressive (dormant) for the next few hours.

Indeed, this pathway appears delayed, only generating $[Me_2N\text{-}BH_2]_2$ after 4 h in conjunction to traces of the new *mono*- and *bis*- hydrides at –8.15 ppm and –11.50 ppm, respectively. New signals such as those at 173.25 ppm (*mono*) and 181.22 ppm (*bis*) in the ^{31}P NMR spectrum seem to correlate with the growth of the new hydride signals in the ^1H NMR spectrum. While the ^{11}B NMR spectrum is similar to case when $RuCl_2$(*p*-cymene)PPh_2(OH) was used, only after 48 h is the preliminary monohydride fully consumed towards the monohydride signal that accompanies dehydrocoupling. This coincided with the loss of the signal at 158.7 ppm as the dominant in the ^{31}P NMR spectrum, and the appearance of the signals at 173.10 ppm and 181.04 ppm. By the end of this process, it is clear that the catalyst containing the *i*-propyl phosphine [$RuCl_2$(*p*-cymene)P^iPr_2(OH)] underperforms the one containing the phenyl phosphine [$RuCl_2$(*p*-cymene)PPh_2(OH)] as it exhibits a sluggish formation of active hydride

species. After 48 h, consumption of Me_2NHBH_3 reached 31% with $RuCl_2$(*p*-cymene)P^iPr_2(OH) in contrast to the catalyst $RuCl_2$(*p*-cymene)PPh_2(OH), which showed ~51% consumption over the same period. The reaction proceeds otherwise similarly, showing slow and full consumption of the Me_2NHBH_3 after 264 h, during which time the hydride species cannot be observed anymore. The difference in reactivity between these two catalysts clearly indicates its dependency on the nature of the phosphine. In general, aryl phosphines are better π-acceptors than alkyl phosphines and therefore experience a greater degree of backdonation from the metal to antibonding orbitals. Given this, ruthenium in $RuCl_2$(*p*-cymene)PPh_2(OH) may favour activation of Me_2NH-BH_3 as the metal has a lower electron density. Hasche described that Ph-substituted Rh(III) ^{R}PSCSP^R pincer complexes were significantly more active than ^{i}Pr analogues.[111] This suggests the effect of ^{i}Pr on the system is likely to be dependent on the activation of hydrogen by ruthenium. Additionally, aryl substituents may promote the deprotonation of P-OH as the resultant charge may be delocalised through the aromatic system.

2.3.3 Catalytic Dehydrogenation of Dimethyl Amine Borane with $RuCl_2$(*p*-cymene)PPh_3

In order to further investigate the effect of the nature of the phosphinous acid ligand on the dehydrogenation of amine boranes, a catalyst containing a non-functionalised triphenyl phosphine ligand was utilised. In this case, the dehydrogenation of Me_2NH-BH_3 catalysed by $RuCl_2$(*p*-cymene)PPh_3 was employed as a benchmark on which to assess the inclusion of phosphinous acid as a site for ligand cooperativity. Expectedly, $RuCl_2$(*p*-cymene)PPh_3 produces a unique pathway resultant from the lack of a co-operative ligand. Notably, in conjunction with formation of both *mono* and *bis*-hydrides, a broad signal appears at ~21.00 ppm (J_{HP} = 58 Hz) in the ^{31}P NMR spectrum. An equally broad signal is viewed at –11.73 ppm in the ^{1}H NMR spectrum which converts into a strong singlet upon decoupling from the boron in ^{1}H{^{11}B} spectrum. Additionally, a doublet becomes visible at –3.74 ppm (J_{HP} = 3.20 Hz) that is reminiscent of a metal coordinated borane. To this extent and in similarity to the reaction with (Me)B-amine borane, $RuCl_2$(*p*-cymene)PPh_3 appears to form an inactive BH_4 complex over the reaction course (Figure 29). This is confirmed in the ^{11}B NMR spectrum which shows the corresponding doublet signal once decoupled from protons at –38.00 ppm (J_{BH} = 53 Hz). Anke added that addition of NMe_2Et can trap free borane and improve catalyst lifetime. Accordingly, the group reported a TON_{MAX} three times higher with the inclusion of 1 mol% of NMe_2Et than without.[79]

Independently, Me_2NHBH_3 is dehydrogenated to a similar distribution as when using $RuCl_2$(*p*-cymene)$PPh_2(OH)$ over 276 h at RT. This involved the formation of *mono*- and *bis*-hydride species. Several other hydride species are also observed towards the end of reaction. These exhibited signals (δ, ppm) at: –11.51 (s), –11.61 (s), –11.78 (s), –12.39 (s), –14.39 (t, J_{HP} = 30 Hz), –15.20 (s), –15.76 (s), –19.05 (t). Therefore, as consequence of PPh_3 ligand in $RuCl_2$(*p*-cymene)PPh_3, the reaction produces a number of hydride species (non-selective) and shows signs of early deactivation. As one of the examples of complexities, the triplet at –14.39 ppm resolves to a singlet once decoupled from the phosphorous in a $^1H\{^{31}P\}$ NMR experiment suggesting two PPh_3 units may be present on a single Ru-centre.

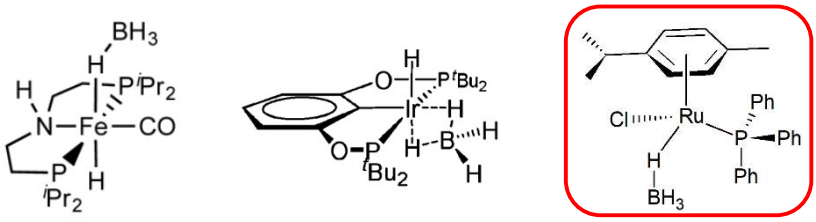

Figure 29 : BH_4 deactivated states of catalyst

2.3.4 Catalytic Dehydrogenation of Dimethyl Amine Borane with $RuCl_2$(*p*-cymene)$PPh_2(CH_2OH)$

Similarly, to the case where $RuCl_2$(*p*-cymene)PPh_3 was used as a pre-catalyst, a phosphine containing a methylene hydroxide group (CH_2OH) was also investigated. As discussed below, this had the ability to dehydrogenate DMAB via a unique pathway. Moreover, the distance of the CH_2OH moiety from the metal centre can encourage additional states. A cluster of novel signals around 28.30 ppm accompanied the formation of the *mono*-hydride (52.41 ppm) by ^{31}P NMR spectroscopy. As discussed previously, resonances within this region are associated with a κ^2-binding modes ($RuCl\{\kappa^2$-(*P*,*O*)-2-$Ph_2PCH_2OH\}$(*p*-cymene)][Cl]) and may lead to significant catalyst activity. Despite the *in-situ* formation of a cationic catalyst, the observation of dehydrogenated products are not as forthcoming as when [$RuCl_2$(*p*-cymene)$PPh_2(OH)$] was used. Additionally, $RuCl_2$(*p*-cymene)$PPh_2(CH_2OH)$ can still be observed as late as 8 h after the start of the reaction in the ^{31}P NMR spectrum. The consumption of $RuCl_2$(*p*-cymene)$PPh_2(CH_2OH)$ provides complex regions (multiple signals) at 51 ppm and 28 ppm.

Owing to access towards κ^2 bonding, the formation of the *bis*-hydride is delayed and was only observed as a minor species even after 12 h. Accordingly, this may suggest why Me_2NHBH_3 remains in 94% abundance up to 12 h. However, following this the consumption of Me_2NH-BH_3 appears to greatly increase (*See RT Graph*), exhibiting the formation of the *bis*-hydride at

increased concentrations from 36 h. Additionally, the enhanced reactivity observed in this case, might have been a consequence from the dominance of a singular *mono*-hydride signal at –8.06 ppm (J_{HP} = 54 Hz) in comparison to other minor species present within the complex region (Figure 30). This appears to correlate to the dominant signal at 52.31 ppm in the ^{31}P NMR spectrum. Similar to $RuCl_2$(*p*-cymene)PPh_2(OH), in this case, the formation of a dominant *mono*-hydride can correlate to the formation of dehydrocoupled products. Following this, a similar relationship to the other catalysts is observed with presence of both *mono*- and *bis*-hydrides species in a highly simplified pathway.

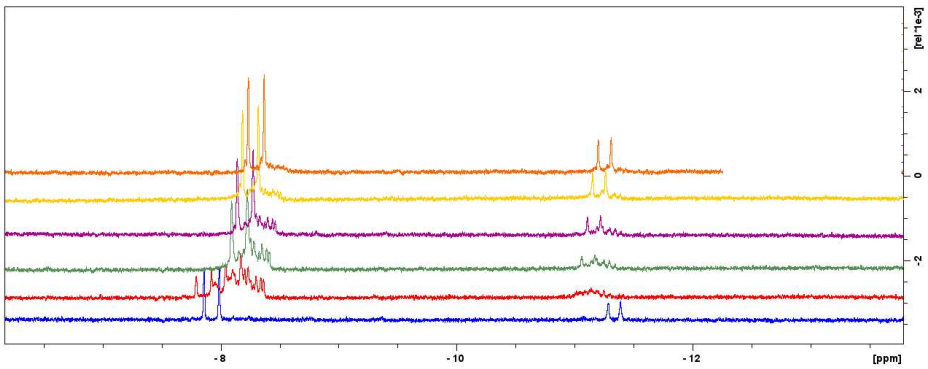

Figure 30: $RuCl_2$(*p*-cymene)$PPh_2(CH_2OH)$ hydride pathway by ^1H NMR spectroscopy

2.3.5 Catalytic Dehydrogenation of Dimethyl Amine Borane with $RuCl_2$(*p*-cymene)PPh_2(HN-Propyl)

Complexes with polar metal–nitrogen bonds are the most prominent representatives within bifunctional catalysis and are continually at the forefront of MLC.[75] This is because electron-rich transition metal complexes with amido ligands experience high N-centred basicity. Additionally, these species can readily interconvert between amido and amine forms. With this in mind, a pre-catalyst containing a phosphine with an amine substituent was utilised. Namely, $RuCl_2$(*p*-cymene)PPh_2(HN-Propyl) should serve as a good comparison to the phosphinous acid-base catalysts as a cooperative ligand. Potentially, the catalyst may exhibit a greater selectivity and activity as complications of B-O bonding are eliminated. Following the catalytic dehydrogenation of amine boranes by ^{31}P NMR spectroscopy presented a simpler reaction course; unlike the previous examples. This catalyst showed complete exclusivity in the formation of the monohydride species throughout the reaction. The signal assigned to the starting complex at 60.02 ppm in the ^{31}P NMR spectrum fully converted into another signal at 82.01 ppm assigned to the corresponding *mono*-hydride species. This conversion took 84 h to be achieve the *mono*-hydride as the sole resonance. Naturally, only one hydride signal is visible in the ^1H NMR spectrum at –8.12 ppm (J_{HP} = 51 Hz). Among the catalysts investigated here,

$RuCl_2$(*p*-cymene)PPh_2(HN-Propyl) is the only one which did not produce the *bis*-hydride species. This might indicate that the formation of the *bis*-hydride species is an active process of the catalyst. Additionally, the *mono*-hydride is the same from throughout the reaction and did not convert into another active species. Both are highly suggestive that the N-Propyl ligand participates in the dehydrogenation of Me_2NHBH_3. Evidence of N-H on the ligand is not observed – obstructed by N-H in amine-borane and not observed in ^{1}H NMR spectrum at the end.

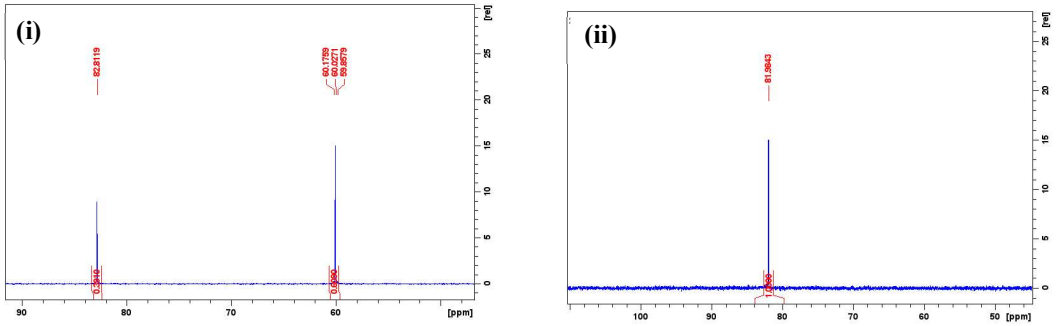

Figure 31: ^{31}P NMR conversion of $RuCl_2$(*p*-cymene)PPh_2(HN-Propyl) in the catalysis of Me_2NH-BH_3 **(i)** ^{31}P NMR spectrum showing clean conversion of the complex to the mono-hydride resonance **(ii)** ^{31}P NMR spectrum showing the mono-hydride species in exclusivity after the complex consumption

2.3.6 The Effect of Temperature on the Catalytic Dehydrogenation of Dimethyl Amine Borane at 5 mol% Catalyst Loading

The catalysis of Me_2NH-BH_3 was conducted with 5 mol% loadings of $RuCl_2$(*p*-cymene)PPh_2(OH) , $RuCl_2$(*p*-cymene)P^iPr_2(OH), $RuCl_2$(*p*-cymene)PPh_3, $RuCl_2$(*p*-cymene)$PPh_2(CH_2OH)$ and $RuCl_2$(*p*-cymene)PPh_2(HN-Propyl) at room temperature. By monitoring the ^{11}B NMR spectrum for the reaction progress, approximate concentrations of Me_2NH-BH_3 can be produced given the integration of the starting material every 12 h until it is consumed. The graph below shows a comparison of the results for the dehydrogenation of amine boranes with the various catalysts tested. Based on the results, the following order is observed; $RuCl_2$(*p*-cymene)PPh_2(OH) > $RuCl_2$(*p*-cymene)$PPh_2(CH_2OH)$ > $RuCl_2$(*p*-cymene)PPh_2(HN-Propyl) > $RuCl_2$(*p*-cymene)P^iPr_2(OH) = $RuCl_2$(*p*-cymene)PPh_3. It is evident from the graph that $RuCl_2$(*p*-cymene)PPh_2(OH) produced the fastest consumption of Me_2NH-BH_3 towards dehydrogenated products. This may be attributable to the rate at which the dihydride (potentially the active species) is formed relative to the start of the reaction.

Further, the reaction profile with $RuCl_2$(*p*-cymene)$PPh_2(CH_2OH)$ as a catalyst appears more sigmoidal in shape, characteristic of an induction period relating to κ^2-bonding. This coordination mode may be responsible for the presence of an induction period observed. This

is also consistent with observations where several hydride species are observed before convergence towards a dominant *mono* and *bis*-species. For the conversion of Me_2NH-BH_3 exceeding 90%, the reactivity difference appears negligible for $RuCl_2$(*p*-cymene)PPh_2(HN-Propyl), $RuCl_2$(*p*-cymene)P^iPr_2(OH) and $RuCl_2$(*p*-cymene)PPh_3 despite unique character in dehydrogenation.

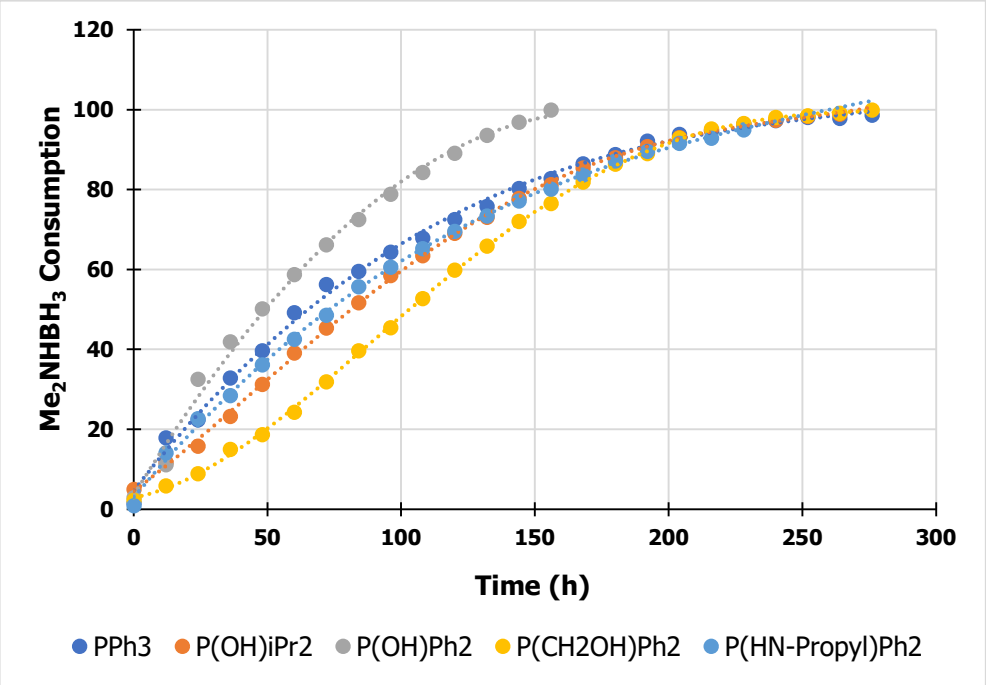

Figure 32: A graph to show the catalytic performance of $RuCl_2$(*p*-cymene)PR_2R' catalysts (5 mol%) in the dehydrogenation of Me_2NHBH_3 at RT.

The effect of temperature is known to be an important pre-requisite for catalyst efficiency. With this in mind, catalytic dehydrogenations were carried out at 70 °C (the temperature was chosen as it is consistent with literature standard conditions for the same transformation). The reaction mixtures in Young's tubes were allowed to heat at 70 °C for 1 h, then removed and analysed by ^{11}B, ^{31}P and ^{1}H NMR spectroscopy. For all catalysts, except $RuCl_2$(*p*-cymene)P^iPr_2(OH), near quantitative conversions were achieved after 1 h. The following order was achieved for the consumption percentage of Me_2NH-BH_3 after 1 h at 70 °C; $RuCl_2$(*p*-cymene)PPh_2(HN-Propyl), $RuCl_2$(*p*-cymene)$PPh_2(CH_2OH)$, $RuCl_2$(*p*-cymene)PPh_2(OH), $RuCl_2$(*p*-cymene)PPh_3, $RuCl_2$(*p*-cymene)P^iPr_2(OH).

Table 2 : **Consumption of Me_2NH-BH_3 by $RuCl_2$(*p*-cymene)PR_2R' catalysts (5 mol%) at 70 °C after 1 h**

Catalyst	Conversion as determined by ^{11}B NMR Spectroscopy (%)
Ru-PPh_2(HN-Propyl)	99.4
Ru-$PPh_2(CH_2OH)$	99.2

Ru-PPh_2(OH)	98.9
$RuPPh_3$	98.5
Ru-P^iPr_2(OH)	87.5

There is no evidence for different reaction pathways due to the change in temperature. Instead, in the cases of all catalysts, the NMR spectrums exhibits stages of completion that match the experiments carried out at room temperature but only occurred faster. For instance, the ^1H NMR spectrum of the mixture at 70 °C when $RuCl_2$(*p*-cymene)$PPh_2(CH_2OH)$ was used as catalyst exhibits a cleaner hydride region with the *mono*- and *bis*-hydride species present. The corresponding reaction at room temperature showed a significant concentration of κ^2-bonding motifs over the first hour. Thus, the effect of heating to 70 ºC can accelerate the reaction. Similarly, the dehydrogenation of amine boranes catalysed by $RuCl_2$(*p*-cymene)PPh_3 shows resemblance to the corresponding case at room temperature – *i.e.* with a number of hydride species and evidence of a partially deactivated complex. At 70 °C, $RuCl_2$(*p*-cymene)PPh_2(OH) only shows the *bis*-hydride signals in the ^1H NMR spectrum which have begun to split towards two distinct hydrides as observed in the room temperature reaction. The result for the catalytic dehydrogenation of amine boranes using $RuCl_2$(*p*-cymene)PPh_2(HN-Propyl) as a catalyst is notable. It seems to be dependent on an increased water content within the reaction. 17% of the product distribution within the ^{11}B NMR spectrum can be assigned as (poly)boric acid. This should only form if water is present in the reaction. For the other catalysts, 5-6% (poly)boric acid was observed as a product, showing a large skew for the $RuCl_2$(*p*-cymene)PPh_2(HN-Propyl) catalysis. Thus, the improved result may be dependent on a hydro-thermolysis style of dehydrogenation. Still, only the monohydride is detected at the reaction end by ^{31}P and ^1H NMR spectroscopy. Another notable result arises from the reaction of $RuCl_2$(*p*-cymene)P^iPr_2(OH) conducted at 70 ºC. Similar to the room temperature comparison to $RuCl_2$(*p*-cymene)PPh_2(OH), the inclusion of alkyl *i*-propyl substituents on the phosphine appears to result in a significant loss in catalytic ability. At 70 ºC, $RuCl_2$(*p*-cymene)P^iPr_2(OH) underperforms the other catalysts, even $RuCl_2$(*p*-cymene)PPh_3 with no possible co-operativity.

The temperature was shown to have dramatic effect on the reaction course. The dehydrogenation of Me_2NHBH_3 was also investigated at 50 °C. Table 3 below compares the conversion of the amine boranes over time at 50 °C.

Three catalysts, $RuCl_2$(*p*-cymene)PPh_2(OH), $RuCl_2$(*p*-cymene)$PPh_2(CH_2OH)$ and $RuCl_2$(*p*-cymene)PPh_2(HN-Propyl) gave conversions lower than 90% in 8 h. This is a substantial decrease in activity in comparison to the conversions obtained at 70 ºC (Table 2). Catalysis

experiments with catalysts $RuCl_2$(*p*-cymene)PPh_2(OH), $RuCl_2$(*p*-cymene)$PPh_2(CH_2OH)$ and $RuCl_2$(*p*-cymene)PPh_2(HN-Propyl) were carried out at 20 ºC, 50 ºC and 70 ºC. This allowed the effect of the temperature on the catalysis to be investigated. The linearised form of the Arrhenius equation was used. Essentially, the initial rates were obtained by following the conversions at the beginning of the reactions. These were calculated for each catalyst at the given temperature by plots of decrease in the concentrations of dimethyl amine borane [DMAB] *vs.* time.

Table 3 : **Consumption of Me_2NH-BH_3 by selected catalysts (5 mol%) at 50 ºC**

	Consumption of DMAB by ^{11}B Integration (%)		
Time (h)	**$RuCl_2$(*p*-cymene) PPh_2(OH)**	**$RuCl_2$(*p*-cymene) $PPh_2(CH_2OH)$**	**$RuCl_2$(*p*-cymene) PPh_2(HN-Propyl)**
1	20.1	17.7	22.3
2	38.2	26.5	32.8
3	49.1	35.8	39.8
4	61.9	46.9	51.7
5	68.6	60.4	56.8
6	76.1	70.2	61.8
7	81.6	81.4	70.1
8	87.8	85.5	75.8

By monitoring the ^{11}B integration values of signals throughout the reaction, "relative conversions" for the concentration of Me_2NHBH_3 could be determined. For example, "relative concentrations" can be determined for [DMAB] by knowing the concentration of [DMAB] at the initial time (T_0) and ^{11}B signal integration at any given time. A key limitation of this conversion stems from the lack of an internal standard as a reference for integration values, as described by Conley[83] and Ortega-Lepe[81]. In addition to this, the ^{11}B integration does not account for boron containing products that precipitated out of solution, as we observe (*See Product Distribution*). The ^{11}B integration and relative concentrations are therefore only corroborated against the previous ^{11}B NMR spectrums recording in order to determining a reaction profile. Reactions, as those conducted for $RuCl_2$(*p*-cymene)PPh_3 and $RuCl_2$(*p*-cymene)P^iPr_2(OH) were only investigated at two temperatures; room temperature and 70 ºC. By only assessing the catalysts at two temperatures, and thus generating only two data points, any analysis of these reactions will be highly inaccurate. Conversions at room temperature showed an exponential decay in which initial rates are calculated by plotting linear trendlines through first points at the start of the conversions. The initial rate measurements for room temperature reactions are shown graphically below and in Table 4.

Table 4 : **Initial Rates (V_0) For Catalysis Experiments (5mol%) Between 293-343 K By Select Catalysis**

		Initial Rate (mol^{-1} dm^3 h^{-1})		
Temperature (K)	**Reaction Conditions**	**Ru-PPh_2(OH)**	**Ru-PPh_2(N-Propyl)**	**Ru-$PPh_2(CH_2OH)$**
293	[DMAB] = 0.57 M	0.0051	0.0034	0.0031
323	[DMAB] = 0.57 M	0.0599	0.0496	0.0613
343	[DMAB] = 0.57 M	0.5636	0.5666	0.5652

(i)

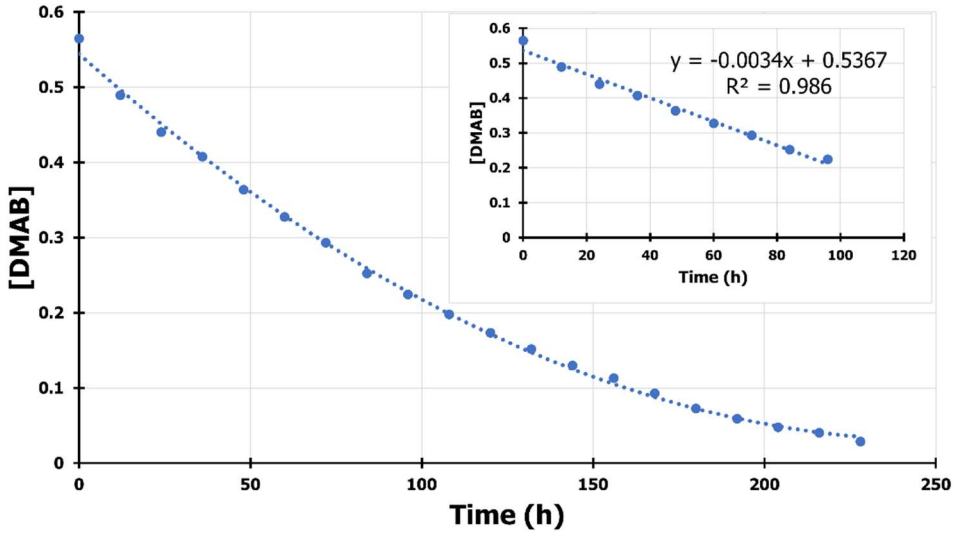

(ii)

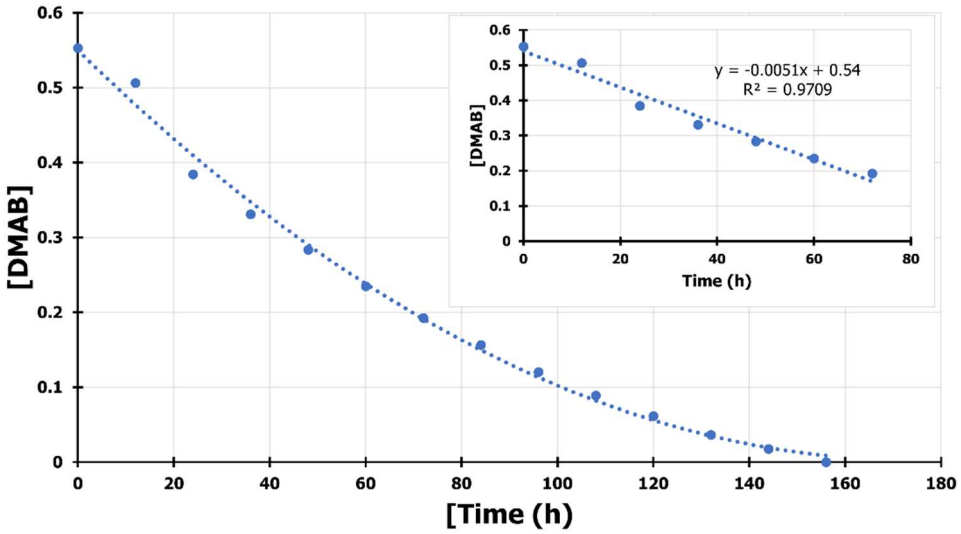

(iii)

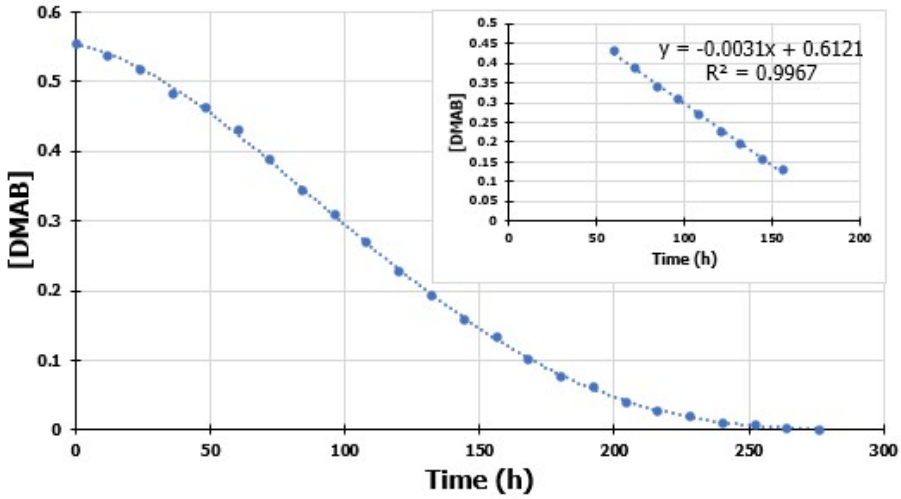

Figure 33: The consumption of Me_2NHBH_3 by $RuCl_2$(*p*-cymene)PR_2R' catalysts (5 mol%) at RT featuring initial rate determinations **(i)** $RuCl_2$(*p*-cymene)PPh_2(HN-Propyl) **(ii)** $RuCl_2$(*p*-cymene)PPh_2(OH) **(iii)** $RuCl_2$(*p*-cymene)$PPh_2(CH_2OH)$

After assigning initial rates (V_0) to the reactions, the effect of temperature on the rate constant was explored through the Arrhenius equation.

$$k = Ae^{-Ea/RT} \textbf{ (Equation 1.4)}$$

$$\text{Ln } k = \ln A - \frac{E_a}{RT} \textbf{ (Equation 1.5)}$$

E_a = Activation Energy, A = Pre-exponential factor, R = 8.314 J $mol^{-1}K^{-1}$,

k = Chemical rate constant, T = Temperature (K)

By applying logarithms to both sides of the Arrhenius equation, a logarithmic form of the equation can be produced (1.5). This equation resembles a straight line when graphs of ln(k) and 1/T are plotted. This produces a straight-line gradient of $-E_a/R$ and ln(A) as the y-intercept. Therefore, the activation energy of the reaction was explored by plotting Arrhenius graphs of ln(k) against 1/T. Natural logarithm plots of rates of reaction conducted at room temperature, 50 ºC and 70 ºC against 1/T produced straight line relationships.

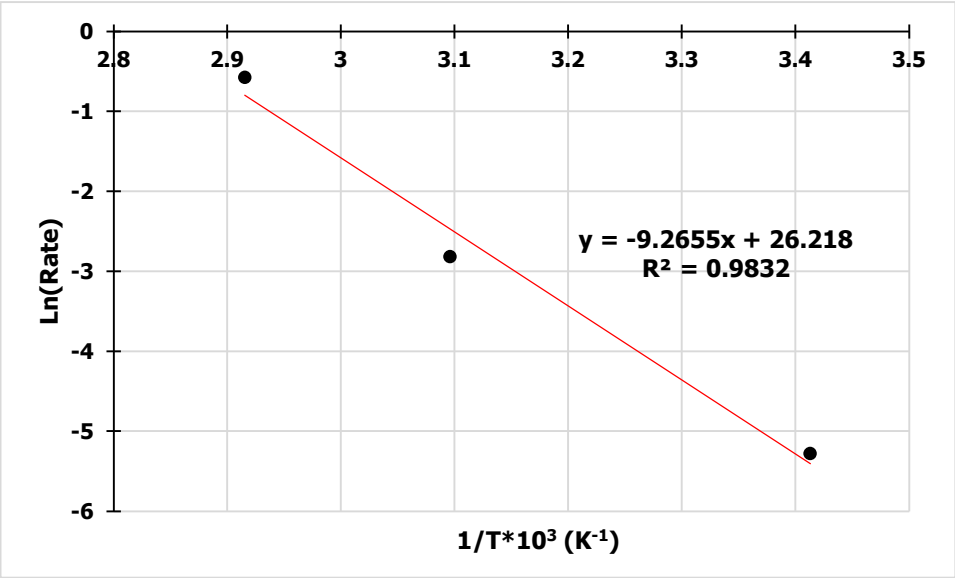

Figure 34: Arrhenius plot generated for $RuCl_2$(*p*-cymene)PPh_2(OH) through experimental initial rates between 293-343 K

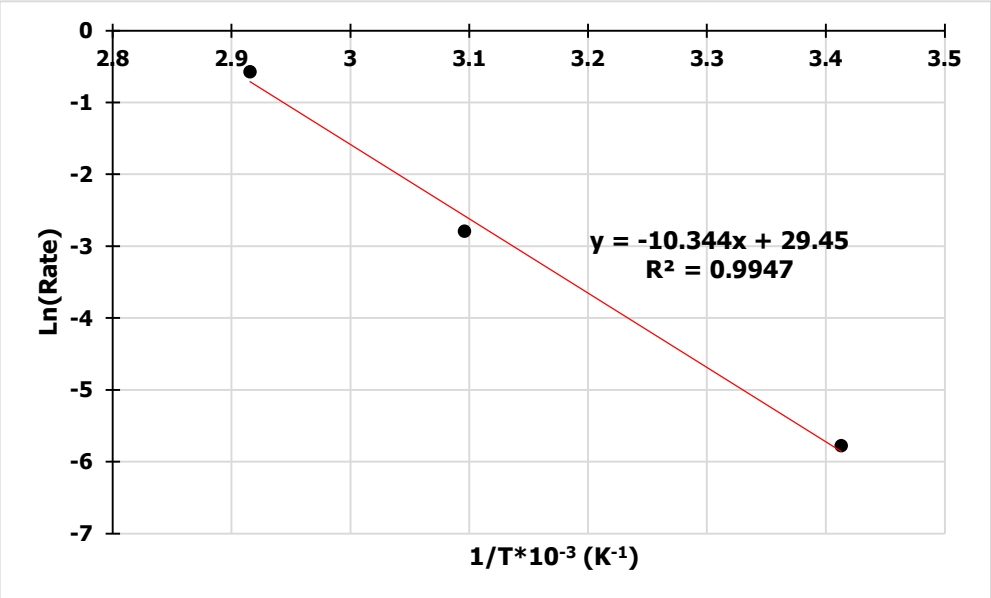

Figure 35: Arrhenius plot generated for $RuCl_2$(*p*-cymene)$PPh_2(CH_2OH)$ through experimental initial rates between 293-343 K

The gradient expressing $-E_a/R$ was then used to calculate the activation energies for $RuCl_2$(*p*-cymene)PPh_2(OH), $RuCl_2$(*p*-cymene)PPh_2(HN-Propyl) and $RuCl_2$(*p*-cymene)$PPh_2(CH_2OH)$. These were determined as 77.03 $kJmol^{-1}$ (18.41 kcal/mol), 83.76 $kJmol^{-1}$ (20.02 kcal/mol) and 86 $kJmol^{-1}$ (20.55 kcal/mol), respectively. This suggests $RuCl_2$(*p*-cymene)PPh_2(OH) as the catalyst that provides the lowest energy pathway. The activation energy obtained for $RuCl_2$(*p*-cymene)PPh_3 over two data points was 85.33 $kJmol^{-1}$ (20.39 kcal/mol). This suggests the inclusion of the phosphinous acid can lead to an increased catalytic activity. Williams reported

that the dissociation of the Shvo's dimer was 28.8 kcal/mol in toluene at room temperature. Still, no activation energies for other ligand co-operative catalysts can be found. Pal and co-workers reported that the activation energy of Cp*Rh complexes for AB dehydrogenation was 25.5 kcal/mol.[112] This shows that the values achieved in these experiments are comparable with literature values.

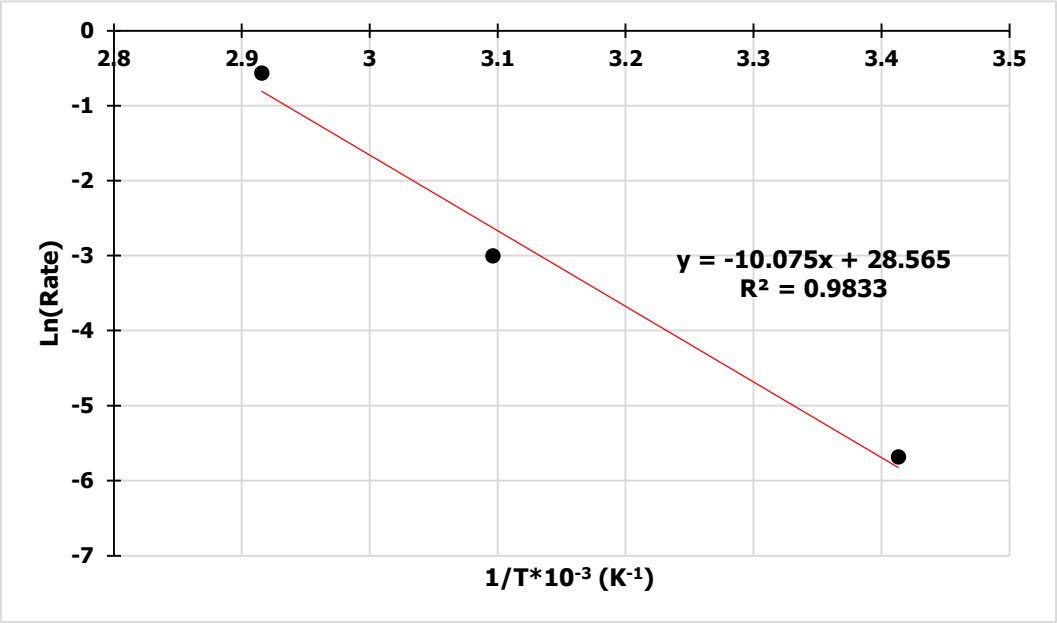

Figure 36: Arrhenius plot generated for $RuCl_2$(*p*-cymene)PPh_2(HN-Propyl) through experimental initial rates between 293-343 K

2.3.7 The Effect of Catalyst Loading in the Dehydrogenation of Dimethyl Amine Borane at 70 °C

For scaling up protocols, low catalytic loadings are ideal in view of costs and separation constraints. Furthermore, the most active catalysts for the dehydrogenation of amine-boranes are known to be active in loadings as minimal as 0.1 mol%. Therefore, the activity of the series of the catalysts was also monitored at 0.1 mol% at 70 °C. This gave the following order of activity: $RuCl_2$(*p*-cymene)PPh_2(HN-Propyl) > $RuCl_2$(*p*-cymene)$PPh_2(CH_2OH)$ = $RuCl_2$(*p*-cymene)PPh_2(OH) > $RuCl_2$(*p*-cymene)PPh_3 > $RuCl_2$(*p*-cymene)P^iPr_2(OH). These can be seen below.

Heating remains to have a more profound effect on the reaction, even at lower loadings. After 1h, only *bis*-hydride species are observed for $RuCl_2$(*p*-cymene)PPh_2(OH), $RuCl_2$(*p*-cymene)$PPh_2(CH_2OH)$, $RuCl_2$(*p*-cymene)P^iPr_2(OH) showing that the sequence of forming the *mono*-hydride which slowly converts to the *bis*-hydride at room temperature can be accelerated. Additionally, in difference to the room temperature reaction of $RuCl_2$(*p*-cymene)PPh_2(HN-Propyl), the *bis*-hydride is observed in this case.

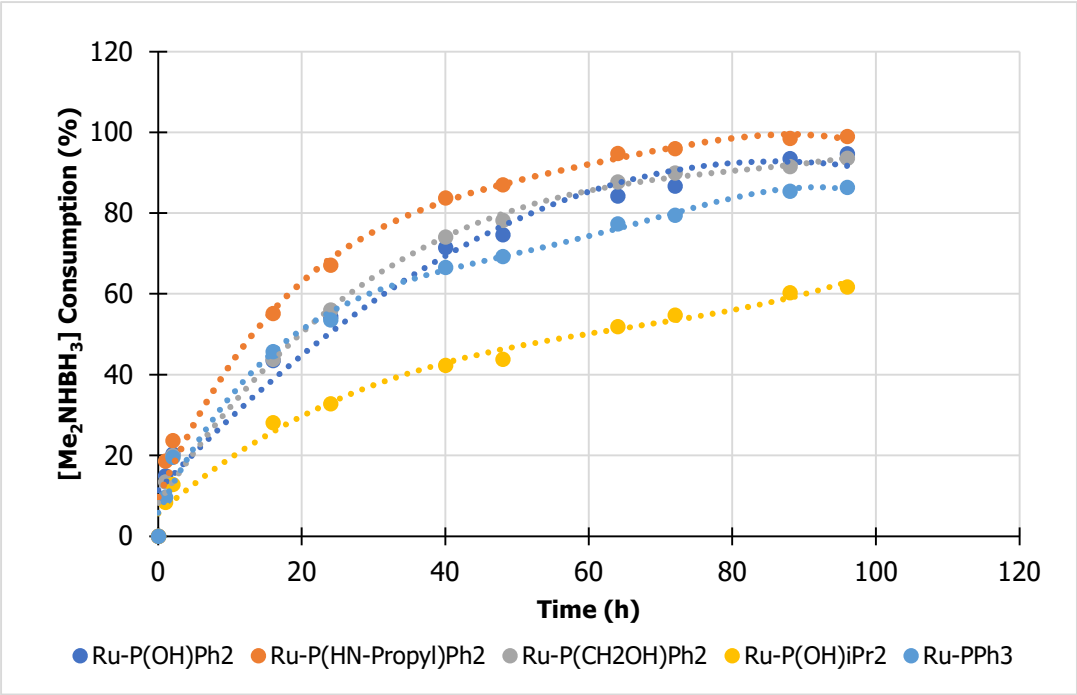

Figure 37: Catalytic Dehydrogenation of Me_2NHBH_3 with $RuCl_2$(*p*-cymene)PR_2R' catalysts (**0.1 mol%**) at 70 ˚C

The efficiency of the catalysts was also evaluated at 1 mol% catalyst loading. The following order was determined; $RuCl_2$(*p*-cymene)$PPh_2(CH_2OH)$, $RuCl_2$(*p*-cymene)PPh_2(HN-Propyl), $RuCl_2$(*p*-cymene)PPh_2(OH), $RuCl_2$(*p*-cymene)PPh_3, $RuCl_2$(*p*-cymene)P^iPr_2(OH).

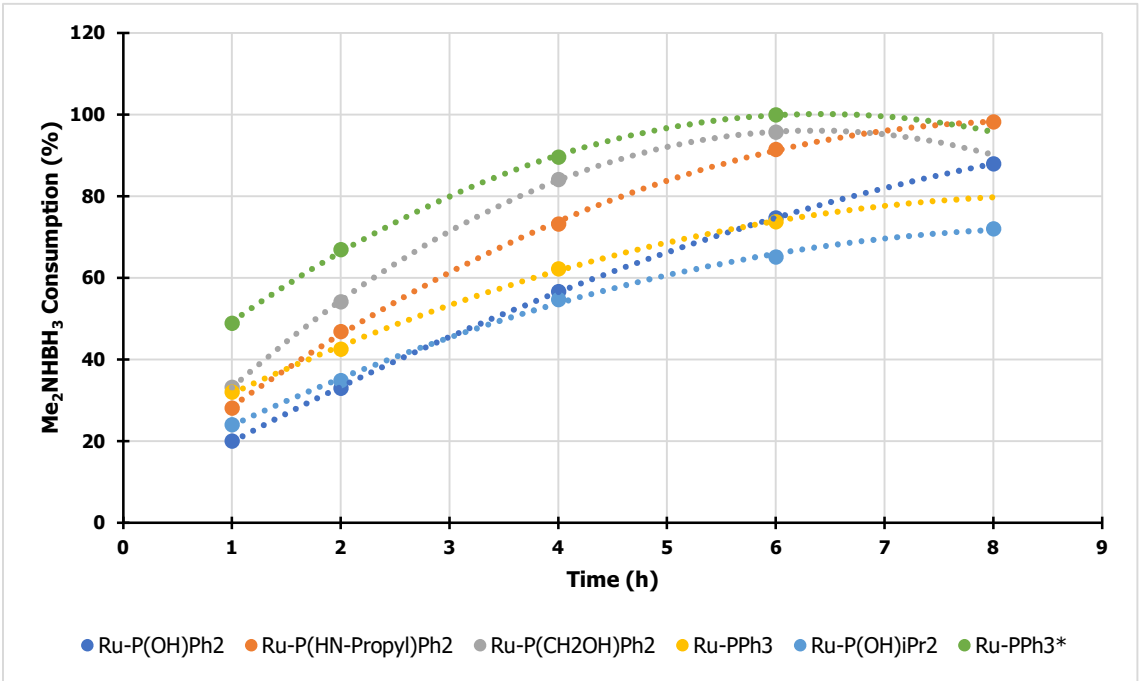

Figure 38: Catalytic Dehydrogenation of Me_2NHBH_3 with $RuCl_2$(*p*-cymene)PR_2R' catalysts (**1 mol%**) at 70 ˚C

An additional entry in the graph is produced from the catalytic reaction of Me_2NHBH_3 with a standard solution of $RuCl_2$(*p*-cymene)PPh_3 in THF that appeared green. Biancalana and co-workers commented that $RuCl_2$(*p*-cymene)PPh_3 solutions in THF can progressively turn green on-air exposure.[113] They identified that $RuCl_2$(*p*-cymene)PPh_3 could afford crystals of the dinuclear, mixed valence Ru^{II}-Ru^{III} species [Ru(μ-Cl)$_3$(η^6-*p*-cymene)$RuCl_2$(κP-PPh_3)] at RT in air. Thus, the improved catalytic ability of the green solution of $RuCl_2$(*p*-cymene)PPh_3 was attributed to a different catalytic motif. Interestingly, this species appeared to outperform the other catalysts.

The efficiency of a few of the catalysts was also evaluated at 0.5 mol% catalyst loading. The following order was determined; $RuCl_2$(*p*-cymene)PPh_2(NH-Propyl) > $RuCl_2$(*p*-cymene)PPh_2(OH) > $RuCl_2$(*p*-cymene)PPh_3.

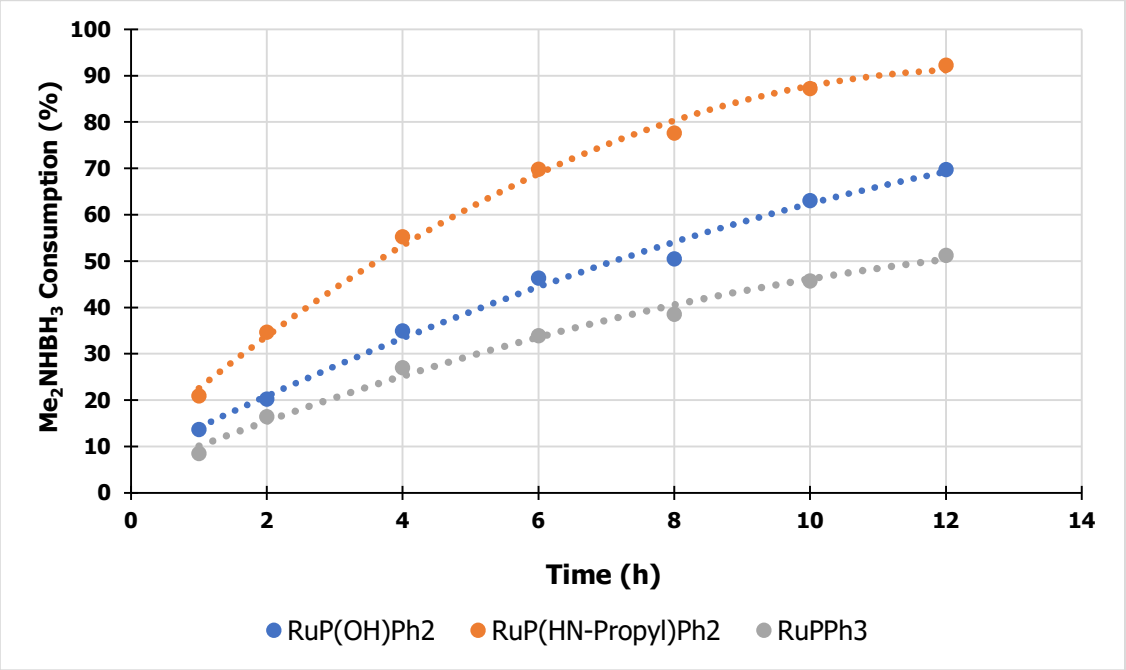

Figure 39: Catalytic Dehydrogenation of Me_2NHBH_3 with $RuCl_2$(*p*-cymene)PR_2R' catalysts (**0.5 mol%**) at 70 °C

2.4 Investigating the Kinetics of the Dimethyl Amine Borane Dehydrogenation

A kinetic profile for AB consumption was generated by plotting [Me_2NHBH_3] against time for the subset of catalysts across all loadings. The concentrations were calculated by "relative conversion" of ^{11}B integration values towards [Me_2NHBH_3]. A plot of ln([Me_2NHBH_3] vs time was linear in all cases, showing a first order dependence on Me_2NHBH_3. The reaction order with respect to the catalyst was determined through initial rate measurements of varying catalyst concentrations and keeping constant [Me_2NHBH_3] = 0.57 M. The following data is

found in Table 5. The slope of the plot of ln(v_0) vs ln([Cat]) provides the reaction rate dependence for the catalyst. For all cases, the catalyst was determined to be first order dependent. This establishes a simple rate equation for the reaction of Rate = k[DMAB][Cat].

Table 5: Initial rates (V_0) For catalysis experiments between 0.1-5 mol% loading by select catalysts. DMAB =0.57M.

		Initial Rates (V_0) (mol^{-1} dm^3 h^{-1})				
Catalytic Loading (mol%)	Catalyst Concentration (M)	$RuPPh_2$ (OH)	$RuPPh_2$ (HN-Propyl)	$RuPPh_2$ (CH_2OH)	Ru PPh_3	RuP^iPr_2 (OH)
5	0.0283	0.5636	0.5666	0.5652	0.5614	0.4989
2.5	0.01415	0.2597	-	0.2713	-	-
1	0.00566	0.1104	0.1013	0.1545	0.0642	0.0482
0.5	0.00283	0.0725	0.0765	-	0.0249	-
0.1	0.000566	0.0072	0.0109	0.0086	0.009	0.0042

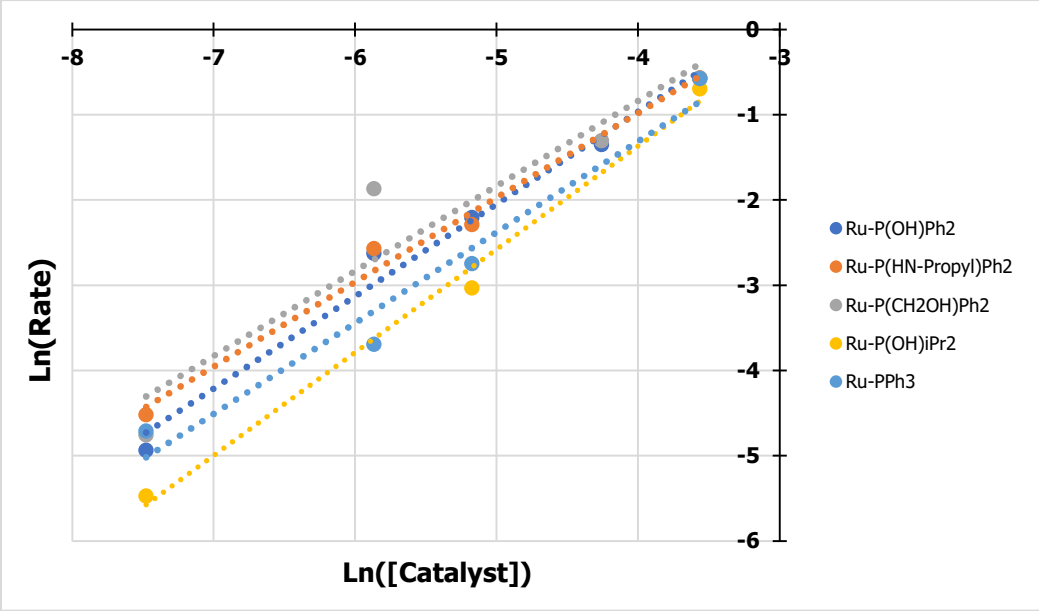

Figure 40: A plot showing the effect of the catalyst concentration on the experimental rate of reaction

2.5 Product Distribution Following Dimethyl Amine Borane Dehydrogenation Catalysis

Whilst performing the dehydrogenation of Me_2NHBH_3, the product distribution was a key factor for discussion across temperature profiles. For this, the distribution predominantly revolves around the formation of $[Me_2NBH_2]_2$ as the main dehydrocoupled product under each respective reaction parameter. It was found that under forcing conditions (70 °C and 5 mol%), $[Me_2NBH_2]_2$ is achieved in lower percentages at an average of 77% of the ^{11}B integration. Comparatively, under less harsh conditions, either lower temperature or low loading at 70 °C, $[Me_2NBH_2]_2$ is produced in >90% conversions. It is observed that this deviation is uniformly

divided across co-products; Me_2NBH_2, $(Me_2N)_2BH$, $B(OH)_3$ and NMe_2H-BH_2Cl rather than identifying a temperature related bias to one product. Additionally, over the course of the catalysis, a colour change from red/orange towards a black solution is consistent between all experiments. It is unclear whether this colour change corresponds to decomposition of the catalyst or towards a dark coloured species. Whilst there is evidence of the formation of alternate hydrides in the above reactions, the observable formation of both the *mono*- and *bis*-hydride imply stability to the complexes. At room temperature this conversion appears gradual, whereas under forcing conditions (70 °C, 5 mol%) the change occurs almost immediately. Although the colour changes cannot be linked to a certain feature of the reaction, it could be dependent on the formation of the *bis*-hydrides as this process too appears highly temperature dependent. Another key feature of the catalysis is the precipitation of colourless crystals. After multiple attempts, these were eventually isolated and analysed by IR. The 2424 cm^{-1} and 1462.72 cm^{-1} stretching band indicates the presence of B-H within the product of reaction. Additionally, ^{11}B NMR spectroscopy shows the species as a triplet at –0.69 ppm ($^1J_{BH}$ = 110 Hz) in $CDCl_3$. Precipitation out of solution could suggest the presence of poly(amino-borane). This is supported by early catalytic tests which showed the presence of the $Me_2NBH_2Me_2NBH_3$. At higher loadings and higher temperatures, this signal is not observed by NMR spectroscopy but the reaction forms a precipitate.

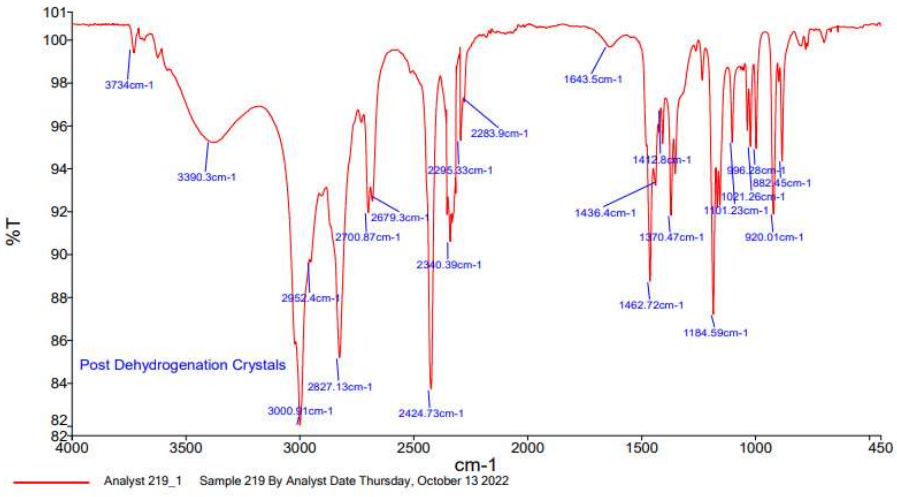

Figure 41: IR of crystals obtained after dehydrogenation of Me_2NHBH_3 with 5 mol% $RuCl_2$(*p*-cymene)PPh_2(OH)

2.6 Catalytic Dehydrogenation of Amine Boranes with $RuCl_2$(*p*-cymene)PPh_2(OH) Variants

To further explore the role of the phosphinous acid ligand in the catalysis of Me_2NH-BH_3, the effect of secondary reactants were investigated on $RuCl_2$(*p*-cymene)$PPh_2(OH)$. The aim was to prepare a cationic version of $[RuCl$(*p*-cymene)$PPh_2(OH)]^+$ and deprotonated complex $RuCl_2$(*p*-cymene)$PPh_2(O^-)$ such that differences in reactivity might indicate the possible role of ligand co-operativity.

2.6.1 Catalytic Dehydrogenation of Amine Boranes with a Cationic $RuCl_2$(*p*-cymene)$PPh_2(OH)$ complex

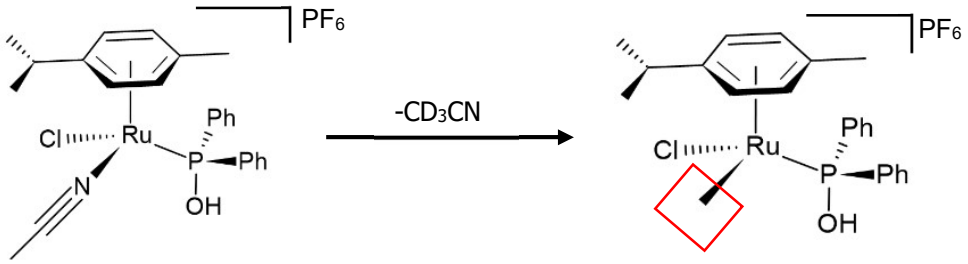

Figure 42: Formation of a vacant site in cationic complex

Cationic variants of catalysts have been shown to offer enhanced reactivities for AB dehydrogenation.[114] In our case, the preparation of a cationic version of $RuCl_2$(*p*-cymene)$PPh_2(OH)$ was motivated not only for enhanced reactivity afforded by the vacant site but by the opportunity to potentially identify the underlying mechanism. Treatment of $RuCl_2$(*p*-cymene)$PPh_2(OH)$ with NH_4PF_6 in acetonitrile at reflux for 20 minutes proved sufficient to install a vacant site, measured by an upfield ^{31}P NMR signal. It is believed that acetonitrile coordinates to the metal centre, which can readily dissociate in the presence of AB to yield an active $16e^-$ complex.

In general, the activity and selectivity of the dehydrocoupling reaction are much improved in the cationic complex, regardless of low-temperature. A catalytic (5 mol%) reaction with Me(B)-amine borane showed that the starting material could be consumed in under 20 minutes, towards $[NH$-$BMe]_3$. Moreover, duplicate sets of hydrides observed in reactions with $RuCl_2$(*p*-cymene)$PPh_2(OH)$ are eliminated – instead, only a single mono-hydride species is observed at – 8.82 ppm as a doublet (J_{HP} = 47 Hz). The ^{31}P NMR spectrum shows that besides the PF_6 signal, only one signal at 82.71 ppm, suggesting exclusive reaction pathway.

The absence of a *bis*-hydride is notable in the ^1H NMR spectrum, implying that the cationic active species is a persistent one and does not fully decompose over time. When the reaction of (Me)B-amine borane and the catalyst is held at –35 °C for 30 minutes, two *mono*-hydride species are initially observed at –8.40 ppm (J_{BH} = 52 Hz) and at –8.85 ppm (J_{BH} = 48 Hz).

However, by the time of the output of the $^{31}P\{^{1}H\}$ and ^{11}B NMR spectra, the result appears the same as previous, relaying a dependence of temperature on the mechanism. Still, the improved result could suggest that Cl abstraction by the amine borane is the rate limiting step of the reaction, whereas in the cationic version, the vacant site of the metal allows direct addition of hydrogen to the metal via σ-H-B bonding (Figure 43).

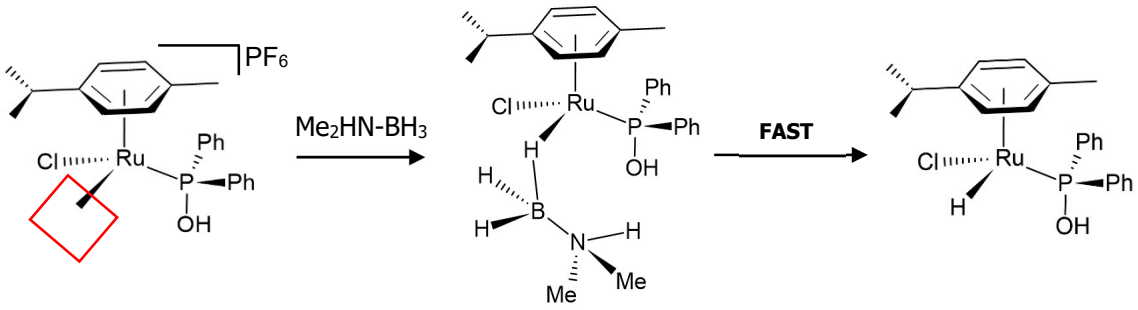

Figure 43 : Monohydride formation in cationic complex via direct Ru-H installation

In reactions of cationic catalyst with Me_2NHBH_3 initially held at –35 °C, the ^{31}P NMR spectrum indicates the presence of a single species at 129.12 ppm along with growth of a hydride (–8.17 ppm, J_{HP} = 52 Hz) in the ^{1}H NMR spectrum. The ^{11}B NMR spectrum shows that Me_2NHBH_3 remains in 85% concentration by ^{11}B integration after the first hour. This suggests an effect of the substrate on the catalytic activity. Similar to the $RuCl_2$(*p*-cymene)PPh_2(OH) catalysis at room temperature, a minor triplet at –2.16 ppm with coupling 115 Hz assigned as Me_2NH-BH_2Cl is observed. This suggests that a similar catalyst activation is occurring between $RuCl_2$(*p*-cymene)PPh_2(OH) and the cationic version. After 20 minutes at room temperature, the ^{1}H NMR spectrum shows two hydrides at –8.17 ppm (J_{HP} = 52 Hz) and –11.35 ppm (J_{HP} = 42 Hz) related to the *mono*- and *bis*-hydride respectively. After 18 h at room temperature, the ^{11}B NMR spectrum shows full consumption of Me_2NHBH_3 towards a variety of dehydrogenated products. This is faster than the reaction of $RuCl_2$(*p*-cymene)PPh_2(OH) at room temperature which took 78 h. Notably, a different product distribution is achieved in comparison to that of $RuCl_2$(*p*-cymene)PPh_2(OH) at room temperature (Figure 44). Specifically, the doublet at 27.73 (J_{BH} = 144 Hz) assigned as $(Me_2N)_2BH$ is achieved as a major product (29%) alongside $[Me_2N\text{-}BH_2]_2$ (17%). The faster consumption of Me_2NH-BH_3 and different product distribution suggest that a different catalytic regime is observed for the catalyst. This is interesting given the initial observations of Me_2NH-BH_2Cl and the *mono*-hydride which suggested a similar reaction was occurring. Additionally, the formation of $(Me_2N)_2BH$ as a major product in the cationic catalyst, indicates that the catalyst may cause B-

N bond cleavage in Me_2NH-BH_3. This may be reconciled through interaction of B-H to the Ru-centre, which activates the cleavage of $NHMe_2$.

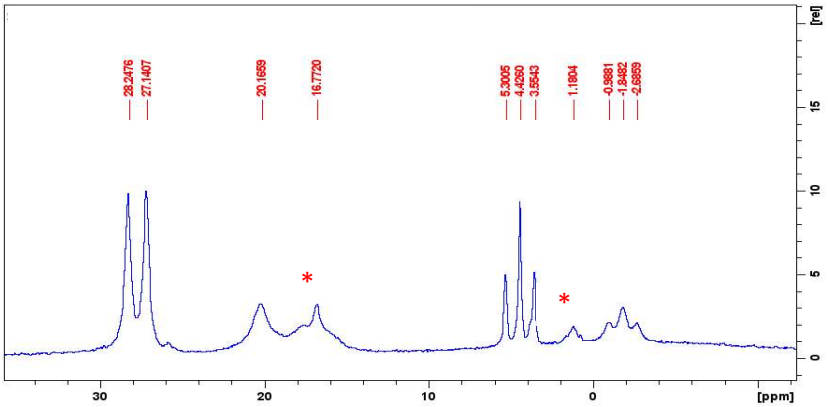

Figure 44: Product Distribution for Cationic-$RuPPh_2(OH)$ and Me_2NH-BH_3 in the ^{11}B NMR Spectrum
*Unassigned Species

2.6.2 The Effect of Base on the Catalysis of Dimethyl Amine Borane with $RuCl_2$(*p*-cymene)PPh_2(OH)

In order to further investigate the effect of the nature of the phosphine ligand on the dehydrogenation of amine boranes, a catalyst containing a deprotonated phosphinous acid moiety was utilised. The aim was to observe a difference in the catalytic activity between P(OH) and P-O^- towards Me_2NH-BH_3 over the course of the reaction. Treating $RuCl_2$(*p*-cymene)PPh_2(OH) with 1 eq. DBU as a base in THF, resulted in a new ^{31}P species upfield at 70.29 ppm in exclusively. This signal does not appear to correlate to any signals observed in the dehydrogenation of Me_2NH-BH_3 with $RuCl_2$(*p*-cymene)PPh_2(OH) conducted at room temperature. The ^1H NMR spectrum of the new complex appeared to show para-cymene signals as doublets at 5.05 ppm (J_{HH} = 5.3 Hz) & 4.89 ppm (J_{HH} = 5.3 Hz) ppm upfield shifted (shielded) relative to $RuCl_2$(*p*-cymene)PPh_2(OH). Ortho and meta protons of the phenyl phosphine also appear shifted in the new complex. Ortho and para protons appear upfield at 8.04 ppm, whilst meta protons are observed at 7.11 ppm in the deprotonated catalyst relative to 7.79 ppm and 7.39 ppm shifts in $RuCl_2$(*p*-cymene)PPh_2(OH). Furthermore, the signal tentatively assigned as the P-OH proton at 6.96 ppm in the ^1H NMR spectrum of $RuCl_2$(*p*-cymene)PPh_2(OH) is not observed after addition of base. On collection of these observations, it was anticipated that deprotonation of the phosphinous acid was successful. Therefore a 5 mol% catalytic loading was added to Me_2NHBH_3 in THF (0.5 mL) under an inert atmosphere, and was monitored by ^{31}P, ^1H and ^{11}B NMR spectroscopy. The ^{11}B NMR spectrum taken after the addition of solvent showed that dehydrogenated products were produced in under 5 minutes. Signals relating to $[Me_2NBH_2]_2$ (5.61, t, $^1J_{BH}$ = 113 Hz), $(Me_2N)_2BH$ (29.2, d, $^1J_{BH}$ =

120 Hz), Me_2NBH_2 (37.9, t, $^1J_{BH}$ = 125 Hz) and an unknown triplet at 2.48 ppm ($^1J_{BH}$ = 110 Hz) were observed in a 20% consumption of the starting material. Notably, the generation of dehydrogenated products, in this case, is much quicker than for $RuCl_2$(*p*-cymene)PPh_2(OH). The ^{31}P NMR spectrum shows that the signal at 128.4 ppm is formed in near exclusivity. Similar to the earlier cases, this appears to correlate to the growth of the active *mono*-hydride at –7.94 ppm (J_{HP} = 53 Hz) in the ^{1}H NMR spectrum. Therefore, unlike $RuCl_2$(*p*-cymene)PPh_2(OH) the formation of the *mono*-hydride is either greatly accelerated or the hydride is formed an alternate way – possibly utilising $[DBU\text{-}H]^+$.

However, as the reaction proceeds the consumption of Me_2NHBH_3 appears to slow down. The ^{31}P NMR spectrum, after 6h, shows that the signal at 128.53 ppm is consumed. ^{31}P signals similar to the catalysis of $RuCl_2$(*p*-cymene)PPh_2(OH) appear downfield at (δ, ppm); 143.87, 139.91, 134.88 and 130.41. The ^{1}H NMR spectrum also shows that the *bis*-hydride signal at –10.66 ppm (J_{HP} = 45 Hz) splits into two signals at –11.11 ppm (J_{HP} = 46 Hz) and –11.13 ppm (J_{HP} = 45 Hz) that shows the catalyst advantage is not maintained throughout the reaction and follows the reactivity of $RuCl_2$(*p*-cymene)PPh_2(OH). A graphical comparison of the conversion of $Me_2NH\text{-}BH_3$ between the two catalysts is shown below.

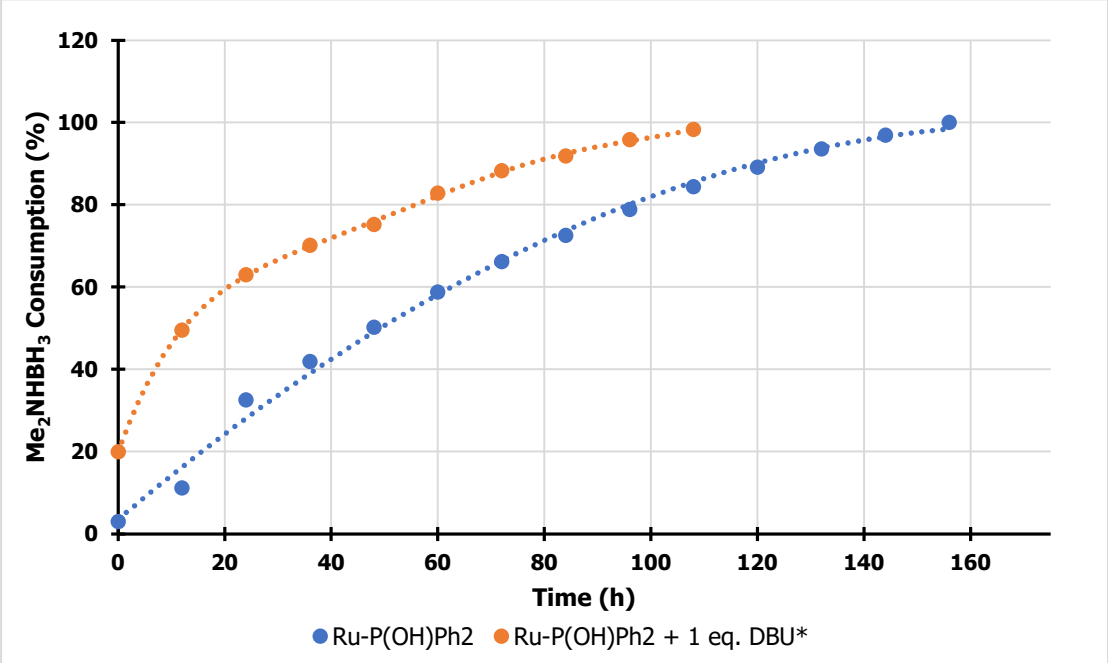

Figure 45: Comparison of Deprotonated Ru-$PPh_2(O^-)$ *vs.* Ru-PPh_2(OH) for the consumption of Me_2NHBH_3 (RT, 5mol%)

Given that the reactive profile between the catalysts appears to be the same after 6 h, this might indicate that the deprotonation of P-OH towards P-O^- is an important mechanistic step in the dehydrogenation of Me_2NHBH_3 with $RuCl_2$(*p*-cymene)PPh_2(OH). Moreover, unknown

resonances in the ^{11}B NMR spectrum between –2 ppm and 4 ppm at the start of the reaction are converted to $[Me_2NHBH_2]_2$ over the reaction. There was no additional signals in the ^{31}P NMR spectrum in this reaction compared to $RuCl_2$(*p*-cymene)PPh_2(OH). This suggests that the P-O^- moiety, even with formal charge, does not lead to the formation of transient/sustained deactivated states for the catalyst. This may be related to the proximity of Ru metal to enable effective co-operative dehydrogenation.

2.7 Stoichiometric Experiments of $RuCl_2$(*p*-cymene)PPh_2(OH) with Amine Boranes

To explore the interaction of the amine borane substrates with $RuCl_2$(*p*-cymene)PPh_2(OH), stoichiometric NMR experiments were conducted. The ambition was to assess whether a cyclic intermediate, involving a bridging hydride might be shown as a dehydrogenative mechanism for the amine boranes. Standard solutions of Me_2NHBH_3 and NH_3BH_2Me were prepared in THF or $CDCl_3$, degassed and added to Youngs Tube's containing $RuCl_2$(*p*-cymene)PPh_2(OH) (20 mg) to achieve stoichiometric ratios. Unfortunately, stoichiometric reaction of $RuCl_2$(*p*-cymene)PPh_2(OH) with H_2MeB-NH_3 and Me_2HN-BH_3 at 20 ºC did not confirm the presence of such intermediates. The ^{11}B NMR spectroscopy for reaction of H_2MeB-NH_3 with $RuCl_2$(*p*-cymene)PPh_2(OH) in $CDCl_3$ at room temperature, showed a single resonance at 33.22 ppm. This was assigned as the [BMe-NH]$_3$ trimeric dehydrogenated product. It is unlikely that the signal corresponds to B-N-O cyclic interaction. The ^1H NMR spectrum shows doublet resonances at; –8.197 ppm (J_{HP} = 54 Hz), –8.54 ppm (J_{HP} = 55 Hz), –8.88 ppm (J_{HP} = 54 Hz) and –11.05 ppm (J_{HP} = 45 Hz), relating to multiple *mono*-hydride species and a single *bis*-hydride. ^{31}P NMR spectroscopy shows the complex resonance as a broad signal at 107.06 ppm in 66%. Para-cymene signals at 5.32 ppm and 5.19 ppm are observed within the ^1H NMR spectrum which correlate to the starting material. By integrating the para cymene signals of the complex relative to the hydrides, the formation of the new hydride resonances were shown to form in less than 4% abundance. Additionally, the ^{31}P NMR spectrum shows 94.34 (s) and 136.54 (s) as a minor species. These resonances do not correlate to the hydride resonances observed in the dehydrogenation of H_2MeB-NH_3 and are not therefore believed to be hydride related.

The equivalent stoichiometric reaction in THF shows H_2MeB-NH_3 can be observed within the first ^{11}B spectrum, alongside –0.77 (br) and 32.30 (s). Similarly, a number of hydrides are observed in the ^1H NMR spectrum at –7.56 (d, J_{HP} = 48.05 Hz), –8.09 (d, J_{HP} = 54 Hz), –8.15 (d, J_{HP} = 56 Hz), –8.33 (d, J_{HP} = 57 Hz), –8.44 (d, J_{HP} = 54 Hz) ppm. The ^{31}P NMR spectrum

similarly shows that 94.36 ppm, 95.88 ppm , 96.90 ppm resonances are also observed in THF, along with a number of downfield resonances which are consistent with the formation of *mono*-hydrides in a higher concentration.

In a reaction with a secondary amine borane, Me_2NH-BH_3, a clean hydride at –7.47 ppm (J_{HP} = 54 Hz) is observed. Similarly, to the dehydrogenation experiments of Me_2NH-BH_3, this appeared to correlate to the 125.14 ppm in the ^{31}P NMR spectrum which shows the activation of the complex. The ^{11}B NMR spectrum indicates the majority of Me_2NH-BH_3 remains unreacted after 10 minutes. A triplet signal at –3.03 ppm ($^1J_{BH}$ = 120 Hz) is consistent with the formation of Me_2NH-BH_2Cl. Additionally, $(Me_2N)_2BH$ at 27.98 ppm (d, $^1J_{BH}$ = 150 Hz) is present within the spectrum. After 2 h, the ^{31}P NMR spectrum shows the signal at 124.8 ppm as a dominant species alongside 102.6 ppm as the remaining starting complex. This signal is consistent with –7.47 ppm as the dominant *mono*-hydride in the ^1H NMR spectrum, although there are several signals observed within this region; –8.48 (d, J_{HP} = 56 Hz), –8.24 (d, J_{HP} = 54 Hz), –8.47 (d, J_{HP} = 54 Hz) ppm. The consumption of Me_2NH-BH_3 in the ^{11}B NMR spectrum produces an extremely broad region between -5 and +5 ppm, which includes –3.08 ppm (t, $^1J_{BH}$ = 120 Hz). This shows that the reaction of Me_2NH-BH_3 with $RuCl_2$(*p*-cymene)PPh_2(OH) does not result in a co-operative activation of the amine-borane. Instead, Me_2NH-BH_3 acts as a halide acceptor for the activation of $RuCl_2$(*p*-cymene)PPh_2(OH). This suggests the P-OH motif is not active as a co-operative ligand towards the amine borane.

Following Me_2NH-BH_3 consumption, the ^{31}P NMR spectrum shows the starting complex remains in 72%. It was observed in the dehydrogenation of Me_2NH-BH_3 by 5 mol% $RuCl_2$(*p*-cymene)PPh_2(OH) that the *mono*-hydride detected at 125 ppm forms completely before the dehydrogenation of excess Me_2NH-BH_3. This is detected by a slight shift in the ^{31}P NMR spectrum and change in the ^{11}B NMR spectrum towards dehydrogenated products. Therefore, the addition of a further equivalent of Me_2NH-BH_3 in the stoichiometric reaction could have fully reacted with the complex to give the *mono*-hydride and further Me_2NH-BH_2Cl. Still, the stability of the mono-hydride remains in question, and the conversion to the *mono*-hydride produced additional minor resonances at 97.31 ppm, 107.3 ppm, 122.92 ppm in the ^{31}P NMR spectrum. Additionally, the ^{11}B NMR spectrum shows that Me_2NH-BH_2Cl is converted to $[Me_2N$-$BH_2]_2$ over the course of a catalytic reaction. Therefore, following the formation of the *mono*-hydride as a single resonance, Me_2NH-BH_2Cl may react further to $[Me_2N$-$BH_2]_2$ and prevent the isolation of the *mono*-hydride. To this extent, a stoichiometric reaction between $RuCl_2$(*p*-cymene)PPh_2(OH) and a tri-N-substituted amine borane which is incapable of

dehydrogenation could be suggested to eliminate this potential issue. However, an amine borane with a N-H bond may be required. Titova et al showed that the activation of the Ir-Cl bond with Me_2NH-BH_3 is initiated through a N-H···Cl interaction.[107] Thus, a reaction with a tri-substituted amine borane may present no activation of the $RuCl_2$(*p*-cymene)PPh_2(OH) pre-catalyst. Instead, a secondary amine borane of type $R^1{}_2NH$-$BHR^2{}_2$ could be preferred.

2.8 Hydride Preparation Reactions for RuHCl(*p*-cymene)PPh_2(OH) and RuH_2(*p*-cymene)PPh_3

The dehydrogenation of the amine boranes appears to be correlated to the formation and reactivity of the *mono*-hydride species. Therefore, the preparation of the *mono*-hydride and *bis*-hydride were targeted. The ambition was to isolate these species and carry out catalysis reactions of amine boranes with them.

2.8.1 Reaction of $RuCl_2$(*p*-cymene)PPh_3 with K_2CO_3 in MeOH

The preparation of the RuHCl(*p*-cymene)PPh_3 and RuH_2(*p*-cymene)PPh_3 have been previously reported using an alkali metal carbonate (1 or 2 equiv.) introduced as a base within primary alcohols.[115] Therefore, a similar reaction was attempted. The addition of $RuCl_2$(*p*-cymene)PPh_3 to a stirring methanol solution of K_2CO_3 at RT quickly afforded a yellow solution in place of a characteristic red solution. For the same reaction, Demerseman and co-workers commented a similar observation as indicative of a β-elimination pathway that affords a metal alkoxide intermediate from metal-chloride precursors.[116] The $^{31}P\{^1H\}$ NMR spectrum shows that the signal for $RuCl_2$(*p*-cymene)PPh_3 at 24.20 ppm has converted to a signal at 34.09 ppm relating to Ru(η^2-O_2CO)(η^6-*p*-cymene)PPh_3.

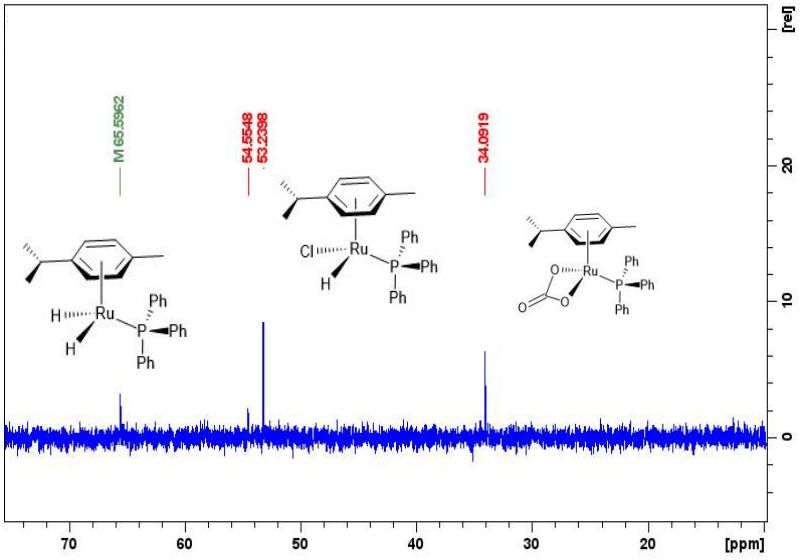

Figure 46 : Intermediates in the reaction of $RuCl_2$(*p*-cymene)PPh_3 via K_2CO_3 in MeOH

Allowing the mixture to reflux for 2 h facilitated the generation of hydride signals in the ^{1}H NMR spectrum that accompanied a secondary colour change towards light brown. After 2 h, the ^{1}H NMR spectrum reveals that both the *mono*-hydride and *bis*-hydride are formed as doublets with chemical shifts of –8.83 ppm (J_{HP} = 54 Hz) and –12.73 ppm (J_{HP} = 43 Hz). The $^{31}P\{^{1}H\}$ NMR spectrum shows besides the metal alkoxide intermediate at 34.09 ppm, the formation of equimolar signals relating to the *mono*-hydride and *bis*-hydride at 53.23 ppm and 65.59 ppm, respectively.

The selectivity towards the *bis*-hydride was improved by extending the reaction time and addition of further amount of K_2CO_3 (0.5 eq.). The ^{31}P NMR spectrum shows that the addition of more K_2CO_3 leads to the consumption of the *mono*-hydride back to the alkoxide complex Ru(η^2-O_2CO). Then, the conversion of Ru(η^2-O_2CO) towards the *bis*-hydride that occurs in methanol is expected from the reaction of the carbonato ligand with 2 molecules of methanol to generate methoxide groups alongside KCl, CO_2 and H_2O. Unfortunately, the *bis*-hydride was not isolated. This occurred from the inability to convert all the remaining metal alkoxide species at 34.09 ppm towards the *bis*-hydride and small reaction scale.

2.8.2 Reaction of $RuCl_2$(*p*-cymene)PPh_3 and $RuCl_2$(*p*-cymene)PPh_2(OH) with $NaBH_4$

The preparation of RuHCl(*p*-cymene)PPh_2(OH) was not attempted with K_2CO_3 in methanol; This is because the P-OH would react with K_2CO_3 and not lead to the isolation of the *mono*-hydride. Instead, the use of $NaBH_4$ as a reducing agent was added to $RuCl_2$(p-cymene)PPh_2(OH). Previously, Alvarez reported a procedure for the quantitative formation of [$RuH_2\{\kappa^1$-(P)-$Ph_2PC_6H_4CH_2$(=O)$\}(\eta^6$-*p*-cymene)] with $NaBH_4$ from [$RuCl_2\{\kappa^1$-(P)-$Ph_2PC_6H_4CH$(=O)$\}(\eta^6$-*p*-cymene)] after observing the species in traces for reactions with K_2CO_3. The reaction of $NaBH_4$ with $RuCl_2$(*p*-cymene)PPh_2(OH) and $RuCl_2$(*p*-cymene)PPh_3 was attempted to explore the differences in reactivity dependent on the phosphinous acid motif.

The addition of $NaBH_4$ (2.2 equiv.) to $RuCl_2$(*p*-cymene)PPh_3 in methanol led to the formation of three hydrides in the ^{1}H NMR spectrum at –6.88 (J_{HP} = 50 Hz), –7.47 (J_{HP} = 53 Hz) and –11.16 (J_{HP} = 43 Hz) in a 3:4:3 relationship. These species appeared to correlate to the resonances; 55.46 ppm (s), 52.39 ppm (s) and 64.77 ppm (s) respectively in the $^{31}P\{^{1}H\}$ NMR spectrum. Concurrently, multiple signals in the region of the C(H)=C(H)- of the para-cymene ligand were observed. These were observed as doublets at 5.69 ppm, 5.63 ppm, 5.55 ppm and 5.26 ppm and were consistent with 5.90 Hz coupling. After 1 h, the –7.47 ppm signal is the only *mono*-hydride that appears along with the *bis*-hydride at –11.16 ppm. These species appear

in 85% concentration determined by the ^{31}P NMR spectroscopy, with 75% of the mono-hydride.

For the equivalent reaction of $NaBH_4$ (2 equiv.) with $RuCl_2$(*p*-cymene)PPh_2(OH) in methanol, the inclusion of the phosphinous acid functionality resulted in a substantial decrease in hydride exclusivity and abundance. The ^1H NMR spectrum showed a doublet at –8.37 ppm (J_{HP} = 53 Hz) and a triplet at –16.60 ppm (J_{HP}= 22 Hz) as the most dominant species, although minor doublet signals are detected at –8.11 ppm (J_{HP} = 50 Hz), –7.82 ppm (J_{HP} = 45 Hz), –11.66 ppm (J_{HP} = 52 Hz). In similarity to the reaction of $RuCl_2$(*p*-cymene)PPh_3, the ^1H NMR spectrum shows the presence multiple species through the number of C(H)=C(H)- signals of the para-cymene ligand. There are two clear doublets observed at 6.26 ppm & 6.20 ppm with a 5.66 Hz coupling that correspond to the $RuCl_2$(*p*-cymene)PPh_2(OH) starting material. Additionally, nearby doublet signals at 5.70 ppm (J_{HH} = 5.60 Hz) and 5.32 ppm (J_{HH} = 5.28 Hz) will likely correspond to the formation of minor hydrides. The $^{31}P\{^1H\}$ NMR spectrum shows 118.53 ppm as the dominant new signal, followed by additional signals at 104.06 ppm, 81.69 ppm, 125.26 ppm, 182.91 ppm. The ^{11}B NMR spectra produces a sharp resonance at 18.46 ppm consistent with $B(OMe)_3$ suggesting all B-H bonds have been cleaved. Similar to $RuCl_2$(*p*-cymene)PPh_3, after 1 h the hydrides resolve to major species; –8.38 ppm (J_{HP} = 54 Hz) and –16.60 ppm (t, J_{HP} = 22.73 Hz), although neither are formed appreciably.

Diaz-Alvarez et al reported the quantitative formation of the *bis*-hydride formed via $NaBH_4$ present with the OH moiety, although the same result could not be demonstrated. This difference in success may be described by a few factors. In their case, the complex exists as [$RuCl_2\{\kappa^1$-(P)-$Ph_2PC_6H_4CH(=O)\}(\eta^6$-*p*-cymene)] prior to the reaction, therefore the aldehyde function is also reduced in to OH, simultaneous to the installation of the *bis*-hydride. Additionally, the chain length of the ligand could facilitate the attack of H^- where the OH functionality in the $Ph_2PC_6H_4CH_2OH$ ligand is situated away from the metal centre. For $RuCl_2$(*p*-cymene)PPh_2(OH), the OH functionality sits directly in the co-ordination sphere of ruthenium possibly sheltering attack. Equally, the OH functionality has direct influence on the metal centre in $RuCl_2$(*p*-cymene) through the phosphorus bond and is involved in hydrogen bonding with Cl ligands which can offer stability against H^-.

2.8.3 Reaction of $RuCl_2$(*p*-cymene)PPh_2(OH) with Et_3SiH

Et_3SiH was tried as an alternate reducing agent to $NaBH_4$ to produce the *mono*-hydride; RuHCl(*p*-cymene)PPh_2(OH). Bagh and co-workers showed that Ru-triazolyidene complexes

with Et_3SiH at 25 ºC to give the corresponding Ru-hydride complexes.[117] The ^{31}P and ^{1}H NMR spectrums of the initial reaction between Et_3SiH and $RuCl_2$(*p*-cymene)$PPh_2(OH)$ in DCM showed no reaction between the reactants. The starting complex in the ^{31}P NMR spectrum at 107.2 ppm showed no deviation even after extended reaction times (22 h). Additionally, the ^{1}H NMR spectrum indicates the presence of both starting reagents unreacted in solution. To try and force reactions between the reagents, an excess of Et_3SiH (4.2 equiv.) was added to the mixture and allowed to stir for an additional 2 h at 45 ºC. The ^{31}P NMR spectrum indicates the development of minor resonances in 15% concentration relative to the starting material. Notably, the signal at 20.16 ppm may indicate the presence of free phosphine. The ^{1}H NMR spectrum indicates an unappreciable amount of the *mono*-hydride at –8.25 ppm (J_{HP} = 52 Hz) and sharp singlet at –10.26 ppm. The formation of a singlet in the ^{1}H NMR spectrum correlates towards a hydride with no ^{31}P coupling, indicating the loss of the phosphorus ligand. To this extent, the hydrido bridged complex [{(η^6-*p*-cymene)RuCl}$_2$(μ-H-μ-Cl)] is reported a singlet that is observed at δ_H –10.18 ppm.[118] Under more forcing conditions using 10 eq of Et_3SiH to $RuCl_2$(*p*-cymene)$PPh_2(OH)$, produces only a minor improvement in the formation of the *mono*-hydride. There is a minor signal at –8.23 ppm (J_{HP} = 54 Hz) in the ^{1}H NMR spectrum and 128.14 ppm in the ^{31}P NMR spectrum.

As the extent of hydride formation can depend on the reaction temperature, the use of alternate solvents (THF, toluene) with higher boiling points was investigated. Performing the reaction at 45 ºC in THF initially appeared to show a similar reluctance for reaction. Although, the formation of a minor *mono*-hydride at –8.23 (J_{HP} = 53 Hz) is accompanied by 128.49 ppm in the ^{31}P NMR spectrum (3%) as an exclusive event. Extending the heating to 70 ºC causes a notable increase in the 129.12 ppm signal in the $^{31}P\{^{1}H\}$, as well as other trace alternatives at 116.82 ppm, 124.91 ppm, 130.11 ppm. Heating to 70 ºC also induces the –8.23 ppm hydride to grow. However, the reaction is non-selective and singlets indicating the loss of phosphorus are observed at –11.94 (s), –13.67 (s), –15.72 (s) along with a triplet resonance at –17.73 with coupling of 15 Hz. Heating to 70 ºC directly with 4.6 equivalents at a lower concentration showed an improvement of exclusivity for the *mono*-hydride up to a 20% conversion before following a similar regression to the prior reactions. The signal at –13.67 (s) was assigned as the Ru(IV) mononuclear dihydride complex [(η^6-*p*-cymene)Ru$(H)_2(SiEt_3)_2$] as the complex was assigned by Chatterjee in a reaction between [(Ru(*p*-cymene)$Cl_2)_2$] and Et_3SiH.[118] Reactions with toluene as a solvent allowing heating to 100 ºC did not produce any improvement in selectivity.

2.9 Mechanistic Proposal for the Catalytic Dehydrogenation of Dimethyl Amine Borane with $RuCl_2$(*p*-cymene)PPh_2(OH)

The earlier examples of ligand co-operative catalysts were transition metal complexes containing Bronsted basic ligands and acidic metal centres. Within these mechanisms, H_2 release from the amine borane is promoted by the transfer of the hydridic hydrogen in the BH moiety to the acidic metal centre and the transfer of proton from the NH moiety to the basic ligand functionality. Based on literature articles[77-82], a few generic mechanistic proposals were considered for the dehydrogenation of amine boranes by phosphinous acid catalysts.

Mechanism 1 involves elimination of hydrogen from a monohydride state to give κ^2-form intermediates, that can support a bifunctional transfer of hydridic BH to the metal centre and NH proton to the P-O/P=O functionality. This is similar to ***Mechanism 2***, inspired by Takahashi, [78] where coordination of AB to the Ru-centre gives a cyclic transition state in which the $H^{\delta+}$ of NH_3 is abstracted by the phosphinous ligand and B-$H^{\delta-}$ is activated by Ru. H-H bond formation can then occur via a concerted process to produce a dihydrogen complex that can dissociate and regenerate the active species.

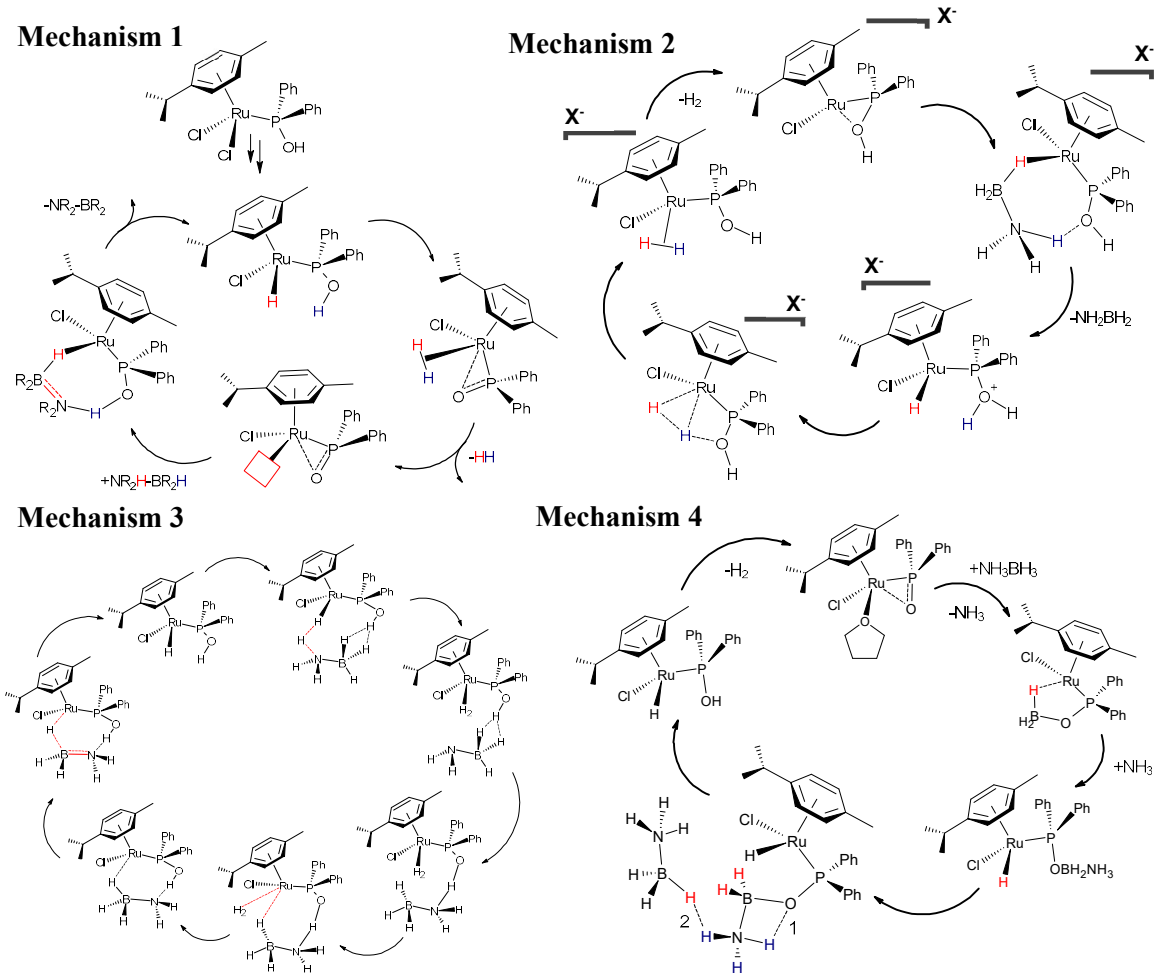

Figure 47 – Mechanistic ideas for the dehydrogenation of amine boranes with $RuCl_2$(*p*-cymene)PPh_2(OH)

Mechanism 3, inspired by Gluer *et al* [77], features complexed-H_2 activation by AB rather than an intermolecular catalytic process to give κ^2-form intermediates. ***Mechanism 4*** considers B-H bond activation to yield Ru-H and PO-$BH_2(NH_3)$ instead of synergistic activation, as described by Liu[85] and Zhou[99]. Given the reaction is performed in the absence of water, bond breakage of the hydroboration intermediate could be expected to result from transfer of $H^{\delta+}$ of NH_3 in a 4-membered concerted transition state (1). Alternatively, outer sphere interactions of complexed-AB with un-coordinated substrate might lead to a chain length regime (2) or deactivation at stoichiometric levels.

By exploring the reactivity of Me_2NH-BH_3 with $RuCl_2$(*p*-cymene)PPh_2(OH) in various reactions, several mechanistic insights can be envisaged. We showed that during the catalytic reactions of Me_2NH-BH_3 with 5 mol% $RuCl_2$(*p*-cymene)PPh_2(OH) at room temperature, that the activation of $RuCl_2$(*p*-cymene)PPh_2(OH) to the *mono*-hydride RuHCl(*p*-cymene)PPh_2(OH) is produced by halide abstraction by the amine borane. This was also demonstrated in the stoichiometric reaction where Me_2NH-BH_2Cl was produced as the sole product. The ^{31}P NMR spectrum shows that this process, detected as the change from 102 ppm to 125 ppm, precedes any detection of dehydrogenated products. This is consistent in the $RuCl_2$(*p*-cymene)P^iPr_2(OH) reaction, which was shown to be slower than the phenyl analogue. Between these reactions, the P-OH motif does not appear to participate with the amine borane, suggesting no co-operativity with the metal centre. Once the *mono*-hydride is formed, dehydrogenated products, namely $[Me_2NBH_2]_2$, are observed in the ^{11}B NMR spectrum. This is followed by the generation of *bis*-hydride. Over the reaction course, the *mono*-hydride is consumed to give the *bis*-hydride. Unfortunately, the preparation of the *mono*- and *bis*-hydrides were unsuccessful.

The catalysis of Me_2NH-BH_3 with both the cationic version and deprotonated complex of $RuCl_2$(*p*-cymene)PPh_2(OH) showed that dehydrogenated products of Me_2NH-BH_3 could be achieved faster. For the cationic version, the vacant site within the complex should facilitate the formation of the *mono*-hydride, likely through the direct addition of B-H to the acidic metal centre. In comparison, the addition of DBU to achieve a deprotonated complex equally showed dehydrogenated products of Me_2NH-BH_3 within 5 minutes. The ^{31}P NMR spectrums confirms that the reaction proceeds through the formation of the *mono*-hydride. Additionally, the reaction appears to follow the pathway of $RuCl_2$(*p*-cymene)PPh_2(OH) which doesn't suggest a different catalytic regime. This was not the case for the cationic catalyst in which a different product distribution in the ^{11}B NMR spectrum was observed. This was suggestive that deprotonation of the P-OH moiety is part of the mechanistic pathway of $RuCl_2$(*p*-

cymene)PPh_2(OH) catalysed Me_2NH-BH_3. To this extent, the reactivity of the deprotonated complex with Me_2NH-BH_3 suggests an initial reactivity between P-O^- and Me_2NH-BH_3.

It is unclear whether the formation of $[Me_2NBH_2]_2$ occurs on the metal centre or off the metal centre. The ^{11}B shows that $[Me_2NBH_2]_2$ is the main product of the dehydrogenation. However, reconciling the observation of a precipitate through the catalysis suggests the presence of boron-containing products not detected in the ^{11}B NMR spectrum. This is believed to be dependent on the formation of polymeric -$[Me_2NBH_2]_n$-.

In culmination of these observations, a mechanism is proposed for the dehydrogenation of Me_2NH-BH_3 by $RuCl_2$(*p*-cymene)PPh_2(OH). The mechanism starts with the activation of $RuCl_2$(*p*-cymene)PPh_2(OH) to the *mono*-hydride by halide abstraction of Me_2NH-BH_3. Given that dehydrogenation of Me_2NH-BH_3 was observed with P-O^-, this suggests that this is the active species. Therefore, hydrogen loss from the catalyst is proposed by the formation of a κ^2 intermediate. This species is expected to be highly reactive and is not detected by ^{31}P NMR spectroscopy. Although signals assigned to this bonding type are observed in $RuCl_2$(*p*-cymene)$PPh_2(CH_2OH)$ showing this reactivity can occur. From there, the amine borane interacts with the catalyst synergistically, with B-H addition to the metal centre and N-H addition to the phosphinous acid. The formation of the *bis*-hydride is believed to be dependent on the activation of the second chloride equivalent by excess Me_2NHBH_3.

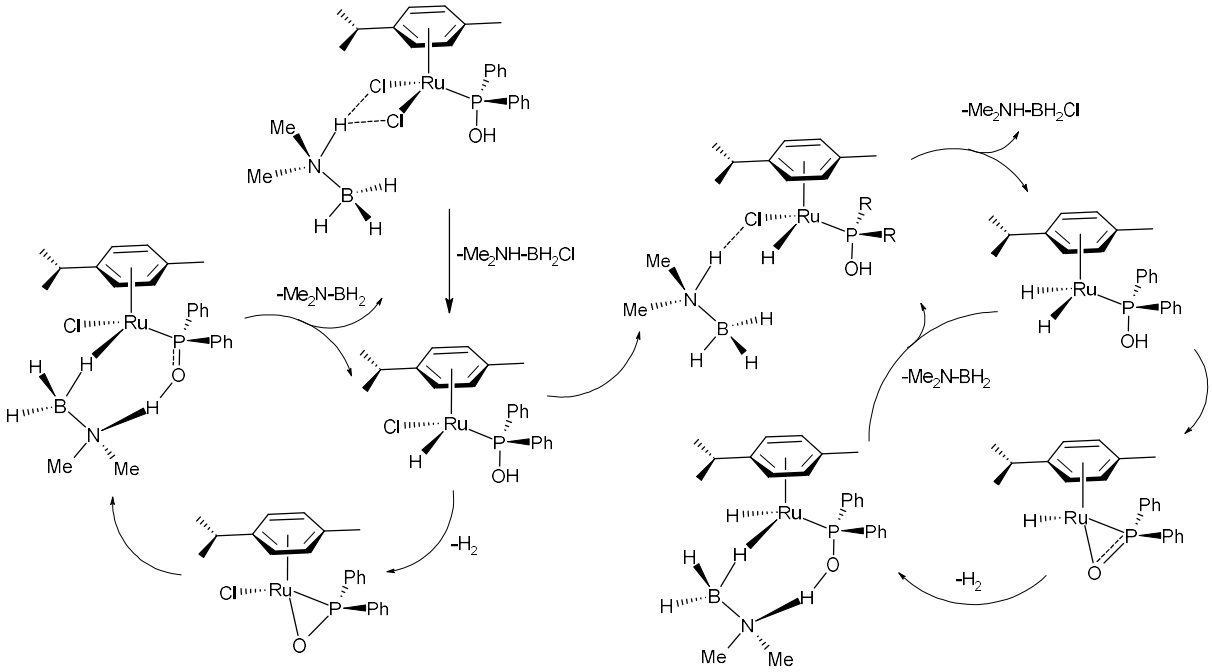

Figure 48 – Mechanistic proposal for the dehydrogenation of Me_2NHBH_3 with $RuCl_2$(*p*-cymene)PPh_2(OH)

It is not certain whether the *bis*-hydride forms directly from the *mono*-hydride. The reaction of $RuCl_2$(*p*-cymene)PPh_2(HN-Propyl) showed that the dehydrogenation of Me_2NH-BH_3 can be achieved without the formation of the *bis*-hydride. This suggests that the *bis*-hydride forms through reactivity of the *mono*-hydride.

3.0 Comparison of the Catalytic Ability of Phosphinous Acid Catalysts to Literature Catalysts

For the catalysis of (Me)B-amine-borane, only two examples are reported in the literature. Campbell and co-workers reported that 1.5 eq H_2 could be released in as little as 10 minutes for (Me)B- amine borane catalysed by a $CoCl_2$ catalyst (5 mol%) at 80 ºC in diglyme.[119] After 36 h, 2,4,6-trimethylborazine [NH-BMe]$_3$ was achieved as the sole resonance in the ^{11}B spectrum. Manners reported the dehydrogenation of (Me)B-amine borane in the presence of [Rh(COD)(μ-Cl)]$_2$ (2.5 mol%, 20 ºC) and IrH_2POCOP (5 mol%, 20 ºC). [Rh(COD)(μ-Cl)]$_2$ produced [NH-BMe]$_3$ as the sole resonance after 1 h, while IrH_2POCOP (5 mol%, 20 ºC) produced [NH-BMe]$_3$ (90%) and $(NH)_2BMe$ (10%). Skeletal nickel was also tested as a catalyst, although led to a significant decrease in activity. The consumption of (Me)B-amine borane by $RuCl_2$(*p*-cymene)PPh_2(OH) and $RuCl_2$(*p*-cymene)$PPh_2(CH_2OH)$ was achieved in under 2 h.

The dehydrocoupling of dimethyl amine borane is well reported in literature by catalysts that can operate in 0.1 mol% loadings. The popular [Rh(1,5-cod)(μ-Cl)]$_2$ has been reported to dehydrogenate Me_2NH-BH_3 in a 0.5 mol% loading in 8 h at 25 ºC. Similarly, [Cp*Rh(μ-Cl)Cl]$_2$ is active for the transformation at 0.5 mol% completing after 112 h at 25 ºC.[120] Generally, (hydrogen bearing) metal complexes incorporating proton-responsive ligands have been proved to be superior catalysts for the dehydrogenation of amine-boranes. To this extent, Sewell and co-workers showed that even simple complexes such as $Rh(PCy_3)_2H_2Cl$ can convert Me_2NHBH_3 in 1.7 h to reach 95% conversion in 2 mol% loading.[121]

To provide a meaningful comparison to a ligand co-operative catalyst, the conversion of Me_2NH-BH_3 in this work can be compared to trans-[Ru(H)$_2$(PMe_3)(PNP^H)] developed by Gluer et al. Equally, the concentration of Me_2NH-BH_3 used in the catalysis of Me_2NH-BH_3 in this case was similar to the research conducted by Gluer. Reactions were carried out at 0.54 M, which is highly comparable to our own case of 0.57 M. Whilst full completion is observed in 28 h, the catalyst shows an initial TOF of 3600 h^{-1} at 2 mol%, with release of 70% hydrogen content (0.7 equiv. H_2) in under a minute. Further, 1 mol% catalysis delivered <0.6 mol% H_2 in under a minute; therefore, the system appears to far exceeds this one. A suggestion may be

drawn to the fact that Catalysts **1-5** undergo activation by Me_2NHBH_3, while $[Ru(H)_2(PMe_3)(PNP^H)]$ exists in its active form. Even so, examples using the deprotonated complex of $RuCl_2$(*p*-cymene)PPh_2(OH) which showed marked improvement at the start underperforms the conversions demonstrated by ligand-cooperative catalysts.

3.1 Considerations to the Reproducibility of Dimethyl Amine Borane Catalysis

There are three main factors that should be discussed as impediments to the catalysis experiments; (1) Effect of Water (2) Complex Stability (3) Catalytic Loading.

3.1.1 The Effect of Water on the Catalysis

During the catalysis reactions of dimethyl amine borane, the ^{11}B NMR spectrum shows that a signal at 21 ppm is produced as a by-product. Titova and co-workers described that broad signals at 21 ppm in the ^{11}B NMR spectrum are due to the hydrolysis of reaction intermediates towards (poly)boric acid.[107] THF used in the catalysis reactions was stored over molecular sieves, degassed, and held in an N_2 atmosphere to minimise water content. However, successive catalytic tests sourced from the stored THF trend to show higher water content; measured indirectly as the formation of (poly)boric acid. Not only does this reflect within the product distribution, but influences the overall reactivity of the catalytic run. For example, a repeat 5 mol% reaction of $RuCl_2$(*p*-cymene)PPh_2(HN-Propyl) with Me_2NHBH_3 conducted at room temperature showed a 41% consumption of Me_2NHBH_3 to dehydrogenated products featuring a 7.5% (poly)boric acid content after only 12h. This vastly outperforms the other catalysts. Additionally, supplementary ^{31}P signals are recorded as 20.79 ppm and 96.85 ppm, the latter of which corresponds to the emergence of the corresponding dihydride (–10.69, J_{HP} = 43 Hz) for $RuCl_2$(*p*-cymene)PPh_2(HN-Propyl) in the ^1H NMR spectrum. For most catalysis, the formation is (poly)boric acid is limited to <6% to enable fair comparison.

3.1.2 Issues Relating to the Stability of Complexes in THF

To evaluate the performance of lower loadings (0.1|0.5|1 mol%) for catalysts **1-5**, standard solutions were prepared. These consisted of 5 mg of the catalyst in 0.5 mL THF, enabling the correct extraction of catalyst by micro syringe (100 µL). As prepared, all standard solutions appeared as orange/red solutions; although after as little as 24h appeared to darken towards a green colour. Biancalana and co-workers commented that $RuCl_2(\eta^6$-*p*-cymene)(κP-Ph_2PR) (R = Phenyl/Phenoxy) complexes are not indefinitely stable in chloroform upon air contact, progressively turning from red to green. They identified that $RuCl_2$(*p*-cymene)PPh_3 could afford crystals of the dinuclear, mixed valence Ru^{II}-Ru^{III} species $[Ru(\mu\text{-}Cl)_3(\eta^6$-*p*-

cymene)$RuCl_2$(κP-PPh_3)] at RT in air. Thus, a similar degradation could be expected for catalysts **1-5** in THF upon air exposure. This again, creates an opportunity for alternate catalytic pathways and does appear to alter the reaction course in experiments. This is clearly observed in 1 mol% loadings of stored-$RuCl_2$(*p*-cymene)PPh_3 which began to outperform phosphinous catalysts. After 1 h, DMAB was consumed up to 70% towards $[Me_2NBH_2]_2$ (53%); far beyond the catalytic potency shown at other intervals. In addition, (poly)boric acid is observed as 9% of the mixture showing the result is likely a combination of contributing factors. The ^{31}P shows signals present at 24.46 ppm, 67.11 ppm and 66.00 ppm. While the last two are certainly dihydride species, the 24.46 ppm lies close to the signal for the $RuPPh_3$ complex which is unlikely to observed in high amounts given the catalytic display. It could be proposed that the enhanced reactivity is direct result of cleavage of the Ru^{II}-Ru^{III} species to give catalytically active Ru(III) and a similar Ru(II) complex. After 3 h, DMAB was consumed in 98%.

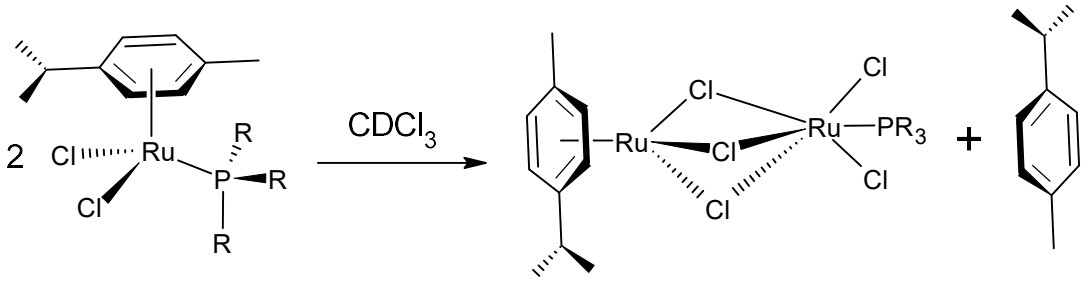

Figure 49: Degradation pathway for Ru-PPh_3 on air exposure

3.1.3 Issues Relating to Catalyst Loading

For <1 mol% systems, aliquots of catalysts were taken by micro syringe from 0.5 mL standards. For 1 mol%, 149-193 μL was the range required of catalysts **1-5**, with amounts decreasing to as little as 15-19 μL for 0.1 mol%. Given this, it is reasonable to expect errors were introduced for achieving the correct loading.

4.0 Conclusions & Future Work

4.1 Conclusions

Ammonia removal from coke oven gas (COG) is integral for the maintenance of TATA Steel Port Talbot and creates a sizeable feedstock for hydrogen storage utilization. Current washing processes create the potential for the acquisition of ammonia within concentrated NH_4^+ aqueous solutions or as NH_3 following incineration at flare stacks, both of which are conducive to amine-borane synthesis. Still, utilization of component waste NH_3 for amine-boranes would require consideration towards the purity, contaminants and stability of reactants and products,

all of which may be influenced by choice of a substituted borane partner. For industrial application at TATA Steel, the ability of the amine borane to reversibly release/gain H_2 exclusively over many cycles would be a key metric to establish. Unfortunately, the synthesis of amine borane substrates, such as NH_3-BH_2(*m*-$(CF_3)_2C_6H_3$) and NH_3-$BH(Et)_2$ in which these characteristics might be favoured were limited due to high reactivates. Thus, the catalytic activation of H_2 from NH_3-BH_2Me & NMe_2H-BH_3 employing ruthenium para-cymene catalysts was also investigated. NH_3-BH_2Me showed that substituent redistributions were possible at elevated temperatures along with the release of H_2. Therefore, although thermolysis of the amine borane would be the simplest method of hydrogen liberation at TATA Steel, the product variety detracts from the reusability of the system. Practicality as a hydrogen storage material would depend on the release of hydrogen at ambient conditions, controlled activation, and release of pure H_2. Catalytic activation of Me(B)-amine borane with $RuCl_2$(*p-cymene*)PPh_2(OH) showed improved product selectivity determined by ^{11}B NMR spectroscopy. The activation of H_2 in these reactions was shown to be possible at room temperature from Me(B)-amine borane and dimethyl amine borane substrates, in difference to control experiments which showed the amine boranes are stable in solution at room temperature. Conducting catalysis at 70^{o}C showed that the rate of hydrogen release could be increased across the catalyst group which is more practical for TATA Steel where hydrogen storage/demand would be required at scale. Further, the use of catalytic loadings reduced to 0.1 mol% were explored. This is an important aspect to better understand to the catalytic efficiency, as well as explore the cost implications of using Ru-based catalysts at TATA Steel. Moreover, the study of the catalytic activation of H_2 for the catalyst subset did serve to better understand their activation/role. A bifunctional ligand co-operative mechanism was anticipated for the activation of (Me)B-amine borane via $RuCl_2$(*p*-cymene)PPh_2(OH); comprised of the transfer of hydridic BH to the metal center and NH proton activation to the basic oxygen functionality. A literature review showed these mechanisms to be possible, although the direct activation of amine-boranes via a phosphinous acid motif in the coordination sphere of a metal has not been previously reported. Minor detection of metallacycle-type hydrides also suggested an alternate catalytic regime, though no hydroboration intermediates (deactivation) were not detected. The installation of a reactive monohydride was shown to succeed through the substitution of B-H with Cl to generate NH_3BH_2Cl in reactions. Comparatively, this process is well defined in Me_2NH-BH_3 catalysis forming Me_2NHBH_2Cl as a distinct pre-activation to any dehydrogenation products. It is interesting that N-H···Cl interactions are not accompanied by simultaneous P-OH activation of B-H, suggesting that P-OH as a moiety does not participate in ligand cooperation.

Secondary, targeted isolation of Ru(P-OH) hydrides were unsuccessful with strong reducing agents such as $NaBH_4$ and Et_3SiH, interpreted as strong intramolecular hydrogen bonding between O-H···Cl. The same hesitancy was not observed in Ru-PPh_3 reaffirming the critical role of P-OH in defining metal-substrate interactions. Still, the *mono*-hydride was assigned as the active species for dehydrogenation based on the previous observations. To this extent, catalytic rate differences observed between $RuCl_2$(*p*-cymene)PPh_2(OH) and $RuCl_2$(*p*-cymene)P^iPr_2(OH) are explainable by the formation and potency of the resulting monohydride. While the ^{31}P NMR spectrums informs that the monohydride formed as pre-activation and the monohydride involved in dehydrogenation are not equivalent, this does not constitute ligand co-operativity. However, reactions related to deprotonating $RuCl_2$(*p*-cymene)PPh_2(OH) prior to catalysis showed remarkable improvement in reactivity and formation of the "active" monohydride immediately. This suggests that is may be P-O^- that can act as a co-operative partner to the metal. Additionally, the mechanistic regime adopts the profile of untreated $RuCl_2$(*p*-cymene)PPh_2(OH) suggesting the species is an important immediate within $RuCl_2$(*p*-cymene)PPh_2(OH) catalysis. An equally enhanced rate was observed for reactions of DMAB with cationic $RuCl_2$(*p*-cymene)PPh_2(OH), although lead to a different product distribution suggesting mechanistic variation. While catalytic differences were observed for $RuCl_2$(*p*-cymene)$PPh_2(CH_2OH)$ and $RuCl_2$(*p*-cymene)PPh_2(HN-Propyl), namely the involvement of κ^2-(P,O) bonding modes and exclusivity to the monohydride respectively, the same ^{11}B product distribution was achieved across all catalysts. ^{11}B monitoring of the solution showed $[Me_2NBH_2]_2$ in 90% selectivity's though observation of precipitate revealed the likely formation of (poly)amino-borane as a reactionary by-product. Kinetic differences were explored between catalysts through "relative conversions" of ^{11}B NMR integrations of $[Me_2NHBH_3]$. Both the catalyst and Me_2NHBH_3 were found to be first order with respect to the reaction, and a basic rate equation was devised; Rate = k[Cat] $[Me_2NHBH_3]$. Temperature dependencies of the reaction were also explored through Arrhenius and Eyring plots. ΔH of catalytic reactions between Me_2NHBH_3 with $RuCl_2$(*p*-cymene)PPh_2(OH), $RuCl_2$(*p*-cymene)PPh_2(HN-Propyl) and $RuCl_2$(*p*-cymene)$PPh_2(CH_2OH)$ were experimentally evaluated as 77.03 kJ mol^{-1}, 83.76 kJ mol^{-1} and 86 kJ mol^{-1} respectively. Additionally, the absence of the dihydride in Ru(N-Propyl) showed that its formation was not caused by oxidative addition of H_2 and likely results from the secondary abstraction of chloride by DMAB substrate. Still the mechanism and involvement of the P-OH motif is not definitively assigned, and would need to be further corroborated. Further, the reusability of the catalyst would also be of interest to define as this would be a key metric for TATA Steel. A catalyst that could be used multiple

times without degradation would enable significant cost savings prompting viability. In reactions with $RuCl_2$(p-cymene)PPh_3, the deactivation towards an inactive BH_4^- complex was detected by ^{11}B NMR spectroscopy, whereas no such products were determined for the phosphinous acid catalysts which shows improvement of the catalyst class. As both the catalyst and amine boranes are air-stable, their reactivity under air would be of interest to assess as this would increase viability at TATA Steel and limit expenditure for specialised procedures such as N_2 atmosphere. Thus, this work established that H_2 release could be promoted from a subset of Ru-based phosphinous acid catalysts and highlighted the potential mechanism of action. For TATA Steel, the reusability of the catalysts and regeneration of the amine borane would need to be demonstrated before consideration. Reactivities using cheaper metal alternatives with the same functionality would also be interesting to explore as a consideration to the cost application.

4.2 Future Work

A list of potential experiments are listed below that could serve as investigative points for further research. These reactions should help to better understand the catalytic system.

1) **The Isolation of the RuHCl(*p*-cymene)PPh_2(OH) *mono*-hydride**

Method 1: Stoichiometric Reaction of $RuCl_2$(*p*-cymene)PPh_2(OH) w/ Me_2NH-BH_3

In the stoichiometric conducted previously, it could have been possible to isolate the hydride exclusively if further equivalents of Me_2NHBH_3 were added. A repeat experiment would therefore be of interest; where should the hydride be isolated, catalytic tests would be improved.

Method 2: Hydride Preparations using $[RuCl_2(p\text{-cymene})]_2$ to $[RuH_2(p\text{-cymene})]_2$

An alternate way to prepare the hydrides for these complexes was thought about. As the P-OH motif of the phosphine ligand seemingly prevents the addition of H^- to the complex, the formation of Ru-H may have to occur prior to the phosphine. Chatterjee showed that one equivalent of Et_3SiH to the $[RuCl_2(p\text{-cymene})]_2$ starting complex resulted in the quantitative formation of the mono hydrido bridged hydride species; $[\{\eta^6\text{-}p\text{-cymene})RuCl_2\}_2(\mu\text{-H-}\mu\text{-Cl})]$. The addition of the phosphinous acid ligand to this complex may result in the formation of the *mono*-hydride and starting complex in equimolar amounts. Although, a different reactivity may be achieved. The addition of two equivalents of Et_3SiH may result in the formation of the

[RuH_2(*p*-cymene)]$_2$ complex. Addition of the phosphine ligand may similarly result in the cleavage of the dimer and isolation of the *bis*-hydride.

The complex [RuH_2(*p*-cymene)]$_2$ has been previously reported to be formed from [$RuCl_2$(*p*-cymene)]$_2$ by Zsigmond and co-workers.[122] In this case, K_2CO_3 in methanol was used as the hydride source, in similarity to the reaction above. Again, should the [RuH_2(*p*-cymene)]$_2$ complex be quantitative in solution, then addition of the phosphine ligand may result in the formation of the bis hydride.

2) Explore the Reusability of the Catalyst

It would be of interest to discover whether the catalyst was active over many dehydrogenation cycles of Me_2NHBH_3 for use at TATA Steel. If the catalyst was only active for one cycle, then the system would not be very appealing. However, if the catalyst can dehydrogenate fresh amine borane, it would be advantageous in terms of cost and sustainability. The key metric in this case would be whether the catalyst showed the same catalytic activity or a loss of catalytic activity. This could be assessed by ^{11}B NMR measurements to record the consumption of the amine-borane. A standard of known concentration would also be required in the reaction mixture.

3) A Reaction of $RuCl_2$(*p*-cymene)PPh_2(OH) with Me_3N-BH_3

A reaction with a tri-N-substituted amine borane could serve to prove the formation of the pre-catalyst is dependent on an initial N-H…Cl interaction. If there is no N-H bond to activate the complex, no catalytic activity should be observed.

4) Testing of $RuCl_2$(p-cymene)PPh_2(OH) with NH_3BH_3

Although Me_2NHBH_3 is investigated for mechanistic studies, ammonia borane is the only substrate with a high enough H_2 capacity to be used as a valid storage material. Therefore, the catalytic ability with AB would be of interest to assess the catalytic activity and selectivity.

5) Testing the performance of P-OMe Catalysts in Comparison to P-OH to Compare Catalytic Activity.

In the above mechanism, the P-OH functionality is expected to play a role in the dehydrogenation of the amine-borane. Therefore, another way to investigate the importance of the P-OH unit is theorised using a methylated P-O functionality. If P-OMe complex rapidly underperformed their P-OH counterparts, this may be suggestive of a role of the OH in the

dehydrogenation of Me_2NHBH_3. Additionally, a negligible difference in catalytic activity; might disapprove any advantage of the P-OH system. Similarly, the preparation of this complex should be the same as the other complexes from $[RuCl_2(p\text{-cymene})]_2$. The addition of the methoxydiphenylphosphine ligand to $[RuCl_2(p\text{-cymene})]_2$ should result in the isolation of the complex. The procedure has been previously reported by Biancalana et al.[113]

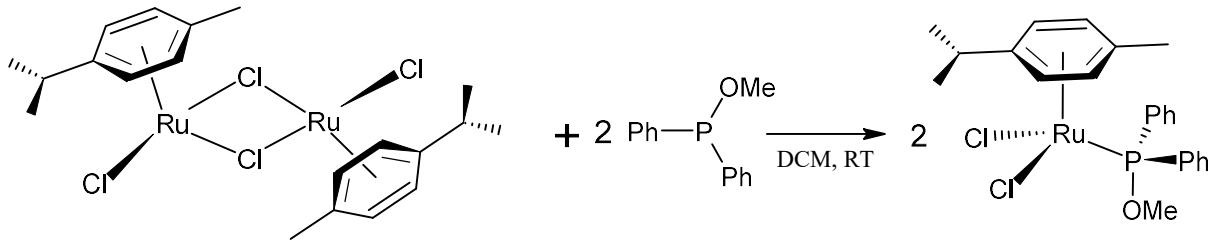

Figure 50 – Preparation of a methylated phosphinous acid catalyst; $RuCl_2$(p-cymene)PPh_2(OMe)

References:

1. D.J. Grant, M.H. Matus, K.D. Anderson, D.M. Camaioni, S.R. Neufeldt, C.F. Lane, D.A. Dixon, *J. Phys. Chem. A*, 2009, **113**, 6121-6132
2. D.J. Heldebrant, A. Karkamkar, J.C. Linehan, T. Autrey, *Energy Environ. Sci.*, 2008, **1**, 156–160
3. J.E. Seo, Y. Kim, Y. Kim K. Kim, J.H. Lee, D.H. Lee, Y. Kim, S.J. Shin, D.M. Kim, S.Y. Kim, T. Kim, C.W. Yoon S.W. Nam, *J Power Sources*, 2014, **254**, 329-337
4. Y. Kim, Y. Kim, S. Yeo, K. Kim, K. Jung-Eun Koh, J.E. Seo, S.J. Shin, D.K. Choi, C.W. Yoon, S.W. Nam, *J Power Sources*, 2013, **229**, 170-178
5. TATA Steel Port Talbot, [Internet], [cited 10/03/2023], [1Screen], Available From https://www.tatasteeleurope.com/corporate/news/160000-tonnes-of-co2-savings-from-tata-steel-blast-furnace-improvement-programme
6. Green Steel, UK Parliament. POSTNOTE 672, May 2022
7. TATA Steel Sustainability Report 2020/2021 Tata Steel's UK Business
8. G. Moral, R. Ortiz-Imedio, A. Ortiz, D. Gorri, A. Ortiz, *Ind. Eng. Chem. Res.*, 2022, **61**, 6106-6124
9. C. Serrenho, Z. S. Mourão, J. Norman, J. M. Cullen, and J. M. Allwood, *Resour. Conserv. Recy.,* 2016, **107**, 174-184
10. S.G. Hewlett, A. Valera-Medina, D.G. Pugh, P.J. Bowen, *Proceedings of the ASME Turbo Expo 2019: Turbomachinery Technical Conference and Exposition. Volume 3: Coal, Biomass, Hydrogen, and Alternative Fuels; Cycle Innovations; Electric Power; Industrial and Cogeneration; Organic Rankine Cycle Power Systems. Phoenix, Arizona, USA. June 17–21, 2019.*
11. India's TATA Steel begins hydrogen gas injection in blast furnace, [Internet], [cited 11/03/2023]. Available at: https://www.reuters.com/business/sustainable-business/indias-tata-steel-begins-hydrogen-gas-injection-trial-blast-furnace-2023-04-24/
12. Ausfelder F, et al. *ChemBioEng Rev,* 2017, **4** (3), 144-210
13. J. Lelieveld, K. Klingmüller, A. Pozzer, R.T. Burnett, A. Haines, V. Ramanathan, *P Natl Acad Sci USA,* 2019, **116** (15), 7192-7197
14. F. Perera, *Int. J. Environ. Res. Public Health,* 2018, **15** (1), 1-17
15. A National Vision of America's Transition To A Hydrogen Economy To 2030 And Beyond, 2002
16. Hydrogen Insights: A perspective on hydrogen investment, market development and cost competitiveness, Hydrogen Council, February 2021
17. S. Niaz, T. Manzoor, A.H. Pandith, *Renew. Sust. Energ. Rev.,* 2015, **50**, 147-469
18. T. Abbasi and S. A. Abbasi, *Renewable Sustainable Energy Rev.*, 2011, **15**, 3034–3040
19. E. Rivard, M. Trudeau, K. Zaghib, *Materials*, 2019, **12**, 1973-1994
20. I. Staffell, D. Scamman, A. V. Abad, P. Balcombe, P.E. Dodds, P. E. Dodds, P. Ekins, N. Shah, K.R. Ward, *Energy Environ. Sci.,* 2019, **12,** 463-491
21. UK Hydrogen Strategy, CP 475, August 2021
22. Energy Information Administration, International Energy Outlook, 2021
23. International Energy Agency, Transport, 2021
24. Transport and Environmental Statistics 2022, GOV.UK
25. N. Brahy, Fuel Cell Electric Buses – Potential for Sustainable Public Transport in Europe, 2015.
26. DOE Technical Targets For Onboard Hydrogen Storage for Light-Duty Vehicles
27. T.Q. Hua, H.S. Roh, R.K. Ahluwalia, *Int. J. Hydrogen Energ.*, 2017, **42** (42), 25121-25129
28. A.M. Abdalla, S. Hossain, O.B. Nisfindy, A.T. Azad, M. Dawood, A.K. Azad, *Energ. Convers. Manage.*, 2018, **165**, 602-627
29. Hydrogen UK, Hydrogen Storage: Delivering on the UK's Energy Needs, Storage Working Group
30. K.C. Ott, Final Report for the DOE Chemical Hydrogen Storage Center of Excellence, 2008
31. A. Zuttel, S. Rentsch, P. Fischer, P. Wenger, P. Sudan, Ph. Mauron, Ch. Emmenegger, *J. Alloys and Compounds*, 2003, 356-357, 515-520
32. Z. Ding, S. Li, Y. Zhou, Z. Chen, W. Yang, W. Ma, L. Shaw, *Nano Materials Science*, 2020, **2** (2), 109-119
33. C.W. Hamilton, R.T. Baker, A. Staubtiz, I. Manners, *Chem. Soc. Rev.,* 2009, **38**, 279–293
34. S.G. Shore, R.W. Parry, *J. Am. Chem. Soc.* 1955, **77**,22, 6084-6085

35. F.H. Stephens, V. Pons, R.T. Baker, *Dalton Trans*., 2007, 2613–2626
36. M. G. Hu, R. A. Geanangel and W. W. Wendlandt, *Thermochim. Acta,* 1978, **23**, 249–255
37. Y.J. Choi, E.C.E. Ronnebro, S. Rassat, A. Karkamkar, G. Maupin, J. Holladay, K. Simmons, K. Brooks, *Phys. Chem. Chem. Phys*., 2014, **16**, 7959-7968
38. U.B. Demirci, *Int. J. of Hydrogen Energ*, 2017, **42** 9978-10013
39. F. Baitalow, J. Baumann, G. Wolf, K. Jaenicke-Rössler and G. Leitner, *Thermochim. Acta*, 2002, **391**, 159–168
40. G. Wolf, J. Baumann, F. Baitalow and F. P. Hoffmann, *Thermochim. Acta*, 2000, **343**, 19–25
41. B. Roy, A. Hajari, V. Kumar, J. Manna and P. Sharma, *Int. J. Hydrogen Energy*, 2018, **43**, 10386–10395
42. A.C. Stowe, W.J. Shaw, J.C. Lineham. B. Schmid, T. Autrey*, Phys. Chem. Chem. Phys*., 2007, **9**, 1831-1836
43. Y. Li, F. Fang, Y. Song, Y. Li, Q. Zhang, L. Ouyang, M. Zhu, D. Sun, *Int. J. Hydrogen Energy*., 2012, **37**, 4274-4279
44. S.B. Kalidindi, J. Joseph, B.R. Jagirdar, *Energy Environ. Sci*, 2009, **2**, 1274-1276
45. D.J. Wolstenholme, K.T. Traboulsee, Y. Hua, L.A. Calhoun, G.S. McGrady, *Chem. Commun*., 2012, **48**, 2597–2599
46. Y.J. Choi, E.C.E. Ronnebro, S. Rassat, A. Karkamkar, G. Maupin, J. Holladay, K. Simmons, K. Brooks, *Phys. Chem. Chem. Phys*., 2014, **16**, 7959-7968
47. O.T. Summerscales, J.C. Gordon, *Dalton Trans*, 2013, **42**, 10075-10084
48. A.D. Sutton, A.K. Burrell, D. A. Dixon, E.B. Garner III, J.C. Gordon, T. Nakagawa, K.C. Ott, J.P. Robinson, M. Vasiliu, *Science*, 2011, **331**, 1426-1429
49. B.L. Davis, D.A. Dixon, E.B. Garner, J.C. Gordon, M. H. Matus, B. Scott, F.H. Stephens, *Angew. Chem. Int. Ed*, 2009, **48**, 6812-6816
50. O.T. Beachley, *Inorg. Chem*. 1967, **6** (5), 870-874
51. M.E. Bowden, I.W.M. Brown, G.J. Gainsford, H. Wong, *Inorganica Chimica Acta*, 2008, **361**, 2147-2153
52. J. Feigerle, N. Smyrl, J. Morrell, A.C. Stowe, United States, N.p., 2010, Web. DOI: 10.1002/9781118019467
53. G.E. Ryschkewitsch, J.W. Wiggins, *Inorg. Chem*., 1970, **9** (2), 314- 317
54. M.P. Confer, D.A. Outlaw, D.A. Dixon, *Comput. Theor. Chem*., 2020, **1189**, 112953
55. Z. Yang, F. Cheng, Z. Tao, J. Liang, J. Chen, *Int. J. Hydr. Energ*., 2012, **37**, 7638-7644
56. L. Li, Q. Gu, Z. Tang, Y. Tan, Q. Li, X. Yu, *J. Mater. Chem. A*., 2013, **1**, 12263
57. D. Neiner, A. Karkamkar, M. Bowden, Y.J. Choi, A. Luedtke, J. Holladay, A. Fisher, N. Symczak, T. Autrey, *Energy Envrion. Sci*., 2011, **4**, 4187-4193
58. F. Leardini, M. J. Valero-Pedraza, E. Perez-Mayoral, R. Cantelli, M. A. Banares, *J. Phys. Chem. C*. 2014, **118**, 17221-17230
59. L. Zhang, S. Li, Y. Tan, Z. Tang, Z. Guo, X. Yu, *J. Mater. Chem. A*. 2014, **2**, 10682-10687
60. M.F. Hawthorne, *J. Am. Chem. Soc*., 1961, **83**, 4, 831-833
61. A.P.M. Robertson, G.R. Whittell, A. Staubitz, K. Lee, A.J. Lough I. Manners, *Eur. J. Inorg. Chem*. 2011, 5279–5287
62. D.A. Resendiz-Lara, N.E. Stubbs, M.I. Arz, N.E. Pridmore, H.A. Sparkes, I. Manners, *Chem. Commun*, 2017, **53**, 11701-11704
63. Shih-Yuan Liu, Hydrogen Storage by Novel CBN Heterocycle Materials Final Report, United States: N.p., 2015, Web doi:10.2172/1221989
64. W. Luo, L.N. Zakharov, Shih-Yuan Liu, *J. Am. Chem. Soc*. 2011, **133**, 13006-13009
65. W. Luo, D. Neiner, A. Karkamkar, K. Parab, E. B. Garner III, D.A. Dixon, D. Matson, T. Autrey, Shih-Yuan Liu, *Dalton Trans*, 2013, **42**, 611-614
66. T.J. Groshens, R.A. Hollins, *Chem. Commun*., 2009, 3089-3091
67. S.S. Mal, F.H. Stephens, R.T. Baker, *Chem. Commun*., 2011, **47**, 2922-2924
68. A.E. Carre-Burritt, B.L. Davis, B.D. Rekken, N. Mack, T.A. Semelsberger, *Energy Environ. Sci*., 2014, **7**, 1653-1656
69. S.M. Whittemore, M. Bowden, A. Karkamkar, K. Parab, D. Neiner, T. Autrey, J.S.A. Ishibashi, G. Chen, Shih-Yuan Liu, D.A. Dixon, *Dalton Trans.* 2016, **45**, 6196-6203
70. T. Nakagawa, A.K. Burrell, R.E. Del Sesto, M.T. Janicke, A.L. Nekimken, G.M. Purdy, B. Paik, R.Q. Zhing, T.A. Semelsberger, B.L. Davis, *RSC Adv*, 2014, 4, 21681-21687

71. T. Semelsberger, J. Graetz, A. Sutton, E.C.E. Ronnebro, *Molecules*, 2021, **26** (6), 1722
72. G. Zhang, D. Morrison, G. Bao, H. Yu, C.W. Yoon, T. Song, J. Lee, A.T. Ung, Z. Huang, *Angew. Chem. Int. Ed.*, 2021, **60**, 11725-11729
73. A. Staubitz, M. Besora, J.N. Harvey, I. Manners, *Inorganic Chemistry*, 2008, 47 (13), 5910-5918
74. C.A. Jaska, K. Temple, A.J. Lough, I. Manners, *J. Am. Chem. Soc.*, 2003, **125**, 9424-9434
75. M.R. Elsby, R.T. Baker, *Chem. Soc. Rev.*, 2020, **49,** 8933-8987
76. M.C. Denney, V. Pons, T.J. Hebden, D.M. Heinekey, K.I. Goldberg, *J. Am. Soc*, 2006, **128**, 12048-12049
77. A. Gluer, M. Forster, V.R. Celinski, J. Schmedt auf der Gunne, M.C. Holthasuen, S. Schneider, *ACS Catal.* 2015, 7214-7217
78. H. Takahashi, T. Watanabe, H. Tobita, *Chemistry Letters*, 2018, **47** (3), 296-299
79. F. Anke, S. Boye, A. Spannenberg, A. Lederer, D. Heller, T. Beweries, *Chem. Eur. J*, **26** (35), 7889-7899
80. A. M. Lunsford, J.H. Blank, S. Moncho, S.C. Haas, S. Muhammad, E.N. Brothers, M.Y. Darensbourg, A.A. Bengali, *Inorg. Chem*, 2016, **55** (2), 964-973
81. I. Ortega-Lepe, A. Rossin, P. Sanchez, L.L. Santos, N. Rendon, E. Alvarez, J. Lopez-Serrano, A. Suarez, *Inorg. Chem*. 2021, **60**, 18490-18502
82. A. Friedrich, M. Drees, S. Schneider, *Chem. Eur. J.* 2009, **15,** 10339 – 10342
83. B.L. Conley, T.J. Williams, *Chem. Commun*, 2010, **46**, 4815-4817
84. W.H. Wang, H.P. Tang, W.D. Lu, Y. Li, M. Bao, Y. Himeda, *ChemCatChem*, **9** (16), 3191-3196
85. J. Liu, J.Y. Chen, M. Jia, B. Ming, J. Jia, R.Z. Liao, C. H. Tung, W. Wang*, ACS Catal*. 2019*, 9*, 3849-3857
86. Y. Pan, Y. Wang, Y. Liang and J. Chen, *Dalton Trans*., 2012, **41**, 871–875
87. G. J. Kim, S. G. Hunt and H. T. Hwang, *Int. J. Hydrogen Energy*, 2020, **45**, 33751–33758
88. G. J. Kim, A. M. Boone, M. Chesnut, J. H. Shin, J. Jung and H. T. Hwang, *Ind. Eng. Chem. Res*., 2020, **59**, 620–626
89. A. Gutowska, L. Li, Y. Shin, C.M. Wang, X.S. Li, J.C. Lineham, R. S. Smith, B.D. Kay, B. Schmid, W. Shaw, M. Gutowski, T. Autrey, *Angew. Chem. Int. Ed*. 2005, **44**, 3758-3582
90. T. Zhang, X. Yang, S. Yang, D. Li, F. Cheng, Z. Tao, J. Chen, *Phys. Chem. Chem. Phys*., 2011, **13**, 18592-18599
91. X. Zhang, L. Kam, R. Trerise, T.J. Williams, *Acc. Chem. Res*. 2017, **50**, 86-95
92. E. Tomas-Mendivil, V. Cadierno, M.I. Menendez, R. Lopez, *Chem. Eur. J*. 2015, 21, 16874-16886
93. L.V. Graux, M. Giorgi, G. Buono, H. Clavier, *Dalton Trans*, 2016, **45**, 6491-6502
94. S. Azpeitia, C. Mendicute-Fierro, M.A. Huertos, A. Rodriguez-Dieguez, J.M. Seco, A.J. Mota, M.A. Garralda, *Eur. J. Inorg. Chem*. 2021, 879–891
95. M. A. Garralda, C. Mendicute-Fierro, A. Rodriguez-Dieguez, J.M. Seco, C. Ubide, I. Zumeta, *Dalton Trans*, 2013, **42**, 11652-11660
96. I. Bustos, Z. Freixa, A. Pazos, C. Mendicute-Fierro, M. A. Garralda, *Eur. J. Inorg. Chem*. 2021, 3131–3138
97. R. Ciganda, M.A. Garralda, L. Ibarlucca, E. Pinilla, M. R. Torres*, Dalton Trans*, 2010, **39**, 7226-7229
98. W.H. Wang, H.P. Tang, W.D. Lu, Y. Li, M. Bao, Y. Himeda, *ChemCatChem*, 2017, **9**, 3191 – 3196
99. Q. Zhou, W. Meng, J. Yang, H. Du, *Angew. Chem. Int. Ed*. 2018, **57**, 12111 –12115
100. B. Singaram, T.E. Cole, H.C. Brown, *Organometallics*, 1984, **3** (5), 774-777
101. B. Singaram, T.E. Cole, H.C. Brown, *Organometallics*, 1984, **3** (10), 1520-1523
102. H.C. Brown, T.E. Cole, M. Srebnik, K.W. Kim, *J. Org. Chem*., 1986, **51**, 4925-4930
103. B. Swanson, D.F. Shriver, J.A. Ibers, *Inorg. Chem*, 1969, 8, 10, 2182-2189
104. H.Helten, A.P.M. Robertson, A. Staubitz, J.R. Vance, M.F. Haddow, I. Manners, *Chem. Eur. J*. 2012, **18**, 4665 – 4680
105. N.E. Stubbs, A. Schafer, A.P.M. Robertson, E.M. Leitao, T. Jurca, H.A. Sparkes, C. H. Woodall, M. F. Haddow, I. Manners, *Inorg. Chem*. 2015, **54**, 10878-10889
106. H. Noth, S. Rojas-Lima, A. Troll, Eur. *J. Inorg. Chem*. 2005, 1895-1906
107. E.M. Titova, E.S. Osipova, A.A. Pavlov, O.A. Filippov, S.V. Safronov, E.S. Shubina, N.V. Belkova, *ACS Catal*., 2017, **7** (4), 2325-2333

108. Z. Lu, L. Schweighauser, H. Hausmann, H.A. Wegner, *Angew. Chem. Int. Ed*, 2015, **54**, 15556-15559
109. A.E. Diaz-Alvarez, C. Vidal, F.J. Suarez, J. Diez, V. Cadierno, P. Crochet, *Organometallics*, 2015, 34, 3670−3677
110. O.J. Metters, A.M. Chapman, A.P.M. Robertson, C.H. Woodall, P. J. Gates, D. F. Wass, I. Manners, *Chem. Commun*., 2014, **50**, 12146-12149
111. P. Hasche, J. Haak, F. Anke, C. Kubis, W. Baumann, H.J. Drexler, H. Jiao, T. Beweries, *Catal. Sci. Technol*., 2021, **11**, 3514-3526
112. S. Pal, S. Kusumoto, K. Nozaki, *Organometallics,* 2018, **37**, 6, 906–914
113. L. Biancalana, S. Zacchini, N. Ferri, M.G. Lupo, G. Pampaloni, F. Marchetti, *Dalton Trans*., 2017, **46**, 16589 – 16604
114. A. Grabulosa, A. Mannu, E. Alberico, S. Denurra, S. Gladiali, G. Muller, *Journal of Molecular Catalysis A: Chemical*, 2012, 363-364, 49-57
115. G. Laurenczy, S. Jedner, E. Alessio, P.J. Dyson, *Inorganic Chemistry Communications*, 2007, 10, 558–562
116. B. Demerseman, M.D. Mbaye, D. Semeril, L.Toupet, C. Bruneau, P.H. Dixneuf*, Eur. J. Inorg*. *Chem*. 2006, 1174–1181
117. B. Bagh, D.W. Stephan, *Dalton Trans*., 2014, **43**, 15638-15645
118. B. Chatterjee, C. Gunanathan, *Chem. Commun.,* 2014, **50**, 888-890
119. P. G. Campbell, Shih-Yuan Liu, *Australian Journal of Chemistry,* 2013, **67** (3) 521-524
120. V. Pons, R.T. Baker, Angew. *Chem. Int. Ed*., 2008, **47**, 9600-9602
121. L.J. Sewell, M.A. Huertos, M.E. Dickinson, A.S. Weller, G.C. Lloyd-Jones*, Inorg. Chem*. 2013, **52**, 4509-4516
122. A. Zsigmond, F. Noheisz, G. Csjernyik, J.E. Backvall, *Topics in Catalysis*, 2002, **19** (1), 119-124
123. D. Zell, S. Warratz, D. Gelman, S.J. Garden, L. Ackermann, Chem. Eur. J., 2016, 22, 1248-1252
124. R. Gonzalez-Fernandez, P. Crochet, V. Cadierno, Molbank, 2021, M1217

4.3 Experimental Procedures

4.3.1 General Remarks

All starting reagents (boronic acids, $LiAlH_4$, NH_4Cl) were purchased from commercial vendors. Tetrahydrofuran as well as NMR solvents (C_6D_6, CD_3CN) were stored in a Youngs ampule under N_2, over 4 Å molecular sieves and was degassed through freeze-pump-thaw cycles. Borane dimethylamine complex (Sigma 97%) was stored in the freezer. All manipulations were conducted under inert atmosphere using standard Schlenk line techniques. All NMR experiments were conducted on a Bruker 400 MHz Ascend 400. Infrared spectra were recorded on a PerkinElmer Spectrum Two ATR FT-IR.

4.3.2 Synthesis of Borohydrides

Synthesis of Lithium Methyl Borohydride

A THF solution (150 mL) of $LiAlH_4$ (2.85g) was prepared in an ice bath as a grey stirring solution under a flow of nitrogen. 3 g of $CH_3B(OH)_2$ was added in portions over 10 minutes and the solution was allowed to subside following each addition. The solution was allowed to stir for 90 mins at room temperature before being allowed to settle. The solution was cannula filtrated over to a fresh 250 mL round bottom flask with a stirring bar. The solvent was removed under vacuum to yield a white powder. The powder was washed with 3 x 10 mL hexane portions. Unknown yield. ^1H NMR δ (CD_3CN): -0.60 (CH_3, m, 3H), -0.20 – 0.41 (BH_3, qq, 3H). ^{11}B NMR δ (CD_3CN): -31.00 (BH_3Me, q, J_{B-H} = 76Hz).

Synthesis of Lithium Phenyl Borohydride

A THF solution (150 mL) of $LiAlH_4$ (1.40 g) was prepared in an ice bath as a grey stirring solution under a flow of nitrogen. 3 g of $PhB(OH)_2$ was added in portions and the solution was allowed to subside following each addition. The solution was allowed to stir for 90 mins at room temperature and then placed to settle. The THF solvent was then cannula filtrated over to a fresh round bottom flask with a stirring bar. The solvent was removed under vacuum to yield a white powder. The product was washed with 3 x 10 mL hexane portions. Unknown Yield. ^1H NMR δ (CD_3CN): 6.97 – 7.52 (Ph, m, 5H), 1.06 – 1.65 (BH_3, qq, 3H). ^{11}B NMR δ (CD_3CN): -25.85 (BH_3Ph, q, J_{B-H} = 80Hz).

Synthesis of Lithium (3,5) Bistriflouromethyl Phenyl Borohydride:

A stirring solution of $LiAlH_4$ (0.66 g, 17.44 mmol) in ~120 mL THF was prepared within a 250 mL round bottom flask. 3 g of 3,5 bis trifluoromethyl phenyl boronic acid was added in portions until full addition. After allowing the reaction to stir overnight at room temperature. The following day, an additional 10 mL dry THF and 0.5 eq of $LiAlH_4$ was added to the reaction. The solution was returned to stirring for 2 h. The sample was then cannula filtrated over to a dry 250 mL round bottom flask with a stirring bar. The following day, 2x50 mL portions of toluene were added to the flask and mildly heated to re-dissolve the borohydride. This solution was cannula filtrated to give a colourless solution and the solvent was removed under vacuum. The sides of the flask were then scraped with a spatula to give a white powder. The bottom of the flask was unable to be removed with a spatula and upon force mildly exploded producing a brown gas. ^{11}B NMR δ (CD_3CN): -27.80 (q, $LiBH_3(CF_3)_2C_6H_3$, J_{BH} = 80Hz), -42.38 (pent, $LiBH_4$, J_{BH} = 81Hz), -5.89 (t, Unassigned, J_{BH} = 80Hz).

Synthesis of Lithium Diethyl Borohydride:

A THF solution (100 mL) of $LiAlH_4$ (0.85 g) is prepared in a dry 250 mL round bottom flask and placed in an ice bath under nitrogen. 2 mL of diethylmethoxyborane was added dropwise

over 10 minutes and the solution was set to stir at room temperature. The solution was cannula filtered over to a dry Schlenk flask fitted with a stirring bar. Over time, both the cannula and stirring bar turned black, and filtration occurred very slowly. The solution was filtered to collect three fractions. These samples were redissolved in THF and cannula transferred to one flask. ^{11}B NMR δ (CD_3CN): -16.82 (t, $LiBH_2Et_2$, J_{BH} = 70Hz), -27.20 (q, $LiBH_3Et$, J_{BH} = 76Hz), -40.95 (pent, $LiBH_4$, J_{BH} = 80Hz)

4.3.3 Synthesis of Amine Boranes

Synthesis of (B-Phenyl) Amine Borane

A 500 mL round bottom flask was charged with $LiBH_3Ph{\cdot}2$ THF (3.107 g, 12.84 mmol) and ammonium chloride (0.76 g, 1.1 eq). Approximately, 30 mL of cold THF was added via cannula to the flask to produce a cloudy solution with un-solubilised ammonia chloride. After 1h stirring under nitrogen at room temperature, the flask was placed under static vacuum, initiating gentle bubbling. The flask was heated to 50 ^oC in a water bath, and gentle bubbling of the sample was observed intermittently for the next hour. The cloudy solution was cannula filtrated to a dry Schlenk flask with a stirring bar. The solvent was removed under vacuum to yield a sticky white material. ^{11}B NMR δ (CD_3CN): -13.77 (t, NH_3-BH_2Ph, J_{B-H} = 95Hz), 29.10 (s). ^{1}H NMR δ (CD_3CN): 6.98-7.31 (NH_3-BH_2Ph, m, 5H), 3.94 (t, 3H, NH_3-BH_2Ph, J_{B-H} = 39Hz), 1.95-2.75 (q, 2H, NH_3-BH_2Ph, J_{B-H} = 93Hz).

Synthesis of (B-Methyl) Amine Borane

A 250 mL round bottom flask was charged with $LiBH_3Me$ (1.85 g, 10.67 mmol) and ammonium chloride (0.62 g, 1.1 eq). Approximately, 30 mL of cold THF was added via cannula to the flask to produce a cloudy solution with un-solubilised ammonia chloride. After 1h stirring under nitrogen at room temperature, the flask was placed under static vacuum, initiating gentle bubbling. The flask was heated to 50 ^oC in a water bath, and gentle bubbling of the sample was observed intermittently for the next hour. The cloudy solution was cannula filtrated to a dry Schlenk flask with a stirring bar. The solvent was removed under vacuum to yield a fine white powder. The product was washed with 3 x 10 mL hexane and dried under vacuum. ^{11}B NMR δ (CD_3CN): -14.19 (t, NH_3BH_2Me, J_{BH} = 95Hz). ^{1}H NMR δ (CD_3CN): -0.11 (s (br), 3H, NH_3-BH_2Me), 1.86 (q (br), J_{BH} = 93Hz, 2H, NH_3-BH_2Me), 3.24 (br, 3H, NH_3-BH_2Me)

Synthesis of (B-Diethyl) Amine Borane

A 250 mL round bottom flask was charged with $LiBH_2Et_2$ (unknown amount) and ammonium chloride (0.60 g) in 30 mL cold THF. The solution was allowed to stir overnight at room temperature. The following morning, a white product had precipitated out of solution. The solvent was then cannula filtrated over to a fresh round bottom flask. The white powder was dried under vacuum. ^{11}B NMR δ (CD_3CN) – 6.45 ppm (t, $^1J_{BH}$ = 89.7 Hz), 48.35 (s).

4.3.4 Preparation of the Catalysts

Generalised Procedure

The catalysts were prepared within the research group according to their literature procedures.[93,123] Catalysts $RuCl_2$(p-cymene)PPh_2OH, $RuCl_2$(p-cymene)P^iPr_2OH and $RuCl_2$(p-cymene)$PPh_2(CH_2OH)$ were prepared according to the following general procedure.

In a Schlenk flask, a solution of $[RuCl_2$(p-cymene)$]_2$ and secondary phosphine oxide (2.2 equiv.) was prepared with 5 mL DCM and allowed to stir for 2h. The reaction mixture was half-concentrated and n-hexane (15 mL) was added to initiate precipitation. The precipitates

were cannula filtered and washed with 2x5 mL portions of hexane to furnish air-stable red powders.

$RuCl_2$(p-cymene)PPh_2OH was produced as an air-stable red powder. ^1H NMR (400 MHz, $CDCl_3$): δ = 7.74-7.66 (m, 4H), 7.51-7.41 (m, 6H), 5.39 (d, $^3J_{HH}$ = 5.2 Hz, 2H), 5.25 (d, $^3J_{HH}$ = 5.8 Hz), 2.49 (sept, $^3J_{HH}$ = 6.98 Hz, 1H), 1.99 (s, 3H), 0.96 (d, $^3J_{HH}$ = 6.94 Hz, 6H). $^{13}C\{^1H\}$ (100.62 MHz, $CDCl_3$): 137.2 (d, J = 58 Hz), 131.6 (d, J = 11.7 Hz), 131.2 (d, 2.4Hz), 128.2 (d, J = 10.6 Hz), 108.6 (s), 96.6 (s), 89.6 (d, J = 5.0 Hz), 86.9 (d, J = 5.7 Hz), 30.3 (s), 21.7 (s), 17.8 (s). $^{31}P\{^1H\}$ (161.97 MHz, $CDCl_3$): 107.1 (s). IR (KBr): 3169.14 (m), 3079.5 (m), 3056 (m), 2961.25 (m), 2877 (m), 1893 (w), 1822.4 (w), 1582.3 (w), 1577.6 (w), 1549.4 (w), 1474 (w), 1434.62 (str), 1375.2 (w), 1332.8 (w), 1260.57 (m), 1158.85 (w), 1171.49 (m), 1106.09 (m), 858.00 (m), 840.04 (m), 796.98 (m), 743 (m), 713.31 (m), 697.65 (m), 565.10 (w), 529.18 (m), 495.42 (m), 463.83 (m).

$RuCl_2$(p-cymene)$PPh_2(CH_2OH)$ was prepared as an air-stable red powder. ^1H NMR (400 MHz, $CDCl_3$): δ 7.90-7.80 (m, 4H), 7.58-7.43 (m, 6H), 5.31 (d, $^3J_{HH}$ = 6Hz, 2H), 5.24 (d, $^3J_{HH}$ = 6Hz, 2H), 4.64 (s, 1H), 2.56 (sept, J = 6.96, 1H), 1.91 (s, 3H), 0.92 (d, $^3J_{HH}$ = 6.99 Hz). $^{13}C\{^1H\}$ (100.62 MHz, $CDCl_3$): 133.42 (d, J =8.30Hz), 132.50 (s), 132.09 (s), 130.97 (d, 2.6Hz), 128.55 (d, J = 9.6Hz), 108.70 (s), 95.40 (s), 89.54 (d, J = 4 Hz), 86.20 (d, J = 5.3 Hz), 63.09 (d, J = 32 Hz), 30.13 (s), 21.52 (s), 17.49 (s). $^{31}P\{^1H\}$ (161.97 MHz, $CDCl_3$): 16.13 (s). IR (KBr): 333.47 (str), 3057 (m), 2908.23 (m), 2867.9 (m), 2362 (w), 1586.9 (w), 1473.4 (m), 1486.7 (m), 1436.15 (str), 1412 (m), 1383.6 (m), 1265.4 (m), 1189.8 (m), 1097.97(m), 1045.01 (m), 862.72 (m), 755.79 (m), 695.48 (m), 581.65 (m), 516.07 (m), 489.77 (m), 472.51(m)

$RuCl_2$(p-cymene)P^iPr_2OH was prepared as an air-stable red powder. ^1H NMR (400 MHz, $CDCl_3$): δ = 5.63 (d, $^3J_{HH}$ = 6.07 Hz, 2H), 5.59 (d, *J* = 5.87 Hz, 2H), 2.79 (sept, $^3J_{HH}$ = 6.87, 1H), 2.66 (octet, $^3J_{HH}$ = 7.10 Hz, 2H), 2.10 (s, 3H), 1.35-1.27 (m, 12H), 1.26 (d, $^3J_{HH}$ = 6.94 Hz, 6H). ^{31}P NMR (161.97 MHz, $CDCl_3$): δ = 134.78 (s). IR (KBr): 3231.71 (m), 3058.73 (w), 2966.15 (m), 2930.28 (m), 2872.80 (m), 2543.17 (w), 1497.50 (m), 1462.57 (m), 1375.48 (m), 1362.95 (m), 1322.97 (m), 1253.41 (m), 1199.58 (m), 1137.74 (m), 1089.12 (m), 1057.96 (m), 1026.13 (m), 965.20 (w), 929.81 (w), 908.00 (w), 881.35 (m), 850.95 (m), 797.41 (m), 736.97 (w), 692.45 (w), 670.40 (m), 656.95 (m), 634.39 (m), 610.05 (m), 570.48 (w), 521.48 (w), 521.99 (m), 508.09 (m), 445.55 (m), 407.30 (w).

Preparation of $RuCl_2$(p-cymene)PPh_2(HN-Propyl)

$RuCl_2$(p-cymene)PPh_2(HN-Propyl) was prepared according to the literature procedure.[124] In a Schlenk flask, a solution of $[RuCl_2(p\text{-cymene})]_2$ and PPh_2Cl (2.2 equiv.) were added to a Schlenk flask with 5 mL DCM and allowed to stir for 2 h. The reaction mixture was half-concentrated and n-hexane (15 mL) was added to initiate precipitation. The precipitate was cannula filtered and washed with 2x5 mL portions of hexane to furnish $[RuCl_2(\eta^6\text{-p-cymene})(PPh_2Cl)]$ as a red powder. To a solution of $[RuCl_2(\eta^6\text{-p-cymene})(PPh_2Cl)]$ in 10 mL of toluene, $^nPrNH_2$ was added (2.1 equiv.). The solution was allowed to stir at room temperature for 1.5 h. The precipitate of the ammonium salt $[^nPrNH_3]Cl$ was removed by cannula filtration. The filtrate was reduced to minimal solvent and n-hexane (15 mL) was added to initiate precipitation of an orange solid, which was washed twice with 5 mL of hexane and vacuum-dried. ^1H NMR (400 MHz, $CDCl_3$): δ 7.96-7.89 (m, 4H), 7.58-7.43 (m, 6H), 5.27 (d, $^3J_{HH}$ = 6Hz, 2H), 5.11 (d, $^3J_{HH}$ = 6Hz, 2H), 3.12 (s, 1H), 2.56 (sept, $^3J_{HH}$ = 6.96, 1H), 2.43-2.37 (m, 2H), 1.91 (s, 3H), 1.27-1.16 (m, 2H), 0.86 (d, $^3J_{HH}$ = 6.9 Hz, 6H), 0.67 (t, 3H, $^3J_{HH}$ = 7.4 Hz) ppm. $^{31}P\{^1H\}$ (161.97 MHz, $CDCl_3$): 59.8 (s). IR (KBr): 3454 (m), 3366.97 (m), 3052.2 (str), 2962.54 (str), 2882 (str), 2697.7 (m), 2541.7 (m), 2182.5 (w), 1577.4 (w), 1514.78 (w), 1463.33

(w), 1432.50 (w), 1404.29 (w), 1096.90 (w), 1034.42 (w), 746.46 (w), 696.16 (w), 546.05 (w), 477.20 (w).

Preparation of $RuCl_2$(p-cymene)PPh_3

100mg of $[RuCl(\mu\text{-}Cl)(p\text{-cymene})]_2$ (0.163 mmoles) was added to a dry Schlenk tube. 2.2 eq. PPh_3 was added to the tube (0.359 mmoles) with 5 mL DCM. The solution was allowed to stir at room temperature for 3h. The flask was placed under vacuum until half of the solvent volume remained. A layer of hexanes (15 mL) was added on top of the solution which caused precipitation of an orange powder. The solvent was cannula filtered off to leave an orange powder. The powder was washed with n-hexane three times and left to dry under vacuum. ^1H NMR (400 MHz, $CDCl_3$): δ = 7.82 (pseudo-t, $^3J_{HH}$ = 8.73 Hz, 6H), 7.43-7.32 (m, 9H), 5.19 (d, $^3J_{HH}$ = 6.02 Hz, 2H), 4.99 (d, $^3J_{HH}$ = 5.68 Hz, 2H), 2.85 (sept, $^3J_{HH}$ = 6.90 Hz, 1H), 1.86 (s, 3H), 1.09 (d, $^3J_{HH}$ = 7 Hz, 6H). $^{13}C\{^1H\}$ (100.62 MHz, $CDCl_3$): 134.4 (d, J = 9.37 Hz), 133.8 (d, J = 46 Hz), 130.2 (d, 2.4Hz), 128.0 (d, J = 9.9 Hz), 111.2 (d, J = 3.3 Hz), 96.0 (s), 89.1 (d, J = 3.2 Hz), 87.2 (d, J = 5.4 Hz), 30.2 (s), 21.9 (s), 17.7 (s). $^{31}P\{^1H\}$ (161.97 MHz, $CDCl_3$): 24.2 (s). IR (KBr): 3049(m), 2959(m), 2329(w), 1960(w), 1761.8 (w), 1572.7 (w), 1483.08(m), 1434.99(m), 1388.3 (w), 1087 (m), 1035.41 (w), 869.14 (w), 742.83 (m), 693.69 (m), 513.80 (m), 497.29 (m), 458.97 (w)

Catalytic Procedure with $[Ru(NCCD_3)Cl(p\text{-cymene})PPh_2OH]PF_6^-$

The reaction of 20 mg of $RuCl_2$(p-cymene)PPh_2OH with NH_4PF_6 (6.42 mg) in 3 mL of CD_3CN at reflux for 10 minutes gave rise to a cationic complex. Two small schlenk flasks were charged with (B-methyl) amine borane (9.1 mg) and another was charged with dimethyl amine borane (10.8 mg) respectively. A 0.8 mL aliquot of the standard solution was added to each schlenk flask. After the addition, one of the Youngs tube of the B-methyl amine borane complex and the sample of dimethyl amine borane were cooled to -35 ºC. A Youngs tube of the (B-methyl) amine borane was submitted for NMR spectroscopy at room temperature. The other samples were submitted for NMR spectroscopy following 30 minutes at -35 ºC.

Catalytic Procedure with $[RuCl_2(p\text{-cymene})PPh_2O^-]$

A solution of 10 mg of $RuCl_2$(p-cymene)PPh_2OH and 3 µL DBU in 0.6 mL THF was prepared in a Youngs tube. 20 mg of dimethyl amine was added to a Youngs tube and submitted for NMR spectroscopy.

4.3.5 Hydride Preparation Reactions

Reaction of $RuCl_2$(p-cymene)PPh_2OH and Et_3SiH

DCM Solvent

A solution of Et_3SiH (13.74 mg, 0.118 mmol) in CH_2Cl_2 (2 mL) was added dropwise to a solution of $RuCl_2$(p-cymene)PPh_2OH (50mg, 0.098 mmol) in CH_2Cl_2 (2 mL) at RT. The reaction mixture was stirred at 45 ºC for 22 h and no change was detected by NMR spectroscopy. To the remaining solution (3 mL), an excess of 50 µL Et_3SiH (4.23 equiv.) was added. After the addition, the solution was stirred for 2 h at 45 ºC. To an NMR aliquot (0.5 mL), an excess of 20 µL (10 equiv.) was added. The sample was heated at 45 ºC for 2 h.

THF Solvent

25 mg of $RuCl_2$(p-cymene)PPh_2OH was placed in a Youngs Tube with 50 µL Et_3SiH (6.35 equiv.) in 0.5 mL THF. The sample was heated to 45 ºC for 2h. The sample then heated to 70 ºC. To improve solubility, in a separate procedure, 34 mg of $RuCl_2$(p-cymene)PPh_2OH was

added to a Schlenk with 4 mL THF. 50 µL Et_3SiH (4.67 equiv.) was added to the Schlenk flask and heated to 70 °C immediately.

Toluene Solvent

17 mg of $RuCl_2$(p-cymene)PPh_2OH was placed in a Youngs tube with 25 µL Et_3SiH (5 equiv.) in 0.5 mL Toluene. The sample was heated to 100 °C for 2h. In a separate procedure, 17 mg of $RuCl_2$(p-cymene)PPh_2OH was placed in a Youngs Tube, with 50 µL Et_3SiH (10 equiv.) in 0.5 mL Toluene. The sample was heated to 100 °C for 2h.

Reaction of $RuCl_2$(p-cymene)PPh_2OH and $NaBH_4$

10 mg $NaBH_4$ was added to a small schlenk flask inside the glovebox and dissolved in 2 mL dry MeOH. Two Youngs tubes were loaded with 10 mg $RuCl_2$(p-cymene)PPh_2OH and 10 mg of $RuCl_2$(p-cymene)PPh_3 respectively. 0.3 mL aliquots of the solution were added to each Youngs tube, and topped up with 0.3 mL dry MeOH. The samples were then submitted and monitored by NMR spectroscopy.

Reaction of $RuCl_2$(p-cymene)PPh_3 and K_2CO_3

30 mL of dry MeOH was added to a Schlenk flask. 75 mg of $RuCl_2$(p-cymene)PPh_3 was added to the flask with 36 mg K_2CO_3. The solution was allowed to stir at room temperature for 30 minutes until the solution was light yellow in colour. The flask was placed under static vacuum and heated to 65 °C (reflux) where the colour changed towards a light brown (whisky colour).

4.3.6 Stoichiometric Reaction Procedures

Stoichiometric Reaction of B-Methyl Amine Borane with $RuCl_2$(p-cymene)PPh_2OH in Chloroform

A standard solution of (B-methyl) amine borane (7.06 mg) in 2 mL $CDCl_3$ was prepared. The solution was degassed over three cycles. 20 mg of $RuCl_2$(p-cymene)PPh_2OH was placed into a Youngs tube. A 0.5 mL (1.76 mg) aliquot of the standard solution was added to the Youngs tube. The sample was then submitted and monitored by NMR spectroscopy.

Stoichiometric Reaction of B-Methyl Amine Borane with $RuCl_2$(p-cymene)PPh_2OH in THF

A standard solution of (B-methyl) amine borane (7.06 mg) in 2 mL dry THF was prepared. The solution was degassed over three cycles. 20 mg of $RuCl_2$(p-cymene)PPh_2OH was placed into a Youngs tube. A 0.5 mL (1.76 mg) aliquot of the standard solution was added to the Youngs tube. The sample was then submitted and monitored by NMR spectroscopy.

Stoichiometric Reaction of Dimethyl Amine Borane with $RuCl_2$(p-cymene)PPh_2OH in THF

A standard solution of 9.4 mg of dimethyl amine borane was prepared in 2 mL THF and degassed over 3 cycles. 20 mg of $RuCl_2$(p-cymene)PPh_2OH (0.0394 mmol) was added to a dry Youngs tube. A 0.5 mL (2.35 mg) of the standard solution was added to the Youngs tube. The sample was then submitted and monitored by NMR spectroscopy.

4.3.7 Catalytic Reactions

General Catalytic Procedure

20 mg of dimethyl amine borane was added to a Youngs tube along with 5 mol% of the catalyst. 0.6 mL dry THF was added to the Youngs tube. The Youngs tube was submitted for NMR spectroscopy and monitored every 12 h at room temperature.

General Catalytic Procedure for Low Catalytic Loadings

Standard solutions consisting of 5 mg of the catalyst in 0.5 mL THF were prepared in 2 mL Schlenk flasks under N_2. 20 mg of dimethyl amine borane was added to Youngs tube. The appropriate volume of catalyst stock solution (Table 6) was added to the Youngs tube using a micro syringe. Dry THF was added into the Youngs tube to produce a sample of 0.6 mL. The Youngs tubes were heated to 70 ºC and measured by NMR spectroscopy. Catalyst reactions of 5 mol% were measured after 1h at 70 ºC. Catalyst reactions of 1 mol% and 0.5 mol% were measured hourly for 2h, and then every 2h. Catalyst reactions of 0.1 mol% were measured every 12 h.

Table 6: Masses of Catalyst Required at Each Loading

	Volume of Catalyst Required (mg)			
Catalyst	5 mol%	1 mol%	0.5 mol%	0.1 mol%
$RuCl_2$(p-cymene)PPh_2OH	8.63	1.72	0.86	0.17
$RuCl_2$(p-cymene)PPh_2(HN-Propyl)	9.33	1.86	0.93	0.186
$RuCl_2$(p-cymene)PPh_3	9.66	1.93	0.96	0.19
$RuCl_2$(p-cymene)$PPh_2(CH_2OH)$	8.87	1.77	0.88	0.18
$RuCl_2$(p-cymene)P^iPr_2OH	7.48	1.49	0.75	0.15

Thermolysis Reactions of B-MeAB

Two Youngs tube were prepared with 14.4 mg and 15.6 mg of (B-methyl) amine borane. 0.5 mL of CD_3CN and C_6D_6 were added to a Youngs tube respectively. The Youngs tubes were monitored by NMR spectroscopy. The Youngs tube were allowed to heat identically at the following temperatures and intervals: Room temperature (0h), 35 ºC (1h), 40 ºC (20h), 50 ºC (27h), 50 ºC (43h), 50 ºC (47h), 50 ºC (51h), 70 ºC (66h), 70 ºC (82h), 75 ºC (86h).